T I M E A N D F R E Q U E N C Y D O M A I N

M O D E L L I N G O F T H E

P I E Z O E L E C T R I C T R A N S D U C E R

PRESENTED BY

GORDON HAYWARD

In the fulfilment of the requirement for the degree of Doctor of Philosophy of the University of Strathclyde

Department of Electronic Science and Telecommunications

December 1981 Glasgow

C O N T E N T S

C O N T E N T S (contd)

Page

C O N T E N T S (contd)

ABSTRACT

A new model for piezoelectric ultrasonic transducers is proposed. Using a systems engineering approach, the concept of feedback is used to explain secondary piezoelectric effects and to clearly describe electro-mechanical interaction. The model is derived from the fundamental piezoelectric equations and it embraces the relevant practical situations where the transducer is subject to arbitrary electrical and mechanical loading. The following main features are incorporated within the model.

a It is valid over a wide range of frequencies,

b It is applicable in both transmission and reception modes,

c It involves realisable elements which are readily simulated, and

d Piezoelectric, pressure and voltage interactions are clearly related.

The model has been verified extensively in computer simulations and water tank measurements of transducer profiles. Extremely close substantiation of the theoretical analyses was obtained, and the model is considered to offer significant advantages over existing transducer analogies.

CHAPTER I

INTRODUCTION

The conversion of electrical energy to mechanical energy and vice versa may be achieved by a number of physically different processes. Such electro-mechanical transducers include magnetostrictive, electro-magnetic, electrostatic, moving coil, piezoelectric and ferroelectric devices. The present application is concerned only with transducer action involving the latter two effects, namely piezoelectricity and ferroelectricity.

1.1 PIEZOELECTRICITY AND FERROELECTRICITY

Piezoelectricity is the phenomenon whereby electric dipoles are generated in certain anisotropic crystals when the material is subjected to a mechanical stress. This is known as the direct piezoelectric effect. The inverse piezoelectric effect occurs when the same materials demonstrate a dimensional change under the influence of an electric field. For a material to exhibit an anisotropic effect such as piezoelectricity, it is a requirement that its crystal structure should have no centre of symmetry. That is, there is at least one axis in the crystal where the atomic arrangement appears different as one proceeds in opposite directions along the axis. Naturally occurring piezoelectric crystals include quartz, tourmaline and rochelle salt.

While the piezoelectric effect is exhibited to a marked degree only in certain anisotropic crystals, all dielectrics

are electrostrictive, in that they show a dimensional change parallel to an applied electric field. In most cases, the magnitude of this effect is relatively small, but some materials, notably certain titanates and zirconates, demonstrate electrostriction to a considerable extent. Such materials form the very important class of electromechanical transducers known as piezoelectric ceramics, or ferroelectrics.

Above a certain temperature (the Curie temperature), the crystal structure of a ferroelectric material does possess a centre of symmetry and thus no resultant dipole moment is possible. Such a crystal, when cooled below the Curie temperature, contains domains for which each electric dipole is aligned in a specific allowed direction. When summed over the entire crystal, the net electric dipole for all of the domains is zero. However, if the crystal is cooled in the presence of an electric field (polling field), the domains tend to align in that allowed direction which is nearest to the direction of the applied electric field. After removal of the polling field, the dipoles cannot easily return to their original positions, and there exists within the ceramic material, a remanent polarisation.

The crystal thus exhibits a permanent electric dipole and when subject to mechanical stress, the lattice distorts, resulting in a change in the total dipole moment of the crystal. The material has thus become piezoelectrically

'polarised' and is hence capable of electro-mechanical transducer action. Such devices are termed ferroelectric because this behaviour presents a physical analogy with the remanent magnetic behaviour of ferromagnetic materials.

In the present application, ferroelectrics are considered to behave like naturally occurring piezoelectric crystals, each having identical relationships between electrical and mechanical quantities. Consequently, the term 'piezoelectric' is used throughout to describe both truly piezoelectric and ferroelectric materials.

1.2 APPLICATION OF PIEZOELECTRIC TRANSDUCERS AND SYSTEM MODELLING

The devices under consideration are assumed to operate, for both transmission and reception, in the thickness mode. That is, each device comprises a thin plate or disc of piezoelectric material which undergoes uniform, compressional vibration in the thickness direction. The fundamental operating frequency of such transducers is generally in the range 0.1 to 10 MHz, although this may deviate considerably, depending on the application and piezoelectric material employed. Operating either as single, independent elements, or as part of an array of identical devices, thickness mode piezoelectric transducers have found widespread application in the following principal areas.

- Underwater sonar, navigation and communications systems.
- Ultrasonic non-destructive testing (ndt) systems.
- Acoustic Emission systems.
- Medical diagnosis.
- Imaging systems, including acoustic holography and tomography.
- Layer thickness testing.
- The measurement and evaluation of some material characteristics.

An essential pre-requisite to the practical implementation of any transducer based system is the availability of a model which accurately predicts transducer performance and response characteristics. Such a model should also embrace the entire acoustic system and as a result, must include the following operating factors.

1 The majority of piezoelectric transducer applications involve some form of transient excitation. Any model must therefore accurately predict transient response characteristics.

2 The mechanical boundary conditions relevant to the particular application.

3 The electrical boundary conditions often exert considerable influence on transducer response. These are often overlooked, especially in transient operation, where accurate modelling of the transmitting and receiving circuitry is required.

It should be noted that the relative complexity of any transducer model is closely related to the particular application and operating conditions. Relatively simple transducer approximations may be sufficient for some continuous wave (CW) applications, whereas more accurate and sophisticated modelling techniques are required for transient operation.

The behaviour of piezoelectric ultrasonic transducers has been widely investigated in the transmission and reception modes. Several models, for example Mason (28), Cook (6), Redwood (36), Martin (27), Kossof (18) and Krimholtz (21) have been proposed to explain this behaviour, but in general they suffer from one or more of the following limitations.

a Some are not truly wideband, being valid only over a narrow range of frequencies in the region of mechanical resonance. Consequently, their application to transient problems is strictly limited.

b None brings out clearly the physical nature of the piezoelectric transduction process.

c Unreal circuit elements such as negative capacitance are frequently employed in the electrical analogues proposed, making exact physical interpretation difficult.

d The effects of external electrical and mechanical loading are usually difficult to interpret.

e Because of the complexity of some of the models, only simple, often impractical situations can be analysed.

1.3 AIMS AND CONTRIBUTIONS OF THE THESIS

A model is described which is the outcome of attempts to eliminate the previously mentioned limitations. Using a systems engineering approach, the concept of feedback is used to explain piezoelectric interaction and to clearly describe the complex electro-mechanical relationships. The resultant model is derived from the fundamental piezoelectric equations and it possesses the following main features.

a It is valid over a wide range of operating frequencies and as such it may be applied to both CW and transient modes of operation.

b The theory is applicable in both transmission and reception modes.

c Feedback mechanisms are involved which clearly relate pressure and voltage interactions.

d The model involves realisable elements which are readily simulated.

e The model embraces relevant practical situations where the transducer is subject to arbitrary electrical and mechanical loading.

f The physical nature of the transduction process, for example primary and secondary piezoelectric interaction, are clearly emphasised and the factors influencing such effects are readily recognisable.

For these reasons, the model is believed to offer significant advantages over existing piezoelectric transducer analogies. Consequently, development of the feedback model is considered to comprise the major contribution of the present work.

In the course of the thesis, the model is verified extensively using computer simulation, voltage measurement and water tank measurement of transducer wave profiles. As a result of such investigations, it is considered that the thesis offers the following additional contributions to piezoelectric system design.

1 The thesis clearly defines all parameters which influence secondary piezoelectric action. The omission of such effects permits considerable simplification of the modelling process, thereby permitting the use of relatively

simple computer algorithms for direct evaluation of transducer response in the time domain.

2 A method is presented which permits accurate modelling of the electronic pulser configuration employed in the great majority of transient excitation systems. Consequently, it is possible to accurately predict and calibrate piezoelectric transducer performance under practical operating conditions.

3 Techniques are described for the simple and accurate measurement of acoustic impedance ratios and/or mechanical bond integrity at the transducer faces. These are considered to offer considerable improvement over existing methods.

4 A new type of membrane hydrophone was employed for the water tank measurements of acoustic pressure wave profiles. It is demonstrated that the transducer model may readily be extended to cover this type of device.

The following chapters (II, III, IV, V) outline development of the feedback model and offer detailed comparisons with existing transducer analogies. Chapters VI and VII extensively discuss transducer action in conjunction with experimental verification, while chapter VIII presents an alternative modelling technique under limited conditions of no secondary piezoelectric action.

CHAPTER II

PIEZOELECTRIC TRANSDUCER MODELLING TECHNIQUES

2.1. INTRODUCTION

This chapter is a review of the various methods which have been employed in order to model the thickness mode piezoelectric transducer. The more important, (and widely applied), transducer analogies are described in some considerable detail, with particular emphasis on the following aspects:-

(i) A clear illustration of the underlying physical concepts involved with piezoelectric transducer behaviour.

(ii) The applicability of the various models in ultrasonic system design.

The concluding section in the chapter describes the proposal of a new model which is believed to offer significant advantages over existing analogies and simulation studies.

The physical behaviour of a piezoelectric transducer may be predicted by a set of linear equations and as a result, it is possible to construct a model which accurately describes operational characteristics of the device. This may be achieved by a variety of methods, all of which must symbolically represent the appropriate governing equations of the system.

Two principal analytic techniques have been developed in order to describe thickness mode transducer properties.

One method, most often applied to resonator theory, involves solving the relevant differential equations with specific boundary conditions (usually zero stress) in order to determine impedance characteristics for a particular vibrational mode. Solutions corresponding to steady state plate vibrations have been given by Tiersten (56) and more recently Meeker (30), who extended the basic analysis to include finite boundary conditions. With this technique, the relationships among transducer material constants are clearly defined, and the method has found principal application in the determination of piezoelectric parameters (15).

A second, much larger group of analyses, incorporates solutions of the relevant differential equations with arbitrary boundary conditions, in order to develop some form of model analogy for the transducer. Because the boundary conditions are arbitrary, this latter concept is of particular interest in ultrasonics systems design. In addition, familiarity with the properties of the analogous model results in a clearer insight into the physical behaviour of the system. Such models include electrical networks, block diagrams, signal flow graphs and analogue or digital simulation diagrams.

In the case of electro-acoustic devices, it has been found convenient in the past to represent such an inter-

disciplinary system by some form of equivalent electrical circuit. That is, the device is modelled by a purely electrical system with governing differential equations of the same form as those describing piezoelectric element behaviour. Common electro-mechanical analogues are those of force-voltage and velocity-current, thereby allowing mechancial system properties to be conveniently evaluated by means of relatively familiar electrical network concepts.

On the other hand, advances in both analogue and digital computer technology have led to the development of mathematical transducer models which are more amenable to simulation analysis. An example of this technique, which is described in section 2.5. of this chapter, involves formulating the transduction process using matrix theory.

Before commencing with the review, it is worthwhile to state briefly the major physical assumptions involved in thickness mode transducer behaviour.

a. The transducer only operates in the thickness mode and has lateral dimensions comprising many wavelengths of sound.

b. The transducer and all surrounding media are loss free.

c. The transducer generates a single mode stress wave. That is, wave modes are uncoupled, thereby permitting description by a single electro-mechanical coupling factor.

d. The transduction process is linear and confined to one dimension.

e. Force and velocity fields are uniform over the surface area of the transducer.

Any deviation from these five basic assumptions is clearly outlined under the appropriate model section.

2.2. THE EQUIVALENT ELECTRICAL CIRCUIT ACCORDING TO W.P. MASON

This section describes the derivation of an exact transducer electrical equivalent circuit (within the confines of earlier assumptions). Basic physical concepts behind the analogy are clearly defined, along with a brief discussion on the relevant model applications.

Much of the original work on piezoelectric transducer dynamic analogies was performed by W.P. Mason (28) and this book provides a classic introduction to equivalent circuit treatments of various piezoelectric configurations. In order to derive the electrical equivalent circuit for a particular transducer, Mason utilised the fundamental piezoelectric relationships, in conjunction with the appropriate wave equation and boundary conditions relevant to that configuration. This technique yields three coupled equations, describing the transducer system in terms of three dependent and three independent variables;

representing a network with one pair of electrical terminals and two pairs of mechanical terminals. By postulating an electromechanical transformer, these equations may be related to an equivalent circuit, the parameters of which are electrical analogues of the coefficients in the original equations.

This model, (or the techniques employed in its derivation) has provided the basis for a large number of subsequent transducer analyses. For example, using the model, Kossof (18) and Thurston (57) developed simplified electrical analogues designed to approximate transducer operation in the vicinity of the first thickness resonance. Redwood (36) and others (8,11,54), using either the basic model or the fundamental equations involved in the derivation, discussed transducer operation under transient conditions. Sittig (50), Papadakis (34) and others have used the basic model to help analyse layered transducer structures. Because of the significance of Mason's model in the historical development of transducer system characterisation, it is well worthwhile at this stage to consider the major aspects involved in the derivation.

Derivation of the Mason Equivalent Circuit

The piezoelectric equations appropriate to the case of a flat, electroded thickness mode transducer are outlined in A1.1, where the relationships between electrical and mechanical quantities are expressed in terms of charge. That is,

$$T = Y^D S_x - hD \qquad \text{Indirect Effect.}$$

T is the mechanical stress.

Y^D is Young's Modulus of Elasticity, measured under conditions of constant electrical displacement.

h is the piezoelectric constant relating stress to applied charge density.

S_x is the mechanical strain.

D is the electrical displacement.

and,

$$E = -hS_x + D/\epsilon^S \qquad \text{Direct Effect.}$$

h relates the electrical field developed per applied mechanical strain.

ϵ^S is the material permittivity measured under conditions of constant strain.

Assuming that the device vibrates only in the x-direction, the piezoelectric relations may be written as follows,

$$T = \frac{Y\partial\xi}{\partial x} - hD$$

$$E = -h\frac{\partial\xi}{\partial x} + D/\varepsilon \qquad \text{——— 1}$$

Where ξ denotes particle displacement within the transducer and the suffixes have been dropped for convenience.

Under the assumption that any applied field is sinusoidal, the disc is expected to undergo sinusoidal expansion and contraction. Consequently, elastic waves travel backwards and forwards inside the transducer. In other words, the mechanical behaviour is similar to that of a transmission line.

Solving the wave equation in one dimension yields,

$$\xi = (Ae^{-j\beta x} + Be^{j\beta x})e^{jwt} \qquad \text{——— 2}$$

A and B are constants determined by boundary conditions at opposite faces of the transducer. By substituting for ξ into the piezoelectric relations, an equation which relates force, F, to the charge on the transducer plates, Q, is obtained;

$$-(F + hQ) = \{(jwZcA)e^{-j\beta x} + (-jwZcB)e^{j\beta x}\}e^{jwt} \quad \text{——————3}$$

Where Zc is the acoustic impedance of the transducer. Differentiating equation 2 with respect to time yields,

$$\frac{\partial \xi}{\partial t} = \frac{1}{Zc}\left[(jwZcA)e^{-j\beta x} - (jwZcB)e^{j\beta x}\right]e^{jwt} \quad \text{——————4}$$

Equations 3 and 4 are formally identical with those of an electrical transmission line of characteristic impedance Zc. The term $\frac{\partial \xi}{\partial t}$ (particle velocity) is analogous to current and - (F+hQ) analogous to voltage.

By integrating the expression for electric field in equation 1, it is possible to obtain the following relationship between voltage and charge.

$$hQ = hCoV + \frac{h^2 Co}{jw}\left[\frac{\partial \xi_2}{\partial t} - \frac{\partial \xi_1}{\partial t}\right] \quad \text{——————5}$$

Where Co is the clamped or static capacitance of the transducer and the expression contained in brackets represents the difference in particle velocity at the rear and front faces. Since the term hQ denotes force, both terms on the right hand side of this equation must also represent forces. By considering the first of these terms, hCoV, as the force generated by an applied voltage V, then hCo becomes a transformation factor relating force to voltage. Mason represented this electrically as a force to voltage 'transformer' of turns ratio hCo, such

that when a voltage is applied across the primary, a force is generated across the secondary and vice versa.

By means of current-velocity and voltage-force analogies, the term $\frac{h^2Co}{jw}$ in equation 5 may be interpreted as a 'mechanical impedance'. That is, $\frac{1}{h^2Co}$ may be considered a mechanical capacitance. However, care must be taken concerning the sign of this quantity. In equation 5 the total driving force is hQ and this must appear across the secondary of the electro-mechanical transformer. This implies that the force term $\frac{h^2Co}{jw}\left[\frac{\partial \xi_2}{\partial t}-\frac{\partial \xi_1}{\partial t}\right]$ is negative in value, otherwise the total force across it and the secondary of the transformer (hCoV) would be of greater value than the total driving force (hQ). Consequently, the element $\frac{1}{h^2Co}$ must be regarded as a negative capacitance. This illustrates one of the drawbacks of dynamical analogies in that unreal circuit elements often have to be used in order to model system characteristics.

In order to fully define the transducer at its electrical terminals, a relationship between input voltage and current must be determined. Since current flowing into the device is given by jWQ, equation 5 yields,

$$I = jwCoV + hCo\left[\frac{\partial \xi_2}{\partial t} - \frac{\partial \xi_1}{\partial t}\right] \text{ ——————6}$$

The first term of this equation represents current flowing into a capacitance Co which is across the primary of the electromechanical transformer. The second term may be construed as an electrical current flowing through the transformer primary due to a flow of 'mechanical current' in the secondary.

The complete equivalent circuit, according to Mason, may be drawn as shown in figure 2.1, which depicts a transducer loaded at front and rear faces by mechanical impedances Z_1 and Z_2 respectively. The transducer is considered a six terminal device, one pair representing the electrical terminals and the other two pairs as mechanical terminals connected to loading media situated at the opposite faces. The transmission line, which is assumed lossless, represents the necessary time delay for mechanical signals to travel through the transducer thickness. A negative capacitance effectively simulates secondary piezoelectric action, while force to voltage conversion is represented by an ideal transformer. Since the model is derived from the fundamental system relationships, it is exact, within the limits of the initial simplifying assumptions, which were stated in section 2.1. In addition, the model is applicable under both continuous wave and transient conditions, although in many instances calculations are extremely complex and the important underlying electromechanical relationships tend to become obscured.

A useful variant of Mason's model, especially convenient for the analysis of steady state systems, may be readily obtained by replacing the transmission line with its lumped T equivalent circuit. The resultant model is shown in figure 2.2.

Although the electrical equivalent circuits of figures 2.1 and 2.2 have served as the basis for very many subsequent transducer analyses, Mason's fundamental model suffers from the following inherent disadvantages.

1. Effects of mechanical loading and backing variations are difficult to determine without recourse to full mathematical analysis. Similarly, the effects of various electrical load terminations on transmission and reception characteristics are not readily envisaged.

2. The electrical equivalent circuits involve the unreal element of negative capacitance. Consequently, physical interpretation of piezoelectric action is difficult to conceive. In addition, the effects of transducer parameter variations on operating performance are not readily predictable.

3. Transient analysis, for all but the simplest of cases, is extremely difficult due to the mathematical complexity involved.

4. Use of the model requires a certain degree of competence in network theory and a knowledge of transmission line behaviour.

As a result of these drawbacks, the exact equivalent circuits have not found widespread acceptance in the analysis of a generalised transduction system. That is, under conditions of arbitrary excitation (force or voltage) and arbitrary electrical or mechanical loading. Instead, analyses based on the Mason Model tend to consider simplified versions, either by constraining the frequency range of interest or interpeting only simple cases of mechanical and electrical loading. However, many of these investigations do provide enhanced understanding of transducer performance and for this reason the more important works are briefly presented in the following section.

2.3 SOME IMPORTANT ELECTRICAL ANALOGUES

2.3 (i) The Basic Lumped Parameter Equivalent Circuit

In the model, the properties of a piezoelectric vibrator are represented by the lumped parameter equivalent circuit shown in figure 2.3. The circuit comprises a series branch consisting of C_1 (the motional capacitance), L_1 (the motional inductance) and R_1 (motional resistance), shunted by a capacitance Co, representing the electrical capacitance of the transducer. L_1 and C_1 are chosen such that they resonate at a frequency equal to the mechanical resonance of the piezoelectric element. By suitable alteration of these components, different modes of vibration may be studied. Mechanical loss is included in this model by means of the resistive component R_1, and the transducer quality factor which is defined by,

$$Q = (L_1C_1)^{1/2}/R_1$$

Inspection of the equivalent circuit shows that two conditions of resonance exist; a series resonant condition when L_1, C_1 and R_1 resonate to produce an impedance minimum, and a parallel condition when the L_1-C_1-R_1 branch is inductive and tunes with Co to produce an impedance maximum. The frequencies at which these conditions occur are defined as the resonance and anti-resonance frequencies respectively.

It should be noted that the representation of a piezoelectric vibrator by this circuit is useful only if the ciruit parameters are constant and independent of frequency. In practice this is not the case and the model is applicable only over a very narrow frequency interval in the vicinity of an isolated mechanical resonance. However, as indicated in the IEEE Standard on Piezoelectricity (15) the model may be extended to incorporate neighbouring resonances by including additional R-L-C branches in parallel with the main R_1-C_1-L_1 branch.

Since it is only valid over a limited range of operating frequencies, this model cannot be applied to transient analysis of transducer behaviour and in acoustic systems the main applications are confined to continuous wave operation in the vicinity of the transducer resonant frequency. Using this equivalent circuit, Thurston (57) analysed transducer bandwidth as a function of mechanical and electrical terminations. Effects of electrical matching networks on improving transducer transmission characteristics were also investigated.

Despite being confined to narrowband systems, this form of representation is widely used in the experimental determination and verification of piezoelectric transducer characteristics. Standard methods of obtaining these

constants basically consist of determining the electrical impedance of a piezoelectric resonator as a function of frequency. In principle, it is necessary to measure the resonance and anti-resonance frequencies along with the free and clamped capacitances in order to determine the relevant material constants. In some instances, accurate measurement of the anti-resonant frequency can be obscured due to the presence of other vibrational modes. For example, radial vibrations are often troublesome when measuring thickness characteristics of piezoelectric discs. In such cases, it is more convenient to characterise the resonator by a lumped parameter circuit and calculate the material constants from the measured parameters of this circuit. A full description concerning the use of this equivalent circuit in determining transducer properties is given in (15) and (16).

2.3ii The Equivalent Circuit According to Kossof

An inspection of Mason's lumped parameter equivalent circuit (fig 2.2) reveals that the term $jZc \tan^{\alpha}/_{2}$ tends towards infinity as the mechanical resonant frequency is approached. Since this term appears in series with both mechanical output ports, transducer behaviour

around this resonance is severely distorted. However, by utilising a standard network identity, Kossof (18) derived an alternative equivalent circuit which effectively overcomes the problem. This equivalent circuit is shown in figure 2.4, depicting a thickness mode transducer mechanically loaded at opposite faces by media of acoustic impedances Z_1 and Z_2. The figure outlines a force F_1, produced at one of the transducer faces, by a voltage v applied to the electrical terminals. Note that the converse is also true, that is, a voltage v produced by an applied force, F_1.

By treating any intermediate layer between the transmitting transducer and irradiated medium as a lossless transmission line, the effects of various backing and matching layers were analysed according to conventional network theory. In a similar manner, the effects of inductive electrical matching circuits on the transmitting, receiving and impedance transfer functions were also investigated. The analyses were performed under steady state operating conditions and all computational results presented in the frequency domain. In this way, changes in bandwidth, centre frequency and transmission characteristics were readily evaluated as functions of mechanical loading (including quarter wave matching), electrical tuning and negative capacitance of the equivalent circuit.

It should be noted that the work done by Kossof was essentially narrowband, being restricted, through mathematical complexity, to a narrow range of frequencies centred around the mechanical resonance. (Approx. 0.5fo-1.5fo where fo is the mechanical resonant frequency, according to Kossof's notation). In addition, the analysis was based almost entirely on network theory, with tuned circuit analogues used to explain resonant behaviour. Consequently, the underlying physical interactions involved in the transduction process tend to be obscured by electrical circuit topology.

2.3iii The Equivalent Circuits of Martin and Sigelmann

Further simplification of Mason's equivalent circuit model is possible if the electrical or acoustic excitation functions are known along with the electrical or mechanical impedance. For a transducer operating as a source, this condition is met if the generator emf and impedance are both known. Operating as a detector, the condition is satisfied if the incident acoustic signal and the acoustic impedance of the loading medium are known. The overall transduction system may then be modelled as a Thevenin mechanical equivalent circuit for the transmitting mode and the Thevenin electrical equivalent circuit for the receiving mode.

In the analysis of Martin and Sigelmann (27), Mason's three-port equivalent circuit was reduced to two, single port networks representing transmission and reception. The circuit appropriate to the transmitting mode consists of a source Fmeq, which is equivalent to that force exerted by the transducer on a perfectly rigid medium, and an impedance Zmeq, which models the mechanical impedance of the device. The corresponding analogy for reception consists of a voltage source Veeq, which corresponds to the open circuit voltage, and an impedance Zeeq, corresponding to the electrical impedance of the transducer. In each case the Thevenin parameters were derived from the constituent equations used by Mason. Both models are outlined in figure 2.5.

Martin and Sigelmann used these equivalent circuits in order to study transducer system behaviour under various conditions of mechanical loading, transducer element size and output resistance of the electrical excitation source. Experimental data for transducer electrical impedance as a function of frequency was in good agreement with the simulated predictions. However, it may be added that their method of adjusting transducer parameters in order to obtain a 'closestfit' for these curves must be questioned, since discrepancies invariably arise due to the presence of radial modes. This is discussed in greater detail in chapter seven.

Although this form of presentation has advantages in that the models are simple and lend themselves fairly readily to computer simulation, the following two disadvantages are apparent.

a. With the formulation of Martin and Sigelmann (27) an extension to a generalised case including transient excitation is extremely difficult.

b. The Thevenin parameters Fmeq, Veeq are effectively black boxes.

Consequently, the electrical model itself gives little or no insight into the physical behaviour of the transduction process. It is significant that in their presentation, Martin and Sigelmann make very little attempt to relate experimental and simulation results to the transducer physical behaviour.

In addition, as pointed out by the authors, the parameter Fmeq implies that one face of the transducer is rigidly clamped. That is, no motion of that face may occur. Since this condition cannot readily be achieved, experimental verification of Fmeq is extremely difficult and simpler techniques of verifying the simulations (such as measurement of electrical impedance as a function of frequency) have to be employed.

2.3iv The Transmission Line Model of Krimholtz, Leedom and Matthaei (KLM Model)

Originally developed to facilitate the analysis of interdigital surface wave transducers (21) this transmission line model of the thickness mode transducer has found application in some ultrasonic systems design (22, 44). While retaining the intuitively satisfying concept of a transmission line, the KLM analysis differs from that of Mason in that the cumbersome distributed coupling of the piezoelectric effect is replaced by a single coupling point at the centre of the transducer. The differences between distributed and single point coupling are incorporated by means of a coupling transformer with a frequency dependent turns ratio, and a series reactance. In this manner, the acoustical and electrical ports may be considered separately, hence aiding the interpretation of various matching schemes.

The KLM model corresponding to a thickness mode piezoelectric transducer is shown in figure 2.6 and a detailed account of its derivation is outlined in (21). In the figure Zc and Vc are the characteristic impedance and velocity associated with the acoustic transmission line. The line length, L, is equivalent to the transducer dimension in the direction of acoustic wave propagation.

Although exact equivalence between this model and that of Mason has been demonstrated (21), basic understanding of the system behaviour is facilitated by the KLM technique. For example, consider a transducer free of any electrical loading. That is, the electrodes are on open circuit. Under these conditions, transducer behaviour is analogous to that of a mechanical transmission line free of electrical loading. This fact is readily observable from figure 2.6, since no current may flow through the transformer primary. However, in the case of Mason's model, this effect is not so readily apparent unless the negative capacitance is transferred to the transformer primary where, under open circuit conditions, it cancels with the clamped capacitance, Co.

Furthermore, in Mason's circuit, the acoustic forces F_1 and F_2 are not developed across the transmission line alone, but are developed partly across the line terminals and partly across the transformer secondary. In the KLM analysis, the forces appear directly across the transmission line terminals. This is physically more acceptable, since it enables a clear distinction to be drawn between the lumped element electrical behaviour and the wave acoustic behaviour of the transducer. The analysis of complex electrical and mechanical matching systems is also simplified. For example, the investigation of multi-layered transducer structures is facilitated since the

equivalent circuits corresponding to each layer may be simply added to the output ports of the model. Use of the KLM technique in this respect has been performed by Silk (44) where the transmission characteristics of a 12-layered transducer system have been investigated. Using similar techniques, Desillets et al (7) developed criteria for optimum broad band transducer design using quarter-wave matching techniques. In each case, a transfer function of the system was obtained in the frequency domain and the effects of finite bond thickness, electrical and mechanical loading were determined. By means of the Inverse Fourier Transform, transfer function impulse response was also investigated, although this was performed only for the simpler electro-mechanical configurations.

Although this model aids physical and computational interpretation of various mechanical matching schemes, the effects of various electrical loading configurations cannot be readily comprehended due to the complex nature of the coupling transformer and series reactance. In consequence, the important phenomenon of secondary piezoelectric action is not clearly illustrated and in this respect the model suffers from the same disadvantages as that of Mason.

So far, the discussion has centred round a group of analyses which tend to be devoted to steady state system performance, despite the fact that both the Mason and KLM equivalent circuits are applicable to wideband systems. In the following section, transient analysis and modelling of the transducer is described along the lines of Cook, Redwood and Filipczynski, all of which yield considerable insight into transient performance.

2.4. TRANSIENT ANALYSIS OF THE PIEZOELECTRIC TRANSDUCER

The transient analyses contained in this section, with the exception of Cook (6) are based on Mason's piezoelectric stress-charge relations. In each case, the development of a system transfer function follows similar lines to those adopted by Mason in the formulation of his equivalent circuit. Apart from the important work of Redwood (36) and Filipczynski (11), no real attempt is made to obtain an electrical analogue of the transducer, the transfer functions themselves being used to study performance under transient conditions.

2.4i The Transient Analysis of Cook

In the analysis according to Cook (6), Mason's fundamental charge relationships were not employed, instead the piezoelectric constant, e, (see Appendix A) was used

to relate stress to an applied voltage. By solving the relevant system and boundary equations for the thickness-mode transducer loaded by real, semi-infinite media, it was shown that the distributed input stress could be represented by two stress generators situated at opposite faces of the transducer. The situation in fig 2.7. where the piezoelectric generator is represented by two lumped stress sources of equal magnitude, eVo(t), where Vo(t) is the voltage applied across the transducer faces. Physically, transient operation of this model may be interpreted as follows:

When an impulse of voltage is applied to the transducer, two stress impulses are initiated at each face, one travelling into the loading medium and the other into the transducer. The relative magnitude of each stress impulse is determined by the appropriate impedance ratio. These impulses reverberate to and fro inside the transducer until they eventually die out due to transmission losses into the surrounding media. Graphical superposition techniques were then used by Cook in order to determine the form and magnitude of the generated acoustic pulse.

In the analysis, effects of the negative capacitance in the transducer transfer function were ignored. Consequently, the model is strictly only applicable to transducers having low values of electro mechanical coupling, such as quartz. Reasonable experimental verification was obtained

for an X-cut quartz crystal, immersed in water, when unit impulse, unit step and sinewave voltages were applied to the input terminals. Nevertheless, the following points should be noted when considering any extension of Cook's model to a more generalised system.

1. Only mechanical behaviour was considered, with no attempt made to include effects of electrical loading on transmitter characteristics.
2. No analysis was performed for the receiving mode.
3. The analysis is only justified for transducers of low values of electromechanical coupling coefficient. That is, K less than 0.1. For higher values of K, applicable to piezoceramic devices, the simple reverberation technique should not be considered as secondary piezoelectric effects must be taken into account.

2.4ii The Transient Analysis of Redwood

Following the analysis adopted by Mason, Redwood (36) obtained transfer functions for the thickness mode transducer during transmission and reception. Commencing with the fundamental system equations, and applying Laplace Transform techniques, solutions were obtained for the transient performance of the piezoelectric transducer corresponding to the following three conditions.

a. The case of an electrically free transducer subject to semi-infinite conditions of mechanical load with arbitrary acoustic impedance.

For this example it was demonstrated that the open circuit voltage produced by an incident stress wave is proportional to the time integral of that stress wave. In addition, due to multiple reverberation within the transducer, the resultant transient wave shape is formed by repetition at regular intervals of the transducer transit time; eventually decaying to zero by virtue of reflection losses at the front and rear faces.

Mathematically, Redwood demonstrated that the open circuit receiver response V(t), due to an incident stress $F_1(t)$ is represented by the following Laplace transfer function,

$$\frac{V(s)}{F_1(s)} = \frac{-h(1-ro)}{sZ_1}\left[1-(1+rx)e^{-sT}+rx(1+ro)e^{-2sT} -rorx(1+rx)e^{-3sT} \ldots\ldots\ldots\right]$$

Where,
s is the Laplace complex variable
ro, rx are reflection coefficients for waves of particle displacement at the transducer front and rear faces respectively. They are less than unity.
$V_1(s)$, $F_1(s)$ are Laplace Transforms of the output voltage and input force respectively.

Consequently, the open circuit voltage follows the integral of the incident force, with the relative amplitudes of successive electrical signals at t = o, T, 2T ..... being given by 1, - (1 + rx), rx(1 + ro) ..... etc. Using graphical techniques, Redwood [36, 37] demonstrated how to construct the overall voltage output for a step input of force applied to the transducer front face. It should be noted that, within the basic assumptions of Mason's model, this transient solution for the electrically free transducer is exact.

b. The case of a rigidly backed receiver with a purely resistive load connected across the electrodes.

Due to mathematical complexity of the analysis and difficulty in obtaining an inverse Laplace Transform solution, Redwood [36] treated the relatively simple case of a transducer rigidly backed at one face. Using this example, he was able to demonstrate that when the transducer is terminated by a small resistive load, the waveform of voltage follows that of the incident force very closely, but not exactly [37]. As the value of resistance is increased, the result tends towards that outlined in the previous case, where the transducer was on electrical open circuit.

Although the physical significance of these results tended to be obscured by mathematical complexity, Redwood was able to show [36,37], by means of simple equivalent circuits, that the differences could be attributed to the negative capacitance present in Mason's model. It will be demonstrated in chapters three and four that such effects are caused by secondary piezoelectric action and that the results may be extended to arbitrary conditions of electrical and mechanical load.

c. The piezoelectric transducer as a generator of ultrasound.

In this case, an exact analysis, valid over all time, was not attempted due to mathematical complexity and the resultant lack of physical interpretation. However, by provisionally ignoring the negative capacitance, a physically meaningful approximation was obtained for the transmitting response of a piezoelectric element (strictly speaking, such an approximation is valid only for devices possessing low values of coupling coefficient). Subsequently, it was demonstrated [36,37], that the transient mechanical behaviour of the transducer is very similar to that of the open circuit receiver, except that there is

no $^{1}/s$ multiplier, i.e. no integration effect occurs. The transfer function obtained by Redwood which describes such a generator is given by,

$$\frac{F_1(s)}{V(s)} = -hCo\frac{(1-ro)}{2}[1-(1+rx)e^{-sT}+rx(1+ro)e^{-2sT}-rorx.$$
$$(1+rx)e^{-3sT} .....]$$

where hCo is the transformation factor relating force to voltage.

Once again, the waveform repeats at integer multiples of the transducer transit time, the amount of ringing being dependent on the reflection coefficients ro and rx. In this approximation, a step function of voltage gives rise to a decaying, repeated step function of force. Note that in the case of the open circuit receiver, a step input of force leads to a decaying, repeated, ramp function of voltage. In both cases Redwood demonstrated how to graphically superimpose the waveforms over every transit period, in order to obtain the full transient response. In an attempt to verify these results an electrical analogue of the transducer was constructed (36). This incoporated an electrical transmission line in order to simulate mechanical behaviour. Excellent agreement was obtained between experimental and theoretical results.

However, it must be stressed that much of the previously discussed analysis is valid only if the negative capacitance present in Mason's model may safely be neglected. In order to examine the effects of this element on transducer transient behaviour, Redwood proposed simplified, but exact equivalent circuits valid only over the first transit interval. That is, over the time interval,

$$o \leqslant t < T$$

These circuits, shown in figure 2.8, provide valuable information concerning the effects of negative capacitance on output voltage and stress waveforms. Such models do make it possible to determine many transient features without recourse to a full theoretical analysis. It is important to note however, that the equivalent circuits, while providing information on the nature of the response, are valid only over a very narrow interval of time. Consequently, they cannot be used to predict overall transient response, and hence the bandwidth, of a transducer configuration.

The analyses of Redwood provided the basis for much further work on transient performance, particularly by Sinha (46 , 47 , 48 , 49), Yadav (62), Carome (4) and Steutzer (54). Sinha employed almost identical methods in order to obtain the response due to a voltage impulse, periodic step

and ramp inputs. In each case the underlying assumptions were similar to those of Redwood.

Steutzer extended Redwood's approach to the case of mechanically free boundaries. For an air-backed and air-loaded transducer, he predicted transient behaviour under two extremes of electrical loading (54); open circuit and short circuit conditions. In each case the excitation waveform was a step input of voltage. For a short circuited, voltage step excited transducer, it was demonstrated that stress and current responses consisted initially of alternating exponential pulses, decaying eventually to a sinewave accompanied by a sequence of sharp spikes.

In addition, Steutzer (55) demonstrated a technique for determining basic thickness mode operating parameters. When a step input of charge is deposited the transducer electrodes from an electrically isolated source, the situation approximates to open circuit excitation. By close observation of the resultant voltage waveform across the electrodes, a simple dynamic measuring technique was devised for obtaining electromechanical coupling factors and acoustic impedance ratios.

2.4iii The Transient Analysis of Filipczynski

In this analysis (11) the influence of negative capacitance was not entirely neglected in evaluating transducer performance. The analysis is similar to that of Redwood in that Laplace Transform techniques are used to obtain system transfer functions.

Filipczynski showed that the negative capacitance has a direct influence on the resonant characteristics of the transducer, effectively determining the mechanical and electrical resonant frequencies. For devices of high electromechanical coupling coefficient ($K>0.1$) it was demonstrated that the mechanical resonant frequency is greater than the electrical resonant frequency, while for K equal to zero, they are identical. By means of a simplified electrical driving system, the influence of negative capacitance was experimentally verified. In addition, a method was described for computing the form and magnitude of the acoustic pulse generated by a piezoelectric transducer of high ($K=0.5$) electromechanical coupling coefficient.when the device is excited by an electrical generator of high output impedance.

By means of an analysis similar to that of Redwood, a voltage-force transfer function was obtained. From this, the equivalent circuit of figure 2.9 was deduced (11). It should be noted that this is essentially equivalent to that derived by Mason, except that the negative capacitance has been placed on the electrical side of the transformer. This equivalence is not unexpected, since the method of derivation is essentially the same in both cases.

From the circuit, it may be observed for the electrodes an open circuit, that the negative capacitance and the transducer clamped capacitance cancel each other. Consequently, if the output impedance of the electrical generator driving such a system were to approximate open circuit conditions, the transducer behaviour would be entirely mechanical and determined by the properties of the transmission line. In fact, the model is now equivalent to that described by Redwood for the transmitting mode.

In an attempt to verify this theory, Filipczynski utilised the experimental configuration shown in figure 2.10. (It may be noted that this ciruit is similar to that used by Steutzer for the determination of transudcer parameters (55)). In this circuit, the thyristor is turned on for a short period of time which is much less than the transducer transit interval. The coupling

capacitor, Cc, then deposits a step function of charge on the transducer electrodes. By selecting Cc at a very low value compared with Co (7pf and 100pf respectively), good electrical isolation is obtained between the thyristor and transducer. It was demonstrated that a step function of charge produced a decaying strain of sawtooth voltage pulses across the transducer. This compared well with the theoretical analysis of the corresponding transfer function.

It should be noted however, that these results were obtained for a highly idealised, inefficient transmitting system. The theory was not extended to a practical system including matching and cabling effects because of the degree of mathematical complexity involved.

Up to this point, the presentation has concentrated on a review of transducer analogies based on electrical equivalent circuits, as these tend to be the most common representations of piezoelectric transducer systems. Consequently, the analysis and identification of transducer behaviour is based on electrical circuit theory utilising network and transmission line concepts.

However, another, more recent mathematical model of the transduction process involves matrix theory in order to formulate the transduction equations. Although a detailed

physical insight is often lost, the technique lends itself very well to computer simulation and for this reason has been incorporated in a number of transducer analyses. The following section presents a brief account of transduction matrix theory, followed by a description of its application to piezoelectric system design.

2.5. MATRIX FORMULATION OF THE TRANSDUCTION EQUATIONS

The input of any transducer in the transmitting mode may be completely characterised by the voltage, V(t) across the transducer, and the current, I(t) flowing through the transducer. The output of the device may be characterised by the distributed field quantities of stress (force/unit area), F(x,t) and velocity U(x,t), for every x in the region of the test medium. By applying the simplifying assumptions discussed earlier; that is, a one dimensional, single mode, linear transduction process, the force and velocity fields may be considered as scalar quantities. The process may then be characterised (29) by a complex matrix which relates the electrical input parameters to the mechanical input parameters in the frequency domain. This matrix, relating any electro-acoustic transducer's input and output parameters is denoted as the transduction matrix, T. That is,

$$\begin{bmatrix} F \\ U \end{bmatrix} = \begin{bmatrix} A & B \\ C & D \end{bmatrix} \begin{bmatrix} V \\ I \end{bmatrix}$$

$$= [T] \begin{bmatrix} V \\ I \end{bmatrix}$$

Applying the same assumptions for a transducer operating in the receiving mode, a transduction matrix relating electrical output parameters to mechanical input parameters is given by,

$$\begin{bmatrix} V \\ I \end{bmatrix} = \begin{bmatrix} A' & B' \\ C' & D' \end{bmatrix} \begin{bmatrix} F \\ U \end{bmatrix}$$

$$= [T'] \begin{bmatrix} F \\ U \end{bmatrix}$$

Where T^1 is the inverse of T.

Although in theory it is possible to characterise the transduction matrix by measuring the input and output parameters, this is very difficult in practice for the thickness mode transducer. The input impedance characteristics of such a transducer are usually a function of the media to which the device is coupled and in addition, the extent of the force and velocity fields can seldom be measured or predicted directly, especially in the case of solid test media.

However, it has been shown that for a particular transducer design, the matrix elements may be computed directly from the material properties of the elements constituting the transducer. In the analyses of Sittig (50, 51), which are primarily concerned with composite,

multi-layered transducer structures, Mason's lumped element equivalent circuit was used in order to formulate the tranduction matrix. Intermediate bonding layers, represented by their electrical transmission line equivalent circuits were also formulated using matrix topology.

As an example of the technique, consider a transducer loaded at one face with a semi-infinite medium of acoustic impedance Z_2, and at the opposite face by a single intermediate layer of finite width. The configuration is shown in figure 2.11. Modelling the intermediate layer by an equivalent, lossless transmission line, and using Mason's lumped element equivalent circuit for the transducer, the overall circuit may be re-drawn in the form of figure 2.12.

By analysing the lumped element circuit, Sittig obtained the following matrix equation relating input voltage and current to output force and velocity for the transducer.

$$\begin{bmatrix} V \\ I \end{bmatrix} = \begin{bmatrix} Ac & Bc \\ Cc & Dc \end{bmatrix} \begin{bmatrix} F_i \\ U_i \end{bmatrix}$$

where,

$$\begin{bmatrix} Ac & Bc \\ Cc & Dc \end{bmatrix} = \frac{1}{\phi Q} \begin{bmatrix} 1 & j\phi^2/wCo \\ jwCo & o \end{bmatrix} \begin{bmatrix} (\cos\alpha c + jZb\sin\alpha c) & Zc(Zb\cos\alpha c + j\sin\alpha c) \\ j\sin\alpha/Zc & 2(\cos\alpha c - 1) + jZb\sin\alpha c \end{bmatrix}$$

$Q = \cos\alpha c - 1 + jZb\sin\alpha c$, $Zb = Z_2/Zc$

For the piezoelectrically inactive layer, the input and output forces and velocities may be related by the following transformation matrix,

$$\begin{bmatrix} F_1 \\ U_1 \end{bmatrix} = \begin{bmatrix} AL & BL \\ CL & DL \end{bmatrix} \begin{bmatrix} Fo \\ Uo \end{bmatrix}$$

where,

$$\begin{bmatrix} AL & BL \\ CL & DL \end{bmatrix} = \begin{bmatrix} \cos\alpha L & jZL\sin\alpha L \\ \frac{j\sin\alpha L}{ZL} & \cos\alpha L \end{bmatrix}$$

The relationship between output force and velocity, Fo, Uo and input voltage and current, V,I is now given by,

$$\begin{bmatrix} V \\ I \end{bmatrix} = \begin{bmatrix} Ac & Bc \\ Cc & Dc \end{bmatrix} \begin{bmatrix} AL & BL \\ CL & DL \end{bmatrix} \begin{bmatrix} Fo \\ Uo \end{bmatrix}$$

Employing this technique, Sittig (51) analysed the effects of bonding and electrode layer thickness on transducer performance, and in particular that configuration of an ultrasonic delay line consisting of transmitting transducer, intermediate delay line medium and receiving transducer. More recently, Lewis (13) used a similar technique in order to analyse a multi-layer transducer configuration typical of ultrasonic imaging and non-destructive testing systems. Frequency response curves were obtained for a variety of matching layers, and by means of an inverse Fourier Transform routine, pulse shapes in the time domain were also studied.

In conclusion, the matrix technique can be extremely useful in the study of multi-layer transducer systems, since it is simple and lends itself ideally to computer simulation. However, the technique provides little insight into physical behaviour; cause and effect relationships being interpreted from computer results. Even with the straightforward case of a transducer loaded by semi-infinite media of each face, a thorough understanding of physical behaviour may only be obtained if some form of physical model is used in conjunction with the computer simulation.

For example, it is possible to enhance physical understanding if changes in a particular matrix parameter were related directly to changes in the same parameter, contained in Mason's equivalent circuit.

2.6. AN ALTERNATIVE APPROACH TO PIEZOELECTRIC TRANSDUCER MODELLING

The great majority of piezoelectric transducer modelling schemes involve device representation by some form of equivalent electrical circuit. This is not without good reason since electrical analogies offer the following advantages.

1. A knowledge of the circuit diagram of the analogous system permits prediction of the transducer behaviour based on network topology alone. For example, series and parallel resonance along with loading effects may readily be described.

2. Standard network theorems and techniques may be applied in order to reduce or simplify the equivalent circuit and hence derive the necessary input/output relationships.

3. It is possible to construct an actual working model of the equivalent circuit. This may be achieved by discrete circuit element implementation, as performed by Redwood (37) or by analogue computer simulation, as illustrated by Dotti (8).

On the other hand, as outlined in some previous sections, electrical analogies suffer from the following disadvantages.

1. Actual physical elements must be identified that are analogous to resistance, capacitance and inductance as do the physical quantities which correspond to voltage and current. This is not always possible in the case of a thickness mode transducer, where, in order to describe secondary piezoelectric action, a negative capacitance was postulated. This is unlike any real circuit element.

2. The physical parameters and variables of the transducer must be converted and expressed in terms of equivalent electrical units. For example, mechanical or acoustical ohms.

3. In some instances, for example in the analysis of Kossof, modification of the equivalent circuit is required. This may only be achieved if the user has a degree or proficiency in electrical circuit theory.

4. If the response of the analogous electrical circuit cannot readily be ascertained by inspection, then it is necessary either to solve the basic differential equations or perform an often complicated network reduction. Both of these may require more effort than dealing with the equations in some alternative manner. For example, the response of a transducer under arbitrary electrical loading cannot readily be predicted from inspection of the Mason or KLM equivalent circuits. The complex mathematical analysis required to obtain such a response invariably obscures the physical significance of the device behaviour.

5. In some instances, for example the basic lumped parameter equivalent circuit, the model is constructed from inspection of the physical system which it represents, rather than directly from a study of the defining differential equations.

6. Basic equations describing the physical phenomena in disciplines other than circuit theory are not used. Consequently, much physical insight into the nature of the transduction process is obscured by electric circuit topology.

The remainder of this section is devoted to the description of an alternative strategy for modelling thickness mode piezoelectric transducer behaviour. This technique, utilising a systems block diagram approach, is considered to overcome many, if not all, of the disadvantages associated with equivalent circuit methods. It should be noted that the application of block diagrams in describing electro-mechanical systems is not new. Preis (35) has used a block diagram approach to model behaviour of the elecro-dynamic loudspeaker, while Ashley (1) utilised closely related signal flow graphs in order to model the same process.

By deriving the relevant force-voltage and voltage-force transduction equations in a form suitable for implementation via a block-diagram, feedback model, a systems approach may be employed to analyse the transfer function. Using this method, the system equations and processes are illustrated quite differently from dynamical analogies, thereby providing new and often better insight into system performance. Representing the transducer system in a systems format offers the following advantages:

1. All the elements of a block-diagram and their interconnections are obtained directly from the fundamental equations of the system which they represent. Each block describes a specific process within the general system in terms of a transfer function which may describe ratios of inter-disciplinary quantities. Consequently, the physical significance behind each process within the transduction system is readily enhanced and by analysing individual blocks, their effect on the overall transfer function may be determined.

2. The interactive coupling among all processes within the transducer system is clearly shown and provided by the block interconnections.

3. Any required input/output relationship may be determined from a straightforward re-arrangement of the systems model. Such graphical manipulations are capable of producing additional insight into the behaviour of the transducer system.

4. Block diagram reduction of any complex, linear system is often a relatively straightforward process. Consequently, the determination of the overall system transfer function is less susceptible to mathematical error.

However, it should be emphasised that the systems method is essentially a frequency domain technique and relies heavily upon the topics of linear systems theory. The user must therefore be conversant with such concepts.as feedback and transfer functions.

In subsequent chapters it will be demonstrated that, by deriving the transduction equations in a manner suitable for systems feedback presentation, a model is obtained which is superior to existing dynamic analogies. It will be shown that the new model permits a very clear insight into transducer operation and the various factors which affect its behaviour both in transmission and reception. The following two chapters present the derivation of such a model, applicable to the general case of arbitrary electrical and mechanical loading.

CHAPTER III

THE PIEZOELECTRIC TRANSDUCER AS A RECEIVER OF ULTRASOUND

3.1 INTRODUCTION

This chapter presents the development of a block-diagram transfer function which accurately describes the behaviour of a piezoelectric transducer when operating as a receiver of ultrasound. As outlined in Appendix A, the term 'piezoelectric' is used to embrace not only naturally occurring piezoelectric materials such as quartz but also polarised ceramics such as barium titanate. The initial part of the theory follows closely the methods adopted by Redwood (36), Filipczynski (11), Stuetzer (54), Dotti (8) and Yamamoto (63), whereby Mason's (28) fundamental piezoelectric equations are used as a starting point in obtaining transducer characteristics. However, in the present case, no attempt is made to produce an electrical analogue of the transducer, which in the case of a piezoelectric disc invokes the unreal component parameter of negative capacitance. Instead, a systems model, utilising the concept of feedback, is proposed in order to clearly explain electro-mechanical interaction. The investigation concerns a completely general case where the transducer is subject to arbitrary electrical and mechanical loading.

The type of transducer under consideration is a thin piezoelectric disc vibrating unidirectionally in its thickness compressional mode. The transducer geometry is outlined in figure 3.1, which shows a thin disc of radius, r, and

thickness, L. In order to simplify mathematical computation, the following assumptions will be made concerning the properties and behaviour of such a device.

1 The diameter of the transducer is much greater than its thickness, thereby permitting the assumption that all mechanical wavefronts are planar in nature. The propagation of undistorted plane waves within the transducer is considered justified in this context, since the ratio of diameter to thickness is in the region of 20:1.

2 A second assumption is that the disc vibrates in a piston-like manner and that acoustic wave motion is in one direction only, the direction normal to the plane surface of the transducer. Consequently, mechanical and electrical quantities such as stress, strain, electric field and displacement are assumed to vary only in the x-direction. This implies that only a single mode of vibration is possible, namely that of the transducer vibrating in its thickness compressional mode. However, in general, the compressional mode is simultaneously accompanied by radial modes as the plate diameter expands and contracts. Redwood (37) and Filipczynski (11) have both indicated that the radial mode can be neglected for thin transducers of large diameter operating into solid media. However, for transducers operating under lightly loaded conditions, for example, radiating into a water bath, the radial mode can be significant. Nevertheless, providing the disc diameter is much

greater than its thickness, the frequency difference between the radial and thickness modes is so large that they can easily be distinguished. Consequently, an analysis of the latter mode may proceed independently.

3 The third assumption is that initially, the transducer and surrounding media are considered loss-free. As a result, all acoustic media are represented by real acoustic impedances, defined as the product of cross sectional area, density and longitudinal velocity. In the case of a transducer bonded to solid media, the energy loss to the surrounding material is usually very much greater than that dissipated through internal friction in the device itself. However, it should be noted that for operation under lightly loaded conditions, a significant loss can occur within the piezoelectric material. The effects of internal mechanical losses within the transducer are discussed in chapter VI.

4 Finally, the analysis is restricted to operation much below the yield stress of the materials employed. That is, where mechanical and electrical quantities are connected by the linear piezoelectric equations as outlined in Appendix A. Consequently, effects such as cavitation, localised plastic deformation and irregular modes of vibration are neglected along with any possible variation in transducer properties due to ageing and thermal effects.

3.2 EQUATIONS OF MOTION FOR A PIEZOELECTRIC PLATE TRANSDUCER

In order that the nature of electrical and mechanical energy propagation may be studied, we consider firstly the basic piezoelectric relations which were originally proposed by Mason (28).

$$\Gamma_x = Y_x^D S_x - h_{33} D_x \qquad \text{Indirect effect}$$

$$E_x = -h_{33} S_x + D_x/\varepsilon_x^S \qquad \text{Direct effect}$$

Y_x^D is the elastic constant in the x-direction, measured under conditions of constant electrical displacement, (electrodes on open circuit) expressed in Newtons per square metre

ε_x^S is the absolute permittivity of the transducer material in the x-direction, measured under conditions of constant strain, in Farads per metre.

D_x is the electric displacement in the x-direction, expressed in coulombs per square metre

E_x is the electric field strength in the x-direction, expressed in volts per metre

Γ_x is the tensile or compressive stress in the x-direction in Newtons per square metre

S_x is the strain, or fractional change in length, in the x-direction

h_{33} is a piezoelectric constant relating the stress developed per applied charge density or the electric field developed per applied mechanical strain. It is usually measured under conditions of constant electrical displacement. The suffix 33 indicates that the constant is applicable to the thickness direction of the crystal.

In addition,

$$S_x = \frac{\partial \xi_x}{\partial x}$$

where ξ_x is the mechanical displacement of an arbitrary point within the transducer.

A full description of the piezoelectric relations is given in Appendix A.

For convenience, the suffices are dropped and hence the piezoelectric relations can be written as follows:

$$\Gamma = \frac{Y\partial \xi}{\partial x} - hD$$

$$E = \frac{-h\partial \xi}{\partial x} + D/\epsilon$$

Assuming that there is no net free charge within the transducer, then Gauss' Law ($\varepsilon_o \oint_s E.ds = \Sigma Q$) yields:

$$\frac{\partial D}{\partial x} = 0$$

therefore $$\frac{\partial \Gamma}{\partial x} = \frac{Y\partial}{\partial x}\left(\frac{\partial \xi}{\partial x}\right) - \frac{h\partial D}{\partial x}$$

ie

$$\frac{\partial \Gamma}{\partial x} = \frac{Y\partial^2 \xi}{\partial x^2} \qquad \text{1}$$

Considering an infinitesimal volume element within the transducer and using Newton's Law relating force to acceleration, it is possible to obtain,

$$\frac{\partial \Gamma}{\partial x} = \rho \frac{\partial^2 \xi}{\partial t^2} \qquad \text{2}$$

Where ρ is the material density.

Equating 1 and 2, the standard wave equation describing mechanical propagation within the transducer is obtained.

$$\frac{\partial^2 \xi}{\partial t^2} = V^2 \frac{\partial^2 \xi}{\partial x^2} \qquad \text{3}$$

where $V^2 = Y/\rho$ is the longitudinal wave velocity in metres per second. It should be noted, as indicated by Redwood (36) that the wave equation for the piezoelectric disc is identical to the wave equation corresponding to propagation in a non-piezoelectric material.

At this point, it is convenient to introduce the Laplace transform which is defined by,

$$G[f(t)] = \int_0^\infty e^{-ST} f(t)dt$$

where S is a complex variable, f(t) is the time function to be transformed and G is the transformation symbol. The solution to equation 3 can now be expressed as:

$$\xi(S) = Ae^{-S(x/V)} + Be^{S(x/V)} \qquad 4$$

This represents two waves travelling inside the disc, one in the positive x-direction and the other in the negative x-direction. A and B are constants defined by the boundary conditions of x = O and x = L (ie at the faces of the transducer).

Before developing the relationship between electrical and mechanical wave quantities, it is interesting to note that since there is no net free charge within the transducer, all free charge must reside on the surface. Consequently, the electrical displacement D can be expressed as follows:

$$D = \frac{Q}{A`} \ C/m^2$$

where $A` = \pi r^2$ is the area of a plane surface of the transducer and Q is the net charge residing on either of the surfaces.

It is now possible to utilise the basic piezoelectric relationships, along with the solution of the wave equation, to relate electro-mechanical wave propagation within the transducer. From the equation describing the indirect effect, we have the relation,

$$\Gamma = Y \frac{\partial \xi}{\partial x} - hD$$

therefore $$\frac{F}{A^{\wedge}} + \frac{hQ}{A^{\wedge}} = Y \frac{\partial \xi}{\partial x}$$

where F is the force in the x-direction

therefore $$F + hQ = A^{\wedge} Y \frac{\partial \xi}{\partial x}$$

Substituting equation 4 into the above expression, a general relationship relating the transforms of force and mechanical displacement inside the transducer is obtained.

$$F(S) + hQ(S) = SZ_C\{-Ae^{-S(x/V_C)} + Be^{S(x/V_C)}\} \quad \text{——————} \quad 5$$

where $Z_C = \rho V_C A^{\wedge}$ is the acoustic impedance of the transducer. Similarly, the equation for force in a non-piezoelectric medium can be found by utilising equations 2 and 4. This yields,

$$F(S) + SZ_m\{-Ae^{-S(x/V_m)} + Be^{S(x/V_m)}\} \quad \text{——————} \quad 6$$

where Z_m is the acoustic impedance of the medium.

Considering now the direct piezoelectric effect, we have:

$$E = -h \frac{\partial \xi}{\partial x} + \frac{D}{\varepsilon}$$

The voltage across the transducer is obtained by integrating the electric field in the transducer over the thickness

$$V = \int_0^L E \, dx$$

$$= \int_0^L \left(-h \frac{\partial \xi}{\partial x} + \frac{Q}{A \varepsilon} \right) dx$$

$$= -h\{ \xi_{(x=L)} - \xi_{(x=0)} \} + \frac{QL}{A \varepsilon}$$

therefore $$V = -h\{ \xi_{(x=L)} - \xi_{(x=0)} \} + \frac{Q}{C_o} \qquad \text{——————} \quad 7$$

where C_o is the bulk, static capacitance of the transducer. The term $\xi_{(x=L)} - \xi_{(x=0)}$ simply indicates the difference in mechanical displacement between the opposite faces of the transducer.

Now consider an arbitrary electrical impedance placed across the transducer terminals, as outlined in figure 3.2. The figure depicts a mechanical wave striking a piezoelectric disc transducer which is electrically loaded by an impedance Z_E. We assume that any externally deposited surface charge

has been allowed to leak away through the load, so that initially, the voltage across the transducer, V(t) is zero. On striking the surface, the mechanical wave induces a polarisation of charge in the transducer, due to the direct piezoelectric effect. A current, I(t) thus flows through the loading impedance, producing a voltage V(t). Consequently, we can obtain a relationship between the charge produced piezoelectrically and the voltage measured across the transducer.

The current, I(t) is related to the charge by the equation,

$$I(t) = \frac{dQ}{dt}$$

Laplace transforming, and assuming zero initial conditions, yields,

$$I(S) = -SQ(S)$$

therefore $$V(S) = -SQ(S)\ Z_E(S)$$

or, $$Q(S) = \frac{-V(S)}{SZ_E(S)}$$

Substituting the above into equation 7 gives for the transform of voltage across the device,

$$V(S) = -h\{\xi_{(x=L)} - \xi_{(x=0)}\}(S) - \frac{V(S)}{SC_oZ_E(S)}$$

Denoting $C_o Z_E(S)$ by $T(S)$, the following expression is readily obtained for the voltage transform across the loaded transducer

$$V(S) = -h\{\xi_{(x=L)} - \xi_{(x=0)}\}(S) \left\{\frac{ST(S)}{1 + ST(S)}\right\} \qquad 8$$

3.3 THE TRANSDUCER AS A RECEIVER OF MECHANICAL WAVES

3.3i Boundary Conditions and Development of the System Equation

Consider a piezoelectric crystal positioned between two non-piezoelectric elastic media, which are assumed to extend indefinitely away from the transducer. The situation is outlined in figure 3.3 which depicts an incident mechanical wave striking the transducer. The incident wave is travelling in medium 1, which has a characteristic impedance Z_1, at a velocity V_1 in the positive x-direction. A_1 is an amplitude factor relating to the incident wave and B_1 is an amplitude factor relating to the reflected wave at the transducer boundary. The transducer has a characteristic impedance Z_C and a longitudinal velocity V_C. A and B are amplitude factors describing the forward and backward travelling waves within the transducer. Similarly, medium 2 has a characteristic impedance Z_2 and a longitudinal velocity V_2. A_2 is an amplitude factor relating to the wave which is transmitted into medium 2. In addition, the following points should be noted.

1 Medium 1 is often referred to as the loading medium with medium 2 as the backing medium, corresponding to the transducer front and rear faces respectively.

2 All acoustic impedances are assumed real, their value per unit area being given by the product of material density and longitudinal velocity.

3 The time taken for mechanical waves to cross the transducer, the transit time, is given by

$$T = \frac{L}{V_C}$$

Such a system is mechanically constrained by two boundary conditions, namely continuity of mechanical displacement and continuity of normal stress. Applying the first of these at each face of the transducer yields,

$$\xi_{1(x=0)} = \xi_{C(x=0)} \text{ and } \xi_{2(x=L)} = \xi_{C(x=L)}$$

where $\xi_1(S) = A_1 e^{-S(x/V_1)} + B_1 e^{S(x/V_1)}$

$$\xi_2(S) = A_2 e^{-S(x/V_2)}$$

$$\xi_C(S) = Ae^{-S(x/V_C)} + Be^{S(x/V_C)}$$

In a similar manner, continuity of normal stress at the boundaries gives rise to the following set of equations.

$$F_{1(x=0)} = F_{C(x=0)} \text{ and } F_{C(x=L)} = F_{2(x=L)}$$

where $F_1(S) = SZ_1[-A_1e^{-S(x/V_1)} + B_1e^{S(x/V_1)}]$

$$F_2(S) = SZ_2[-A_2e^{-S(x/V_2)}]$$

$$F_C(S) + hQ(S) = SZ_C[-Ae^{-S(x/V_C)} + Be^{S(x/V_C)}]$$

These boundary conditions give rise to four equations involving A, B, A_1, B_1 and B_2.

$$A_1 + B_1 = A + B$$

$$SZ_1(-A_1 + B_1) = SZ_C(-A + B) - hQ(S)$$

$$A_2e^{-S(L/V_2)} = Ae^{-S(L/V_C)} + Be^{S(L/V_C)} \qquad 9$$

$$SZ_C[-Ae^{-S(L/V_C)} + Be^{S(L/V_C)}] - hQ(S) = SZ_2[-A_2e^{-S(L/V_2)}]$$

If we assume that there is an arbitrary electrical impedance, having a Laplace transform, $Z_E(S)$, connected across the electrodes of the transducer, then an expression for the transform of voltage across the crystal is given by equation 8.

$$V(S) = -h\{\xi_{(x=L)} - \xi_{(x=0)}\}(S) \left\{\frac{ST(S)}{1 + ST(S)}\right\}$$

therefore

$$V(S) = -h\{A(e^{-ST} - 1) + B(e^{ST} - 1)\} \left\{\frac{ST(S)}{1 + ST(S)}\right\} \qquad 10$$

It is necessary to obtain expressions for A and B in terms of A_1, the incident mechanical wave. From equation 9 it is possible to obtain the following expressions:

$$SZ_1(-2A_1 + A + B) = SZ_C(-A + B) - hQ(S)$$

and

$$SZ_C(-Ae^{-ST} + Be^{ST}) - hQ(S) = -SZ_2(Ae^{-ST} + Be^{ST})$$

The first of these two equations can be written in the form:

$$A - B\frac{(Z_C - Z_1)}{(Z_C + Z_1)} - \frac{2A_1Z_1}{(Z_C + Z_1)} + \frac{hQ(S)}{S(Z_C + Z_1)} = 0$$

The second equation can similarly be expressed in the manner below.

$$-Ae^{-ST}\frac{(Z_C - Z_2)}{(Z_C + Z_2)} + Be^{ST}\frac{-hQ(S)}{S(Z_C + Z_2)} = 0$$

We define

$$R_B = \frac{(Z_C - Z_2)}{(Z_C + Z_2)} \quad \text{and} \quad R_F = \frac{(Z_C - Z_1)}{(Z_C + Z_1)}$$

The previous two equations now become,

$$A - BR_F = A_1(1 - R_F) - \frac{hQ(S)}{S(Z_C + Z_1)} \qquad \text{11}$$

and

$$AR_B e^{-2ST} - B = - \frac{hQ(S)e^{-ST}}{S(Z_C + Z_2)} \qquad \text{11}$$

Equations 11 are more conveniently expressed in matrix form.

$$\begin{bmatrix} 1 & -R_F \\ R_B e^{-2ST} & -1 \end{bmatrix} \begin{bmatrix} A \\ B \end{bmatrix} = \begin{bmatrix} \left\{A_1(1 - R_F) - \frac{hQ(S)}{S(Z_C + Z_1)}\right\} \\ \left\{- \frac{hQ(S)e^{-ST}}{S(Z_C + Z_2)}\right\} \end{bmatrix}$$

Solving the above matrix equation yields for A and B,

$$\begin{bmatrix} A \\ B \end{bmatrix} = \frac{1}{\Delta} \begin{bmatrix} 1 & -R_F \\ R_B e^{-2ST} & -1 \end{bmatrix} \begin{bmatrix} \left\{A_1(1 - R_F) - \frac{hQ(S)}{S(Z_C + Z_1)}\right\} \\ \left\{- \frac{hQ(S)e^{-ST}}{S(Z_C + Z_2)}\right\} \end{bmatrix}$$

where $\Delta = 1 - R_B R_F e^{-2ST}$.

We can thus obtain two expressions for A and B viz:

$$A = \frac{(J_1)(L)}{\Delta} \qquad \text{12}$$

$$B = \frac{(J_2)(L)}{\Delta}$$

where J_1, J_2 and L are the following matrices:

$$(J_1) = (1 \qquad -R_F e^{-ST})$$

$$(J_2) = e^{-ST}(R_B e^{-ST} \qquad -1)$$

$$(L) = \begin{bmatrix} \left\{A_1(1 - R_F) - \dfrac{hQ(S)}{S(Z_C + Z_1)}\right\} \\ \\ \left\{\dfrac{-hQ(S)}{S(Z_C + Z_2)}\right\} \end{bmatrix}$$

Substituting equation 12 into equation 10, the following expression for the transform of voltage across the transducer is obtained.

$$V(S) = -h\left\{\frac{(J_1)(L)}{\Delta}(e^{-ST} - 1) + \frac{(J_2)(L)}{\Delta}(e^{ST} - 1)\right\}\left\{\frac{ST(S)}{1 + ST(S)}\right\}$$

$$= -h\left[(J_1)e^{-ST} - (J_1) + (J_2)e^{ST} - (J_2)\right]\frac{(L)}{\Delta}\left\{\frac{ST(S)}{1 + ST(S)}\right\}$$

Substituting for (J_1) and (J_2) and rearranging terms produces an expression for the voltage transform:

$$V(S) = h\left[\{(1 - e^{-ST}).(1 - R_B e^{-ST})\}\{(1 - e^{-ST}).(1 - R_F e^{-ST})\}\right] \cdot$$

$$\times\frac{(L)}{\Delta}\left\{\frac{ST(S)}{1 + ST(S)}\right\}$$

Letting $U(S) = \dfrac{ST(S)}{1 + ST(S)}$, we may write,

$$V(S) = \frac{(K)(L)}{\Delta} h(1 - e^{-ST}) U(S) \qquad 13$$

where $(K) = \left\{(1 - R_B e^{-ST})(1 - R_F e^{-ST})\right\}$

Equation 13 represents the mechanical response of a lossless, piezoelectric transducer under arbitrary conditions of electrical loading. As such, it is a general equation describing fully the transient behaviour of the transducer when it is operating in the receiving mode. Consequently, equation 13 shall be termed the system equation of the electrically loaded piezoelectric receiver.

3.3ii Development of the Closed Loop Transfer Function

The system equation obtained in the previous section is essentially a transfer function relating, in the S-domain, the voltage developed across the transducer, V(S) to the incident mechanical value, which for the moment is denoted by the amplitude factor A_1. However, in this form, it is neither amenable to mathematical evaluation or physical interpretation. In the present section, a block diagram model of the transducer is developed. The model is based on a closed loop, feedback system which not only lends itself to mathematical analysis, but provides a ready insight into the physical behaviour of a piezoelectric receiver.

In the previous section it was shown that the voltage across the transducer was related to the surface charge by the

following transform relationship,

$$Q(S) = \frac{-V(S)}{SZ_E(S)} = \frac{-C_o V(S)}{ST(S)}$$

Substituting into equation 13 for Q(S) gives,

$$V(S) = \frac{h(1 - e^{-ST})}{(1 - R_B R_F e^{-2ST})} U(S)\left\{A_1(1 - R_F)(1 - R_B e^{-ST}) + \right.$$

$$\left. + \frac{hC_o V(S)}{S^2 T(S)} \left[\frac{(1 - R_B e^{-ST})}{(Z_C + Z_1)} + \frac{(1 - R_F e^{-ST})}{(Z_C + Z_2)}\right]\right\} \qquad 14$$

The amplitude factor A_1 will now be examined in more detail. A_1 denotes the incident mechanical wave, which is assumed to be planar and undistorted. It is required, after the manner of Redwood (36), to describe the incident wave in terms of force or pressure. The expression for the initial wave of force striking the transducer is given by the following transform equation.

$$F_1(S) = SZ_1(-A_1 e^{-S(x/V_1)} + Be^{S(x/V_1)})$$

By considering only the incident wave at x = 0,

$$A_1 = \frac{-F_1(S)}{SZ_1} \qquad 15$$

One additional quantity remains to be defined, the electro-mechanical coupling coefficient, K, of a piezoelectric transducer. It is a measure of the efficiency of the device when converting electrical voltage to mechanical displacement and vice versa.

$$K = h_{33}\left[\frac{\varepsilon^{S}_{33}}{Y^{D}_{33}}\right]^{\frac{1}{2}}$$

where all parameters and suffixes are as previously defined.

Dropping the suffixes for simplicity, we may write,

$$K^2 = \frac{h^2\varepsilon}{Y}$$

The permittivity, ε, is related to the static capacity of the transducer by the equation,

$$\varepsilon = \frac{LC_o}{A}$$

Also, the elastic constant, Y, is related to the longitudinal velocity by the expression,

$$Y = V_C{}^2\,\rho$$

By direct substitution and noting that $\frac{L}{V_C} = T$, $Z_C = AV_C\rho$, we may write,

$$h^2C_o = \frac{K^2Z_C}{T} \qquad \text{16}$$

Now let

$$K_F(S) = \frac{(1 - e^{-ST})(1 - R_B e^{-ST})}{(1 - R_B R_F e^{-2ST})}$$

and

$$K_B(S) = \frac{(1 - e^{-ST})(1 - R_F e^{-ST})}{(1 - R_B R_F e^{-2ST})} \qquad \text{17}$$

Substituting equations 15, 16 and 17 into equation 14 results in the following expression for V(S).

$$V(S) = U(S)\left\{\frac{-hF_1(S)}{SZ_1}(1 - R_F)K_F(S) + \right.$$

$$\left. + \frac{K^2Z_CV(S)}{S^2T(S)T}\left[\frac{K_F(S)}{(Z_C + Z_1)} + \frac{K_B(S)}{(Z_C + Z_2)}\right]\right\}$$

$$\text{therefore} \quad \frac{V(S)}{U(S)} = \frac{-F_1(S)K^2K_F(S)}{SThC_o}\frac{2Z_C}{(Z_C + Z_1)}$$

$$+ \frac{V(S)K^2K_F(S)}{SThC_o}\left[\frac{hC_o}{ST(S)}\right]\frac{Z_C}{(Z_C + Z_1)}$$

$$+ \frac{V(S)K^2K_B(S)}{SThC_o}\left[\frac{hC_o}{ST(S)}\right]\frac{Z_C}{(Z_C + Z_2)}$$

If we now let,

$$M(S) = \frac{K^2}{STHC_o}, \qquad W(S) = U(S)M(S)$$

$$N(S) = \frac{hC_o}{2ST}$$

$$T_F = \frac{2Z_C}{Z_C + Z_1}$$

$$T_B = \frac{2Z_C}{Z_C + Z_2}$$

Then,

$$V(S) = -F_1(S)W(S)K_F(S)T_F + V(S)W(S)K_F(S)N(S)T_F +$$

$$+ V(S)W(S)K_B(S)N(S)T_B \qquad \text{18}$$

This equation can now be expressed in the form of a transfer function for the transducer in reception. The transfer function, H(S), is defined as,

$$H(S) = \frac{\text{Transformed Output Voltage}}{\text{Transformed Input Force}} = \frac{V(S)}{F_1(S)}$$

Collecting terms in equation 18 and solving for V(S) in terms of $F_1(S)$ yields:

$$H(S) = \frac{-W(S)K_F(S)T_F}{1 - \{W(S)K_F(S)N(S)T_F + W(S)K_B(S)N(S)T_B\}}$$

This equation is the generalised transfer function for an electrically loaded piezoelectric disc operating in the receiving mode. When expressed in this manner, it is known as the system closed loop transfer function. It is now possible to express the transfer function in block diagram form, as a closed loop, feedback system. Before doing so, however, a brief review of block diagram and feedback nomenclature is required.

A block diagram of a typical feedback system is shown in figure 3.4. The various parameters in the system are defined as follows. (All quantities are expressed in the S-domain).

R(S) is the Laplace transform of the input signal.

C(S) is the transformed output signal.

G(S) is the direct or forward transfer function.

X(S) is the feedback transfer function.

E(S) is the error signal.

$\pm$ indicates whether the feedback is positive (+) or negative (-).

$H(S) = \frac{C(S)}{R(S)}$ is the system transfer function or the ratio of output to input, in the S-domain.

For the simple system outlined in figure 3.4, it is readily shown that, for a positive feedback system,

$$\frac{C(S)}{R(S)} = \frac{G(S)}{1 - G(S)X(S)}$$

While for a negative feedback system,

$$\frac{C(S)}{R(S)} = \frac{G(S)}{1 + G(S)X(S)}$$

The foregoing theory can now be utilised to obtain a feedback representation of the piezoelectric transducer in reception. Equation 19 is now written in the form,

$$-H(S) = \frac{W(S)K_F(S)T_F}{1 - W(S)K_F(S)N(S)T_F - W(S)K_B(S)N(S)T_B} \qquad \text{20}$$

This can now be expressed in the form of a closed loop, positive feedback system, as indicated in the block diagram of figure 3.5. The equivalence of equation 20 and the block diagram can be explained as follows:

Referring to figure 3.5, we may write,

$$E(S) = J(S)N(S) + F_1(S)$$

$$J(S) = W(S)\{E(S)K_F(S)T_F + J(S)N(S)K_B(S)T_B\}$$

$$= W(S)\{J(S)N(S)K_F(S)T_F + F_1(S)K_F(S)T_F + J(S)N(S)K_B(S)T_B\}$$

therefore

$$J(S)\{1 - W(S)K_F(S)N(S)T_F - W(S)K_B(S)N(S)T_B\} = F_1(S)W(S)K_F(S)T_F$$

$$V(S) = -J(S)$$

therefore

$$\frac{V(S)}{F_1(S)} = \frac{-W(S)K_F(S)T_F}{1 - W(S)K_F(S)N(S)T_F - W(S)K_B(S)N(S)T_B}$$

This equation is identical to equation 20, hence verifying the validity of the block diagram. It is now required to examine in detail each component of the block diagram in order to obtain a physical interpretation of the overall feedback model.

3.4 PHYSICAL SIGNIFICANCE OF THE FEEDBACK MODEL

In order to understand the physical significance of some of the parameters contained in the block diagram, it is important to differentiate clearly between a function of force (pressure) and a function of particle displacement. In addition, a brief review of plane wave interaction at a boundary is essential.

Consider, after the manner of Blitz (2), a packet of plane waves incident normally to a plane boundary which separates two media A and B, each having characteristic impedances Z_A and Z_B respectively. Part of the incident sound energy is reflected back into medium A and the remainder transmitted into medium B. The general situation is outlined in figure 3.6 where P_I, P_R and P_T represent values of acoustic pressure for incident, reflected and transmitted waves. The corresponding values of particle displacement are:

$$\xi_I,\ \xi_R \text{ and } \xi_T$$

The relationships between pressure and particle displacement are,

$$P_I = \frac{\partial \xi_I}{\partial t} Z_A = S\xi_I Z_A \quad \text{(Laplace transforming)}$$

$$P_R(S) = -S\xi_R Z_A$$

$$P_T(S) = S\xi_T Z_B$$

As usual, two boundary conditions apply, ie continuity of pressure and continuity of normal displacement.

$$P_T = P_I + P_R$$

$$\xi_T = \xi_I + \xi_R$$

Using these two equations it is readily shown that, (Blitz (1)),

$$\frac{P_T}{P_I} = \frac{2Z_B}{Z_A + Z_B} = \text{transmission coefficient for waves of force}$$

$$\frac{P_R}{P_I} = \frac{Z_B - Z_A}{Z_B + Z_A} = \text{reflection coefficient for waves of force}$$

$$\frac{\xi_T}{\xi_I} = \frac{2Z_A}{Z_A + Z_B} = \text{transmission coefficient for particle displacements}$$

$$\frac{\xi_R}{\xi_I} = \frac{Z_A - Z_B}{Z_A + Z_B}$$ = reflection coefficient for particle displacements.

It should be noted from the above that reflection coefficients for particle displacements are 180 degrees out of phase with the reflection coefficients of pressure. It is now required to apply all of this information to the block diagram shown in figure 3.5.

It is possible to rearrange figure 3.5 by removing the block T_F from the forward path and instead placing it in both the feedback and input paths. This new arrangement is shown in figure 3.7.

The term $T_F = \frac{2Z_C}{Z_C + Z_1}$ is simply the transmission coefficient for waves of force travelling into the transducer from the front face medium. The remainder of the forward loop now comprises the product of $K_F(S)$ and $W(S)$. This can be written as,

$$\text{Forward path} = K_F(S)W(S)(-1)$$

Neglecting for the moment the negative sign and expanding $W(S)$ yields:

$$K_F(S)U(S)M(S)$$

$$= K_F(S)U(S)\frac{K^2}{SThC_o}$$

$$= K_F(S)U(S)\frac{h}{SZ_C}$$

where the term $\frac{1}{SZ_C}$ is a conversion factor which converts the pressure function inside the transducer to one of particle displacement. Consequently, if there is a wave of force, with a Laplace transform $F_1(S)$ incident on the transducer front face, then a wave of particle displacement, having a transform $D_1(S)$, is transmitted into the device. The physical situation is outlined in figure 3.8a, with the equivalent block diagram representation shown in figure 3.8b.

It is now possible to examine the block $K_F(S)$, which is defined by the following expression,

$$K_F(S) = \frac{(1 - e^{-ST})(1 - R_B e^{-ST})}{(1 - R_F R_B e^{-2ST})}$$

where,

$R_F = \frac{Z_C - Z_1}{Z_C + Z_1}$ Reflection coefficient for pressure waves incident on the transducer front face

$R_B = \frac{Z_C - Z_2}{Z_C + Z_2}$ Reflection coefficient for pressure waves incident on the transducer rear face.

Now consider a function of particle displacement propagating through the transducer. Since the transducer at present is

assumed lossless, the wave will undergo multiple, distortionless reflections as it passes back and forth between the two faces of the disc. Thus, on noting that the reflection coefficients for particle displacement are 180 degrees out of phase with those of pressure, figure 3.9a may be constructed. From the figure, the total particle displacements at the transducer front face are given by the series,

$$\xi_F = D_1(t = 0) + D_1R_B(1 + R_F)(t = 2T) + D_1R_FR_B^2(1 + R_F)$$

$$(t = 4T) + D_1R_F^2R_B^3(1 + R_F)(t = 6T) \ .....$$

Now, representing a delay of one transducer transit time, T, by the Laplace delay operator e^{-ST}, the transformed series becomes:

$$\xi_F(S) = D_1(S)\left\{1 + R_B(1 + R_F)e^{-2ST} + R_FR_B^2(1 + R_F)e^{-4ST} + \right.$$

$$\left. + R_F^2R_B^3(1 + R_F)e^{-6ST} \ .....\right\}$$

$$= D_1(S)\left\{1 + R_B(1 + R_F)e^{-2ST}\left[1 + R_FR_Be^{-2ST} + \right.\right.$$

$$\left.\left. + R_F^2R_B^2e^{-4ST} \ .....\right]\right\}$$

$$= D_1(S)\left\{1 + R_B(1 + R_F)e^{-2ST}\left[\sum_{n=0}^{\infty}(R_FR_B)^ne^{-2nST}\right]\right\}$$

The term inside the square brackets is a geometric progression whose sum to infinity is given by the following expression:

$$S_\infty = \frac{1}{1 - R_F R_B e^{-2ST}}$$

The transformed series representing front face displacements is now reduced to the form,

$$\xi_F(S) = D_1(S)\left\{1 + \frac{R_B(1 + R_F)e^{-2ST}}{1 - R_F R_B e^{-2ST}}\right\}$$

$$\text{therefore} \quad \xi_F(S) = D_1(S)\left\{\frac{1 + R_B e^{-2ST}}{1 - R_F R_B e^{-2ST}}\right\} \qquad \text{21}$$

In a similar manner, the transformed displacements of the rear face are represented by the series,

$$\xi_B(S) = D_1(S)(1 + R_B)e^{-ST} + D_1 R_F R_B (1 + R_B)e^{-3ST} +$$

$$+ D_1 R_F^2 R_B^2 (1 + R_B)e^{-5ST} + D_1 R_F^3 R_B^3 (1 + R_B)e^{-7ST} \ldots$$

$$= D_1(S)(1 + R_B)e^{-ST}\left\{1 + R_F R_B e^{-2ST} + R_F^2 R_B^2 e^{-4ST} +\right.$$

$$\left. + R_F^3 R_B^3 e^{-6ST} \ldots\ldots \right\}$$

$$= D_1(S)(1 + R_B)e^{-ST} \sum_{n=0}^{n=\infty} (R_F R_B)^n e^{-2nST}$$

$$\text{therefore} \quad \xi_B(S) = \frac{D_1(S)(1 + R_B)e^{-ST}}{1 - R_F R_B e^{-2ST}} \qquad \text{22}$$

Now recall that the voltage developed across the transducer is proportional to the difference in displacements between the opposite faces, or more exactly, from equation 8,

$$V(S) \propto h\left\{\xi_F(S) - \xi_B(S)\right\}$$

where

$$\xi_F(S) - \xi_B(S) = D_1(S)\left\{\frac{1 + R_B e^{-2ST} - e^{-ST}\ (1 + R_B)}{1 - R_F R_B e^{-ST}}\right\}$$

$$= D_1(S)\left\{\frac{(1 - e^{-ST})(1 - R_B e^{-ST})}{(1 - R_F R_B e^{-2ST})}\right\}$$

$$= D_1(S) K_F(S)$$

Consequently, the term $K_F(S)$ represents physically the difference in particle displacement between the front and rear faces when an impulse of force is incident on the front face. The time domain representation of K_F is shown in figure 3.9b. $K_F(t)$ consists of a train of weighted impulse functions, alternately changing in sign and separated by the transducer transit interval, T. The weighting factors are, 1, $-(1 + R_B)$, $R_B(1 + R_F)$, $-R_F R_B(1 + R_B)$, $R_F R_B^2(1 + R_F)$ ..... etc and these are determined by the mechanical qualities of the front and rear face media. K_F shall be defined as the front face reverberation factor of the transducer. Essentially, it represents the difference in displacement

between the front and rear faces when an ideal impulse function of displacement is incident on the front face.

It should be noted that, due to changes of phase inherent in K_F, the type of feedback alternates between positive and negative at each instant of phase reversal. This feature is given detailed analysis in chapter V, when transducer electrical impedance is discussed.

The remaining two terms in the forward loop are h and U(S). Since h simply represents the piezoelectric conversion from displacement to voltage, the complete forward loop of the block diagram may be drawn as shown in figure 3.10.

The term U(S) is the Laplace transform of a function which represents the modification of the voltage waveform by the external electrical load.

$$U(S) = \frac{SC_oZ_E(S)}{1 + SC_oZ_E(S)}$$

This is a Laplace transform of the transfer function of an electrical network equivalent to that shown in figure 3.11. In the figure, which is the electrical equivalent circuit at the transducer electrodes, I_o is the current flowing out of the transducer and through the external load. V_T is the voltage generated piezoelectrically by the transducer and V_o is the output voltage generated across the load. From

the diagram, it is clear that Z_E has a considerable effect on the form and magnitude of the output voltage waveform. For Z_E equal to infinity, the transducer electrodes are on open circuit and hence the output current, I_o, is equal to zero. That is, no current may flow out of the transducer and hence there is no nett voltage attenuation. When the electrodes are on short circuit, the output current, I_o, is a maximum and the output voltage, V_o, is equal to zero. For this case, there is, as expected, complete voltage attenuation. The function U(S) is thus defined as the voltage attenuation factor.

Under conditions of arbitrary electrical load, current I_o flows out of the transducer, resulting in a change of electrical charge on the transducer electrodes. It will now be demonstrated that the alteration in charge is responsible for the feedback terms contained in figure 3.5 and that it is a direct indication of a secondary piezoelectric effect as discussed in Appendix A.

Consider initially the particular feedback loop relating to the transducer front face. The two elements contained in this loop are T_F and N(S). That is,

Front face feedback loop = T_F N(S)

$$= \frac{2Z_C}{Z_C + Z_1} \quad \frac{hC_o}{2ST}$$

$$= \frac{Z_C}{Z_C + Z_1} \quad \frac{h}{S} \quad \frac{1}{Z_E(S)}$$

The output voltage generated by the transducer across the external load is thus applied directly to the block $\frac{h}{SZ_E(S)}$, which can be split up into three separate units as indicated in figure 3.12.

Defining,

$$Y_E(S) = \frac{1}{Z_E(S)}$$

This is simply the admittance of the external electrical load and serves to relate the transformed output current, $I_o(S)$ to the transformed output voltage, $V_o(S)$. The function Y_E is consequently defined as the feedback admittance function.

The transformed output current, $I_o(S)$ is then integrated (figure 3.12) to form the charge transform $Q_o(S)$. Due to the inverse piezoelectric effect, the charge Q_o produces a force, F_o at both faces of the transducer. As indicated by Redwood (37), a portion of the force is transmitted into the load and backing media and a portion transmitted into the transducer. The transformed fraction propagating into the transducer at its front face is given by,

$$F_{OT}(S) = \frac{Z_C}{Z_C + Z_1} F_o(S)$$

(Front)

This expression serves to complete the feedback loop and hence FOT(S) represents a transform of the force being fed back into the transducer at its front face. The force F_{OT} can thus generate a voltage in a manner identical to that of the incident force.

The overall block diagram relating to the transducer front face can thus be drawn as in figure 3.13. It is important to notice, that for the transducer on open circuit, no current can flow out of the device, and hence there is no feedback. That is, the response of a piezoelectric receiver with no electrical load, is simply the forward transducer function. On the other hand, with the electrodes on short circuit (ie $Z_E = 0$), the output current, and hence the feedback, is at a maximum value. The output voltage is, of course, zero. Since the overall magnitude of the feedback loop is proportional to the square of the electro-mechanical coupling coefficient, some researchers, notably Stuetzer (55), have used the short circuit termination to measure and compare transducer parameters.

The feedback loop of figure 3.5 relating to the transducer rear face has not yet been considered. In addition to generating a wave of force at the front face, the output

voltage also produces, in an identical manner, a stress wave at the transducer back face. This wave of force must also contribute, as indicated in figure 3.5, to the overall feedback of the system. In this case, the transform of the wave of force generated into the transducer is given by,

$$FOT(S) = T_B N(S) V_o(S)$$

$$= \frac{Z_C}{Z_C + Z_2} \frac{h}{SZ_E} V_o(S)$$

This expression, apart from the transmission coefficient, is identical to that obtained at the transducer front face. In fact, it is readily shown that the transducer rear face behaves in an identical manner to the front face, except that the reflection coefficients generally differ due to unequal backing and load materials. Consequently, identical transfer function blocks are valid for the rear face, except that R_B must be replaced by R_F and vice versa. For example, consider the wave generated due to secondary piezoelectric action at the transducer rear face. This function of force is converted to a function of particle displacement by the conversion factor $\frac{1}{SZ_C}$. However, the term relating to the difference in particle displacement is now given by $K_B(S)$ where,

$$K_B(S) = \frac{(1 - e^{-ST})(1 - R_F e^{-ST})}{(1 - R_F R_B e^{-ST})}.$$

This expression is identical to $K_F(S)$ except that R_F has replaced R_B and vice versa. It thus follows, that for the general case where external forces $F_1(t)$ and $F_2(t)$ are applied to the front and rear faces respectively, the overall block diagram of figure 3.14 is applicable. This represents a completely general model of a lossless, arbitrary loaded (both electrically and mechanically) piezoelectric receiver. The device is shown as a three port network, with secondary effects being modelled using the concept of feedback, which vanishes completely when the transducer is electrically on open circuit. The individual elements in figure 3.14 may be summarised as follows:

T_F Transmission coefficient of waves of force striking the front face

T_B Transmission coefficient for waves of force striking the rear face

$\frac{1}{SZ_C}$ Conversion factor relating force to particle displacement

K_F Difference between front and rear face displacements when a wave of force leaves the transducer front face. It is defined as the front face reverberation factor

K_B Difference between front and rear face displacements when a wave of force leaves the transducer rear face. It is defined as the rear face reverberation factor

h The piezoelectric constant relating particle displacement to voltage or electrical charge to force

U The voltage attenuation factor due to an external electrical load

Y_E The feedback admittance, resulting in current flow out of the transducer.

Before developing a systems model for the piezoelectric transmitter, it is worthwhile at this stage to compare the present model with one of the reduced, circuit models devloped by Redwood (34) for the piezoelectric receiver.

3.5 COMPARISON OF THE FEEDBACK MODEL WITH THE EQUIVALENT CIRCUIT OF REDWOOD

By utilising Mason's concept of negative capacitance, Redwood (36) postulated the equivalent 'electrical' circuit shown in 3.15. Due to the mathematical complexity of his analysis, he treated only simple cases of piezoelectric transducers in reception. Figure 3.15 is hence only applicable under the following constraints,

1 The transducer is rigidly backed. That is, Z_2 is equal to infinity and no contribution whatsoever can be expected from the rear face.

2 The model is only valid during the time interval $0 < t < T$, ie over the first transit interval. Consequently, multiple reflections within the transducer are omitted.

3 The electrical load is purely resistive.

The transfer function of the circuit shown in figure 3.15 may be written as follows:

$$\frac{hC_oV(S)}{2F(S)} = \frac{-SRh^2C_o}{S^2RC_oZ + SZ - h^2C_o}$$

where $Z = Z_1 + Z_C$

$$\text{therefore} \quad \frac{V(S)}{F(S)} = \frac{-2hC_oRS}{S^2RC_oZ + SZ - h^2C_o} \qquad \text{23}$$

Now consider the generalised model shown in figure 3.14. For a rigidly backed transducer no contributions are obtained from the rear face during the time interval $0 < t < T$, $K_F(S)$ reduces to unity. The equivalent block diagram for such a device is shown in figure 3.16, where, as in Redwood's model, the electrical loading is a pure resistance, R.

The transfer function of such a system can be expressed as,

$$\frac{V(S)}{F(S)} = \frac{-T_F \frac{h}{SZ_C} U(S)}{1 - T_F \frac{h}{SZ_C} U(S) \frac{h}{2SR}}$$

where $$U(S) = \frac{SRC_o}{1 + SRC_o}$$

$$T_F = \frac{2Z_C}{Z_C + Z_1} = \frac{Z_C}{Z}$$

Substituting for U(S) and T_F yields for the transfer function,

$$\frac{V(S)}{F(S)} = \frac{\frac{-2hRC_o}{Z(1 + SRC_o)}}{1 - \frac{h^2C_o}{SZ(1 + SRC_o)}}$$

therefore $$\frac{V(S)}{F(S)} = \frac{-2hC_oRS}{S^2RC_oZ + SZ - h^2C_o} \qquad \text{24}$$

Equations 23 and 24 are formally identical, hence demonstrating the equivalence of the two approaches, for this relatively simple example.

It should be pointed out, that although an extension of Redwood's model to the more general situation is mathematically possible, the physical significance of transducer behaviour

is almost completely obscured. This is certainly not the case with the systems feedback model where the effect each component has on transducer behaviour may readily be observed.

3.7 CONCLUDING REMARKS

A block diagram representation of the piezoelectric transducer acting in the receiving mode has been developed. The model is exact within the constraints of the initial assumptions. In addition, it is valid over all frequencies and conditions of electrical and mechanical loading. Each element within the block diagram has been related to a recognisable physical quantity involved in the transduction process. Consequently, the overall model illustrates very clearly the complex electro-mechanical interactions which occur. Secondary piezoelectric effects are illustrated using the concept of feedback and the conditions under which such effects may be of importance are clearly demonstrated. In summary, the amount of feedback (or secondary piezoelectric action) is dependent on the following factors:

1 The magnitude and nature of the electrical load. It was shown that under conditions of electrical open circuit, there is no current flow out of the transducer and hence no secondary action.

2 The amount of feedback is directly proportional to the square of the electro-mechanical coupling coefficient. Consequently, for transducers of low coupling coefficient, such as quartz, secondary effects may be negligible.

3 The amount of feedback is in general, inversely proportional to frequency. At higher frequencies, secondary action has less effect on transducer performance.

4 The amount of feedback is dependent on conditions of mechanical loading at the front and rear faces. This follows directly from the presence of the blocks $T_F/2$ and $T_B/2$ in the feedback loops. However, it should be noted that this cannot be employed to minimise secondary piezoelectric action since each block appears in the input path of the diagram.

In subsequent chapters, the model is used to predict response characteristics of a piezoelectric receiver in both time and frequency domains, with particular emphasis on the effects of electrical loading. However, before this is undertaken, transducer performance as a generator of ultrasound must be considered. The following chapter describes the generalised behaviour of a transducer in the transmitting mode.

CHAPTER IV

THE PIEZOELECTRIC TRANSDUCER AS A TRANSMITTER OF ULTRASOUND

4.1 INTRODUCTION

This chapter describes the development of a feedback model which accurately describes piezoelectric transducer behaviour when the device is acting as a generator of ultrasound. All of the physical assumptions made in the previous chapter are again applied. That is, plane wave propagation is assumed in a thin, lossless, piezoelectric disc which vibrates undirectionally in its thickness mode. The transducer is also assumed to operate under arbitrary external mechanical and electrical boundary conditions.

As in chapter III, no attempt is made to derive a direct electrical analogue of the piezoelectric transmitter. A block diagram systems approach, yielding a feedback transfer function, is again adopted. The resultant model is shown to clearly illustrate the interaction between electrical and mechanical quantities. As in the case of the receiver, importance of secondary piezoelectric effects is clearly outlined.

4.2 THE TRANSDUCER AS A TRANSMITTER OF MECHANICAL WAVES

4.2i Mechanical Boundary Conditions

Consider, after the manner of chapter III, a piezoelectric crystal positioned between two non-piezoelectric elastic media, which are assumed to extend indefinitely away from

the device. The transducer is then subjected to an arbitrary electrical excitation which causes stress waves to propagate into both front and rear media. In addition, waves of force are generated at both surfaces inside the crystal, directed towards the plate centre. The physical situation is shown in figure 4.1, which outlines the general mechanical boundary conditions. The terms A and B are amplitude factors, relating to the waves of force inside the transducer, while B_1 and A_2 describe waves propagating into the front and rear media respectively. Medium 1, corresponding to the front face, is defined by its real characteristic impedance Z_1 and medium 2, (at the rear face) by the real characteristic impedance Z_2. The transducer has, as before, a real characteristic impedance Z_C.

The present situation is almost identical to that described for the piezoelectric receiver in chapter III, figure 3.3. The difference is that for the transmitter, there is no incident wave of force, A_1. Consequently, the initial part of the present analysis will correspond exactly to that in Section 3.3i, except that A_1 is set to zero.

Equations 12 in chapter III may therefore be used directly to give expressions for the amplitude factors, A and B, of the waves of force inside the transducer, ie

$$A = \frac{(J_1)(L')}{\Delta} \qquad B = \frac{(J_2)(L')}{\Delta}$$

where

$$(J_1) = (1 - R_F e^{-ST})$$

$$(J_2) = e^{-ST}(R_B e^{-ST} - 1)$$

$$(L') = \begin{bmatrix} \frac{-hQ(S)}{S(Z_C + Z_1)} \\ \\ \frac{-hQ(S)}{S(Z_C + Z_2)} \end{bmatrix} = \frac{-hQ(S)}{2SZ_C} \begin{bmatrix} T_F \\ \\ T_B \end{bmatrix}$$

$$\Delta = 1 - R_F R_B e^{-2ST}$$

where R_F and R_B are reflection coefficients for pressure waves incident on the front and rear faces of the transducer.

4.2ii Relationship Between Force and Charge During Transmission

In this section, a relationship is developed between the charge deposited on the transducer electrodes and the forces created at each face. A general expression relating the transforms of force and charge at any point x inside the transducer was given in chapter III, equation 5, ie

$$F_x(S) + hQ(S) = SZ_C\{-Ae^{-S(x/V_C)} + Be^{S(x/V_C)}\}$$

Substituting for A and B yields,

$$F_x(S) + hQ(S) = SZ_C\left\{\frac{-(J_1)(L')}{\Delta} e^{-S(x/V_C)} + \frac{(J_2)(L')}{\Delta} e^{S(x/V_C)}\right\}$$

therefore

$$F_x(S) + hQ(S) = \frac{-hQ(S)}{2\Delta}\left\{-(J_1)e^{-S(x/V_C)} + (J_2)e^{S(x/V_C)}\right\}\begin{bmatrix} T_F \\ T_B \end{bmatrix}$$

therefore

$$F_x(S) = -hQ(S)\left\{1 - \frac{(J_1)\begin{bmatrix} T_F \\ T_B \end{bmatrix}}{2\Delta} e^{-S(x/V_C)} + \frac{(J_2)\begin{bmatrix} T_F \\ T_B \end{bmatrix}}{2\Delta} e^{S(x/V_C)}\right\} - 1$$

This equation describes the general Laplace transform relationship between the force or stress at any position x within the transducer and the charge on the electrodes. In the case of a piezoelectric transmitter, the interest is primarily centred on the forces at the transducer front and rear faces. That is, at x = 0 and x = L respectively.

Using equation 1, the force generated at the transducer front face can be obtained using the following transform equation.

$$F_F(S) = -hQ(S)\left\{1 - \frac{(J_1)\begin{bmatrix} T_F \\ T_B \end{bmatrix}}{2\Delta} + \frac{(J_2)\begin{bmatrix} T_F \\ T_B \end{bmatrix}}{2\Delta}\right\}$$

$$= \frac{-hQ(S)}{2\Delta}\left\{2\Delta - T_F + T_B R_F e^{-ST} + T_F R_B e^{-2ST} - T_B e^{-ST}\right\}$$

Noting that, $T_F = (1 + R_F)$, $T_B = (1 + R_B)$ gives,

$$F_F(S) = \frac{-hQ(S)}{2\Delta}\left\{(1 - R_F) - e^{-ST}(1 - R_F)\right.$$

$$\left. - R_B e^{-ST}(1 - R_F) + R_B e^{-2ST}(1 - R_F)\right\}$$

$$= \frac{-hQ(S)(1 - R_F)}{2}\left\{\frac{(1 - e^{-ST})(1 - R_B e^{-ST})}{(1 - R_F R_B e^{-2ST})}\right\}$$

Consequently, an expression for the transform of the stress wave generated at the front face is given by,

$$F_F(S) = -hQ(S)\frac{Z_1}{(Z_C + Z_1)}K_F(S) \qquad \text{——————} \quad 2$$

The force generated at the transducer rear face (x = L) can be obtained in a similar manner. By substituting for x in equation 1, the following expression is readily obtained.

$$F_B(S) = \frac{-hQ(S)}{2\Delta}\left\{2\Delta - (J_1)\begin{bmatrix}T_F\\T_B\end{bmatrix}e^{-ST} + (J_2)\begin{bmatrix}T_F\\T_B\end{bmatrix}e^{ST}\right\}$$

$$= \frac{-hQ(S)}{2\Delta}\left\{2\Delta - T_F e^{-ST} + T_B R_F e^{-2ST} + T_F R_B e^{-ST} - T_B\right\}$$

$$= \frac{-hQ(S)(1 - R_B)}{2}\left\{\frac{(1 - e^{-ST})(1 - R_F e^{-ST})}{1 - R_F R_B e^{-2ST}}\right\}$$

The Laplace transform of the stress wave generated at the rear face of the transducer is thus given by,

$$F_B(S) = -hQ(S) \frac{Z_2}{(Z_C + Z_2)} K_B(S) \qquad 3$$

Equations 2 and 3 are Laplace transforms of the waves of force which radiate into the surrounding media when a piezoelectric disc is electrically stimulated by a function of charge whose Laplace transform is Q(S). Each equation is effectively a transfer function relating output force to the charge on the transducer electrodes.

At this stage, it would be extremely useful to consider the physical implications of these two equations, since they are of fundamental importance in the development of the transmitting model.

When a quantity of charge is deposited on the transducer electrodes, stresses are set up at both front and rear faces due to the inverse piezoelectric effect. These stresses cause waves of force to propagate into the surrounding media, as well as into the transducer material. The Laplace transforms of these forces are given by,

Laplace transform of the initial force generated into the load medium $= -hQ(S)\frac{Z_1}{(Z_C + Z_1)}$

Laplace transform of the initial force generated into the backing medium

$$= -hQ(S)\frac{Z_2}{(Z_C + Z_2)}$$

Laplace transform of the initial force generated into the transducer at the front face

$$= \frac{hQ(S)Z_C}{(Z_C + Z_1)} = a_T(S)$$

Laplace transform of the initial force generated into the transducer at the rear face

$$= \frac{hQ(S)Z_C}{(Z_C + Z_2)} = b_T(S)$$

Where hQ(S) corresponds to the Laplace transform of the initial force generated at each face of the transducer due to piezoelectric action.

The previous four expressions are indicated diagramatically in figure 4.2a, where the notation is that of Redwood (37), ie waves travelling into the transducer material are assumed positive. These expressions have a direct analogy with the division of voltage in a series resistive electrical circuit, as shown in figure 4.2b. In the figure, V is the excitation voltage analogous to the initial force, hQ. V_C and V_1 are the voltages across resistances Z_C and Z_1 respectively. Consequently, V_C is analogous to the wave of force directed into the transducer at the front face, and V_1 is analogous

to that force directed away from the transducer.

Since the internal quantities of force, a_T and b_T, reverberate back and forth within the transducer, it is possible to verify equations 2 and 3 in a more fundamental, physically meaningful manner by constructing the lattice diagram of figure 4.3.

From the figure, substituting for a_T and b_T and noting that

$$\frac{Z_C}{Z_C + Z_1} = \frac{1 + R_F}{2}$$

$$\frac{Z_C}{Z_C + Z_2} = \frac{1 + R_B}{2}$$

it is possible to obtain the following S-domain series for stress waves leaving the transducer front face.

$$F_1(S) = hQ(S)\left\{\frac{-(1 - R_F)}{2} + (1 - R_F)\,\frac{(1 + R_B)}{2}\,e^{-ST}\right.$$

$$- R_B(1 - R_F)\,\frac{(1 + R_F)}{2}\,e^{-2ST}$$

$$\left. + R_F R_B(1 - R_F)\,\frac{(1 + R_B)}{2}\,e^{-3ST} \;.....\right\}$$

$$= -hQ(S)\ \frac{(1 - R_F)}{2}\ \Big\{1 - (1 + R_B)e^{-ST} + R_B(1 + R_F)e^{-2ST}$$

$$- R_F R_B(1 + R_B)e^{-3ST} + R_F R_B^2(1 + R_F)e^{-4ST} \ .....\Big\}$$

$$= -hQ(S)\ \frac{(1 - R_F)}{2}\ \Big\{1 + R_B(1 + R_F)e^{-2ST} \sum_{n=0}^{\infty} (R_F R_B)^n\ e^{-2nST}$$

$$- (1 + R_B)e^{-ST} \sum_{n=0}^{\infty} (R_F R_B)^n\ e^{-2nST}\Big\}$$

Taking the sum to infinity for a geometric progression yields the following transform of the stress wave leaving the front face:

$$F_1(S) = -hQ(S)\ \frac{(1 - R_F)}{2}\ \Big\{1 + \frac{R_B(1 + R_F)e^{-2ST} - (1 + R_B)e^{-ST}}{1 - R_F R_B e^{-2ST}}\Big\}$$

$$= -hQ(S)\ \frac{(1 - R_F)}{2}\ \Big\{\frac{(1 - e^{-ST})(1 - R_B e^{-ST})}{1 - R_F R_B e^{-2ST}}\Big\}$$

Consequently, a transformed expression for the waves of force generated into the load medium is given by,

$$F_1(S) = -hQ(S)\ \frac{Z_1}{(Z_C + Z_1)}\ K_F(S)$$

This is identical to the expression given by equation 2, ie the lattice diagram has been used to corroborate the force/

charge relationship. In an analogous manner, the series corresponding to the stress waves leaving the rear face can be obtained. From figure 4.3 we have,

$$F_2(S) = -hQ(S) \frac{Z_2}{(Z_C + Z_2)} \left\{1 - (1 + R_F)e^{-ST} + R_F(1 + R_B)e^{-2ST} - R_F R_B(1 + R_F)e^{-3ST} \ldots . \right\}$$

$$= -hQ(S) \frac{Z_2}{Z_C + Z_2} \left\{\frac{(1 - e^{-ST})(1 - R_F e^{-ST})}{1 - R_F R_B e^{-2ST}}\right\}$$

therefore $$F_2(S) = -hQ(S) \frac{Z_2}{Z_C + Z_2} K_B(S)$$

This is identical in form to equation 3. Consequently, the inverse Laplace transforms of equations 2 and 3 each represent a time series of waves of force leaving the transducer front and rear faces respectively. The time series is produced by multiple reflections occurring inside the transducer as the opposite faces displace under the stimulus of applied charge.

Furthermore, in the previous chapter it was demonstrated that $K_F(t)$ and $K_B(t)$ were time series describing the difference in displacement produced at opposite faces of the crystal under conditions of external mechanical stress. That

is, with a mechanical wave incident on the front and rear face respectively. However, in the present context, $K_F(t)$ and $K_B(t)$ describe the stress behaviour at each face of the transducer when the surfaces are simultaneously displaced due to the inverse piezoelectric effect, ie by the application of a function of charge to the electrodes. It should thus be noted that, although the expressions in each case are mathematically identical, they represent physically different situations.

One additional relationship is required before a complete model of the piezoelectric transmitter may be developed. In the following section, a correspondence is presented between the surface charge Laplace transform Q(S) and the transformed voltage across the transducer electrodes, V(S).

4.3 Relationship Between Voltage and Charge for the Transmitting Mode

From equation 7, chapter III, it may be written,

$$V(S) = -h\{\xi_{x=L} - \xi_{x=0}\}(S) + \frac{Q(S)}{C_o} \qquad \text{——————} 4$$

From equation 10, chapter III,

$$-h\{\xi_{x=L} - \xi_{x=0}\}(S) = -h\{A(e^{-ST} - 1) + B(e^{ST} - 1)\}$$

Substituting for A and B yields,

$$-h\{\xi_{x=L} - \xi_{x=0}\}(S) = \frac{-h}{\Delta}\{[J_1](e^{-ST} - 1) + [J_2](e^{ST} - 1)\}[L']$$

$$= \frac{h^2Q(S)}{2SZ_C\Delta}\left\{[J_1]\begin{bmatrix}T_F\\T_B\end{bmatrix}(e^{-ST} - 1) + [J_2]\begin{bmatrix}T_F\\T_B\end{bmatrix}(e^{ST} - 1)\right\}$$

$$= \frac{h^2Q(S)}{2SZ_C\Delta}\{T_F(e^{-ST} - 1 + R_Be^{-ST} - R_Be^{-2ST})$$

$$+ T_B(e^{-ST} - 1 + R_Fe^{-ST} - R_Be^{-2ST})\}$$

$$= \frac{-h^2Q(S)}{S}\left\{\frac{(1 - e^{-ST})(1 - R_Be^{-ST})}{(1 - R_FR_Be^{-2ST})}\frac{1}{(Z_C + Z_1)}\right.$$

$$\left. + \frac{(1 - e^{-ST})(1 - R_Fe^{-ST})}{(1 - R_FR_Be^{-2ST})}\frac{1}{(Z_C + Z_2)}\right\}$$

$$= \frac{-h^2Q(S)}{S}\left\{\frac{K_F(S)}{(Z_C + Z_1)} + \frac{K_B(S)}{(Z_C + Z_2)}\right\}$$

Substituting directly into equation 4 results in the following expression for the transform of voltage across the transducer

$$V(S) = \frac{-h^2Q(S)}{S}\left\{\frac{K_F(S)}{(Z_C + Z_1)} + \frac{K_B(S)}{(Z_C + Z_2)}\right\} + \frac{Q(S)}{C_o}$$

or,

$$V(S) = \frac{Q(S)}{C_o}\left\{1 - \frac{h^2 C_o}{SZ_C}\left[K_F(S)\,\frac{T_F}{2} + K_B(S)\,\frac{T_B}{2}\right]\right\} \qquad 5$$

Equation 5 describes the relationship (in the S-domain) between the voltage measured across the transducer terminals and the charge on the electrodes. It is worth noting that the electrical impedance of the transducer is readily obtained from this expression. Defining the electrical operational impedance as:

$$Z_T(S) = \frac{V(S)}{I(S)} = \frac{V(S)}{SQ(S)},$$

then

$$Z_T(S) = \frac{1}{SC_o}\left\{1 - \frac{h^2 C_o}{SZ_C}\left[K_F(S)\,\frac{T_F}{2} + K_B(S)\,\frac{T_B}{2}\right]\right\} \qquad 6$$

This equation is extensively analysed in the next chapter concerning device impedance characteristics.

Using equations 2, 3 and 5, it is now possible to obtain a transfer function which relates the output wave of force to the input excitation voltage.

4.4 GENERAL TRANSFER FUNCTION OF THE PIEZOELECTRIC TRANSMITTER

The remainder of this chapter outlines the development of a systems feedback model describing the piezoelectric trans-

mitter. The model, which can be readily adapted to suit any type of electrical configuration, not only outlines piezoelectric operation, but also affords a clear insight into the interaction between electrical and mechanical parts of the system.

In the present section a transfer function relating excitation voltage to output force is developed. The transducer is assumed to have an arbitrary electrical load, Z_E, connected across its terminals and it is driven from a non-ideal voltage source, having an output impedance Z_o. The overall situation is outlined in figure 4.4, where $I_T(S)$ is defined as the Laplace transform of current through the transducer.

From the figure, a transfer function relating the transformed input voltage to the transform of current through the transducer may be obtained from

$$\frac{I_T(S)}{e(S)} = \frac{Z_E}{Z_T(Z_o + Z_E) + Z_o Z_E}$$

where Z_E, Z_o and Z_T are generally functions of S

$$= \frac{\dfrac{Z_E}{(Z_o + Z_E)}}{Z_T + \dfrac{Z_o Z_E}{Z_o + Z_E}}$$

$$= \frac{a(S)}{Z_T(S) + b(S)}$$

therefore $$I_T(S) = \frac{a(S)e(S)}{Z_T(S) + b(S)}$$

therefore $$Q(S) = \frac{a(S)e(S)}{S\{Z_T(S) + b(S)\}} \qquad \text{7}$$

Expressions for the transformed force functions at the transducer front and rear faces are given by equations 2 and 3.

$$F_F(S) = -hQ(S) \frac{A_F}{2} K_F(S)$$

$$F_B(S) = -hQ(S) \frac{A_B}{2} K_B(S)$$

where $$\frac{A_F}{2} = \frac{Z_1}{Z_C + Z_1}, \quad \frac{A_B}{2} = \frac{Z_2}{Z_C + Z_2}$$

Substituting from equation 7 for $F_F(S)$ yields the following transfer function relating the transform of force generated at the front face to the transform of the input voltage.

$$\frac{F_F(S)}{e(S)} = \frac{-ha(S)}{S\{Z_T(S) + b(S)\}} \left[\frac{A_F}{2}\right] K_F(S)$$

Substituting from equation 6 for Z_T yields,

$$\frac{F_F(S)}{e(S)} = \frac{-ha(S)\left[\frac{A_F}{2}\right]K_F(S)}{\left[\frac{1 + b(S)C_oS}{C_o}\right] - \frac{h^2}{SZ_C}\left[K_F(S)\,\frac{T_F}{2} + K_B(S)\,\frac{T_B}{2}\right]}$$

letting $$Y(S) = \frac{C_o}{1 + b(S)C_oS}$$

yields,

$$\frac{F_F(S)}{e(S)} = \frac{-ha(S)\left[\frac{A_F}{2}\right]Y(S)K_F(S)}{1 - \frac{h^2}{SZ_C}Y(S)\left[K_F(S)\,\frac{T_F}{2} + K_B(S)\,\frac{T_B}{2}\right]} \qquad 8$$

This equation is a general transfer function relating the stress wave generated into the load medium to the input voltage. In a similar manner, it can readily be shown that the stress wave generated into the backing medium is related to the input voltage by the following equation

$$\frac{F_B(S)}{e(S)} = \frac{-ha(S)\left[\frac{A_B}{2}\right]Y(S)K_B(S)}{1 - \frac{h^2}{SZ_C}Y(S)\left[K_F(S)\,\frac{T_F}{2} + K_B(S)\,\frac{T_B}{2}\right]} \qquad 9$$

Equations 8 and 9 are in the form of feedback transfer functions and as a result, the overall block diagram of figure 4.5 may be constructed. The equivalence between the

diagram and, for example, equation 8, may be readily verified as follows. From figure 4.5 we have:

$$E(S) = e(S)a(S) + P(S) + Q(S)$$

$$P(S) = E(S)Y(S)hK_F(S)\ \frac{T_F}{2}\ \frac{h}{SZ_C}$$

$$Q(S) = E(S)Y(S)hK_B(S)\ \frac{T_B}{2}\ \frac{h}{SZ_C}$$

$$-F_F(S) = E(S)Y(S)hK_F(S)\ \frac{A_F}{2}$$

Substituting the last three equations into the first, and removing E(S) gives

$$-F_F(S) = \frac{a(S)e(S)hK_F(S)\ \frac{A_F}{2}}{1 - \frac{h^2}{SZ_C}\,Y(S)\left[K_F(S)\ \frac{T_F}{2} + K_B(S)\ \frac{T_B}{2}\right]}$$

This is equivalent to equation 8, hence verifying the validity of the block diagram. As in the case of the piezoelectric receiver, it is now required to examine in detail each component of the block diagram in order to obtain a rigorous physical interpretation of the feedback model.

4.5 PHYSICAL SIGNIFICANCE OF THE POSITIVE FEEDBACK TRANSMISSION MODEL

Referring to figure 4.5, it is possible to move the block Y(S) from the forward loop and place it in the input and feedback paths. This is analogous to the operation carried out in the case of the piezoelectric receiver, where the block T_F was repositioned in an identical manner.

Consider firstly the input path, which is now represented by,

$$\text{Input path} = a(S)Y(S)e(S)$$

$$= \frac{a(S)C_o}{1 + b(S)SC_o}\, e(S)$$

$$= \frac{1}{S}\left(\frac{a(S)SC_o}{1 + b(S)SC_o}\right) e(S)$$

Substituting for a and b gives,

$$\frac{1}{S}\left(\frac{\dfrac{Z_E SC_o}{Z_o + Z_E}}{1 + \dfrac{Z_o Z_E}{Z_o + Z_E} SC_o}\right) e(S)$$

where Z_E and Z_o are in general functions of S

$$= \frac{1}{S}\left[\frac{Z_E SC_o}{Z_o + Z_E + Z_o Z_E SC_o}\right] e(S) \qquad \text{10}$$

Now consider the electrical circuit shown in figure 4.6. The transform of current through the capacitance C_o, is given by:

$$I(S) = \frac{Z_E}{\frac{(Z_o + Z_E)}{SC_o} + Z_o Z_E}\, e(S)$$

This is almost identical to equation 10, except for the factor 1/S. However, it is known that the transformed current I(S) through the capacitor is related to the charge on the capacitor electrodes by the following expression,

$$I(S) = SQ_C(S)$$

where $Q_C(S)$ is the transform of charge on the capacitor plates. Equation 10, which represents the input path of the block diagram is hence a transfer function relating the charge on the plates of a capacitance C_o, to the driving voltage, e. Since C_o is the bulk, static capacitance of the transducer, the equivalent circuit shown in figure 4.6 does in fact, represent the electrical input of the model as viewed from the driving source. However, it is important to note at this stage that the input impedance of the transducer is not simply the impedance of the static capacitance

C_o. It will be demonstrated in a later section that the input impedance characteristics are greatly modified by the resonant nature of the transducer, in conjunction with the effects of secondary piezoelectric action.

Now consider the significance of the block Y(S), which has been repositioned in each feedback path.

$$Y(S) = \frac{1}{S}\left[\frac{SC_o}{1 + b(S)SC_o}\right]$$

$$= \frac{1}{S}\left[\frac{SC_o}{1 + \dfrac{Z_E Z_o SC_o}{(Z_E + Z_o)}}\right] \qquad \text{11}$$

where Z_E and Z_o are generally function of S.

The term inside the square brackets is readily shown to be the admittance of the electrical network outlined in figure 4.7.

In the figure, V_F refers to the feedback voltage and I_F refers to the feedback current. However, in order to physically justify these two terms, some of the remaining parameters of figure 4.5 must first be explained.

Considering initially the forward loop; the input to the block, h, consists of the charge transform $Q_C(S)$ as explained previously. The parameter, h, is simply the piezoelectric

conversion factor relating charge to stress and hence the input to the blocks $K_F(S)$ and $K_B(S)$ is one of force. This is to be expected, since, as explained in Section 4.2ii, $K_F(S)$ represents a transformed time series of waves of force generated at the transducer front face. A fraction of this force is transmitted into the load medium, that fraction being given by $A_F/2$, where

$$\frac{A_F}{2} = \frac{Z_1}{Z_C + Z_1}$$

Also, a fraction of the force generated at the front face is transmitted back into the transducer, this fraction being given by $T_F/2$, where

$$\frac{T_F}{2} = \frac{Z_C}{Z_C + Z_1}$$

This force, which represents the force in the front face feedback loop, is then transformed into a function of particle displacement by the block $1/SZ_C$. The function of particle displacement is in turn converted to one of voltage by the piezoelectric conversion factor, h, in the feedback loop. This corresponds to the feedback voltage V_F which in turn gives rise to the feedback current I_F as indicated in figure 4.7. The current I_F is related to a feedback function of charge, Q_F, where in Laplace notation,

$$Q_F(S) = \frac{I_F(S)}{S}$$

Consequently, the relationship between $Q_F(S)$ and $V_F(S)$ is given by the following equation,

$$Q_F(S) = Y(S)\ V_F(S)$$

$$= \frac{1}{S}\ Y_F(S)\ V_F(S)$$

where Y_F is the admittance of the equivalent electrical network shown in figure 4.7.

It is now possible to construct a systems block diagram which accurately describes the behaviour of a piezoelectric transducer when operating in the transmitting mode. This is shown in figure 4.8 which depicts a completely general model of a lossless, piezoelectric transmitter. As in the case of the piezoelectric receiver, the device is shown as a three port network utilising the concept of feedback to model secondary piezoelectric effects.

The individual elements of figure 4.8 may be summarised as follows:

e — Input excitation voltage

Y_I — Operational admittance of the equivalent electrical circuit at the transducer input

h	Conversion factor from charge to force or from particle displacement to voltage
K_F	Time series describing front face stresses, the front face reverberation factor
K_B	Time series describing rear face stresses, the rear face reverberation factor
$\frac{A_F}{2}$	Fraction of front face stress transmitted into the load medium
$\frac{A_B}{2}$	Fraction of rear face stress transmitted into the backing medium
$\frac{T_F}{2}$	Fraction of front face stress transmitted into the transducer
$\frac{T_B}{2}$	Fraction of rear face stress transmitted into the transducer
$\frac{1}{SZ_C}$	Conversion factor from stress to particle displacement
V_F	Feedback voltage in front face feedback loop.
V_B	Feedback voltage in rear face feedback loop
Y_F	Operational electrical admittance in each feedback loop

Q_C Charge generated on the transducer electrodes by the driving voltage

Q_F Charge generated due to the front face feedback loop

Q_B Charge generated due to the rear face feedback loop.

It may be clearly seen from figure 4.8 that the amount of feedback is dependent on the following four principal factors.

1 As in the case of the receiving model, the amount of feedback is again proportional to the square of the electromechanical coupling coefficient. For example, both feedback loops contain the term h/Z_C, which may be written as follows,

$$\frac{h}{Z_C} = \frac{h^2 C_o}{h C_o Z_C}$$

$$= \frac{K^2}{h C_o T}$$

Consequently, for transducer materials with low values of K, such as quartz (ie where K is less than 0.2), the percentage feedback is relatively low. However, for some ceramic materials, K is in the region of 0.5-0.7 and in such instances a significant feedback contribution may

arise. Similar observations have occurred in other transducer analyses, particularly those of Filipczynski (11) and Redwood (37). As explained in a previous chapter both of these utilise the concept of negative capacitance in order to explain what is effectively a feedback phenomenon. The arguments as to whether or not this 'component' could safely be neglected centred round the value of K. On an intuitive basis, the effects of feedback can be modelled by postulating a negative capacitance, since such a concept would lead to exponentially increasing functions in the time domain. Similar behaviour is to be expected in a feedback system.

2 The amount of feedback is dependent on the load and backing materials, since the stresses transmitted into the transducer depend on the factors T_F and T_B. Consequently the largest amount of feedback occurs when the transducer is air loaded and air backed and the smallest amount occurs when the device is ideally matched at both faces. As a result, values of K are usually measured with the transducer in the mechanically free state. The transducer transmitting characteristics are thus highly dependent on the external mechanical boundary conditions.

3 The amount of feedback is dependent on the electrical characteristics of the driving source and also on the characteristics of any external electrical load. Zero

feedback occurs for both Z_E and Z_O equal to infinity, rising to a maximum when both these components are themselves zero. Such effects can be of great importance when assessing transducer operation and a further more complete investigation of these is performed in later chapters.

4 The quantity of charge feedback to the transducer electrodes decreases with frequency. At high frequencies the device assumes the characteristics of the forward paths in figure 4.8, with the transducer behaving electrically like a simple capacitor. The frequency response characteristics of both transmitter and receiver are discussed in a later chapter.

Before leaving the present section, some additional points are worth noting.

Firstly, as in the case of the piezoelectric receiver, the feedback alternates between positive and negative as the functions K_F and K_B undergo phase reversal. Consequently, the total charge on the transducer plates alternately increases and decreases with each mechanical reflection. As a result, the current through the device also fluctuates, giving rise to a complex electrical impedance characteristic. The relationship between feedback and the transducer impedance characteristic is presented in the next chapter.

Secondly, for a practical piezoelectric transmitter, the feedback loops must invariably be taken into consideration. Secondary piezoelectric effects are in fact absent if both Z_E and Z_o are infinite. However, such conditions result in zero output from the device and are hence impractical. Similarly a low value of K, while reducing the effects of feedback, results in an inefficient transducer. This situation does not arise in the case of the piezoelectric receiver where secondary effects disappear completely when the transducer has no external electrical load.

Thirdly, as in the case of the piezoelectric receiver, an inversion factor, -1, appears in the block diagram. This corresponds to the statement made in Appendix A, whereby the resultant stress has a direction opposite to that of the incident electrical field and vice versa. In the transmitting mode, a positive stress generated at the transducer front face corresponds to a negative excitation voltage.

4.6 CONCLUDING REMARKS

A block diagram model of the piezoelectric transducer acting as a generator of ultrasound has been developed. The model is exact within the constraints of the initial simplifying assumptions. It is wideband and valid under arbitrary conditions of electrical and mechanical loading. The physical significance of each element in the block

diagram has been carefully developed in order to obtain a clear and distinct relationship between electrical and mechanical quantities. In addition, the factors which control secondary piezoelectric action are readily defined, along with the importance of this effect on the overall transfer function. It is considered that no other transducer model illustrates these concepts with the same degree of clarity, either in transmission or reception. For example, it has been demonstrated that no feedback effect occurs for the receiving transducer under conditions of electrical open circuit. This is not the case with the efficient transmitter, since the generator output impedance nearly always results in a degree of secondary piezoelectric action.

In subsequent chapters, the influence of the various elements contained in both transmitting and receiving block diagrams is investigated in detail. With the aid of computer simulation graphs, the major factors affecting transducer performance are demonstrated. Where possible, the simulations are corroborated by experimental results.

CHAPTER V

FEEDBACK REPRESENTATION OF TRANSDUCER OPERATIONAL IMPEDANCE

5.1 INTRODUCTION

This chapter presents an analysis of transducer electrical impedance under a wide variety of mechanical loading conditions. A systems model is used to describe this impedance, which is representative of the electrical input impedance in the transmitting mode and the electrical output impedance for the receiving mode. The analysis is valid over all frequencies within the constraints of the initial simplifying assumptions outlined in chapter 3, section 3.1.

For a fixed voltage input, the total current flowing through the transducer is considered as the vector sum of two current quantities. Firstly, there is an input current, arising directly from the applied voltage source and secondly, there is a feedback current which is generated by secondary piezoelectric action. Although analyses of transducer electrical impedance are widespread and hence well defined, it is believed that by treating the problem in this manner, an extremely valuable insight into the nature of the electrical characteristics is provided. By careful analysis of the individual blocks within the feedback model, complex variations in the impedance characteristics are readily explained and the physical processes which contribute to such deviations are clearly isolated.

Consequently, analysis of the individual blocks within the feedback system are carried out in considerable

detail, with particular emphasis on those factors which determine the total amount of current feedback. Detailed investigation of such parameters as K_F and K_B are also justified due to their involvement in subsequent chapters, where transmitter and receiver characteristics are similarly analysed.

A number of computer simulations are presented and where possible, the description of relevant characteristics is performed by the systems feedback approach. A Tektronix 4051 graphics terminal was used in conjunction with appropriate software in order to generate the simulation diagrams. The program provides simulated magnitude and phase characteristics for all, or sections of the model over a wide range of frequency and mechanical loading conditions. A complete BASIC listing of the program is provided in Appendix (E). Unless otherwise stated, nominal data used in the simulation is outlined in table 5.1.

5.2 TRANSDUCER OPERATIONAL IMPEDANCE

An expression for the electrical impedance of the piezoelectric transducer was derived in the previous chapter. That is, a transfer function relating transducer voltage to current and described by the following equation.

$$\frac{V_T(s)}{I_T(s)} = \frac{1}{SC_o}\left[1 - \frac{K^2}{ST}\left(K_F(s)\,\frac{\mathcal{Z}_c}{\mathcal{Z}_c+\mathcal{Z}_1} + K_B(s)\,\frac{\mathcal{Z}_c}{\mathcal{Z}_c+\mathcal{Z}_2}\right)\right]$$

$$= \mathcal{Z}_T(s) \qquad (1)$$

where,

V_T is the voltage across the transducer element

I_T is the current through the transducer element

Z_T is the transducer electrical impedance.

The characteristics of this expression may be conveniently evaluated by adopting a systems approach. A relationship between voltage V_T and current I_T is outlined in the feedback block diagram of figure 5.1. Although the transfer function of this system describes electrical admittance, the equivalence with equation 1 may readily be observed. However, in order to appreciate the physical implications of the operational transfer function, it is more convenient to substitute for K^2/T and re-arrange the blocks to obtain the diagram outlined in figure 5.2.

On application of a voltage V_T, to the transducer electrodes, a current I flows through the bulk capacitance (C_o), of the device. As described in the previous chapter, two forces, F_F and F_B, are produced at the front and rear faces respectively. A fraction of each force is transmitted into the load and backing media and the remainder into the transducer. By means of secondary piezoelectric action, these forces travelling inside the device produce feedback currents I_F and I_B at the input summing point. Since the feedback is shown as being positive, the resultant current through the transducer is the sum of the input current through the bulk capacitance and the feedback currents produced

by front and rear face displacements. This process is outlined in figure 5.2 where the various relationships between force, particle displacement and current are clearly defined.

Investigation of figures 5.1 and 5.2 reveals that the electrical impedance of the lossless transducer is a complex function whose behaviour is dependent on many parameters. For example, it is apparent that no feedback effects may occur under the following operating conditions:

i) When the electromechanical coupling factor is equal to zero. Although an absolute value of zero for k is impossible in practice, in some instances the value is so low that secondary effects may be neglected.

ii) When the functions K_F and K_B are equal to zero. This condition also implies that no force is generated, either into the transducer or surrounding media. Since K_F and K_B are reverberation factors analogous to the behaviour of a lossless transmission line, it is to be expected that destructive interference may occur at particular frequencies, resulting in zero mechanical transmission.

iii) When the operating frequency is high. That is, effects of secondary piezoelectric action diminish with increasing frequency. This is to

be expected on the basis that particle displacement is inversely proportional to the frequency of an applied force.

iv) When the functions T_F and T_B are equal to zero. This implies that both front and rear faces are totally rigid, resulting in no mechanical displacement. Such a situation is unlikely to be encountered in practice.

It may also be observed, that for no secondary piezoelectric action, the electrical behaviour of a transducer element corresponds exactly to that of a pure capacitance. Furthermore, while conditions of zero feedback are generally impractical, these factors all combine to determine the total amount of current feedback, and hence the electrical impedance characteristics.

The nature of the transducer impedance under no loss conditions has been subject to many analyses and as a result, the overall behaviour is well defined. However, in this context, it is considered that a systems feedback approach is by far the best technique for explanation of this complex phenomenon. Consequently, the following section involves a detailed explanation of the electrical impedance characteristics, with particular emphasis on the roles played by individual blocks within the systems model.

5.3 ANALYSIS OF ELECTRICAL IMPEDANCE

In order to evaluate the effects of secondary piezoelectric action on the impedance characteristics, consider firstly the specific case of a piezoelectric resonator. That is, device operation in the mechanically free state. Such a situation is approximated by an air backed, air loaded transducer and is of importance in the determination of some piezoelectric parameters.

5.3.1 Impedance of the Lossless Piezoelectric Resonator

For a mechanically free transducer, R_F and R_B are equal to unity. Consequently, the expression for the transform of electrical input impedance may be written as follows.

$$\mathcal{Z}_{TR}(s) = \frac{1}{SC_o}\left[1 - \frac{K^2}{ST}\left(K_{FR}(s) + K_{BR}(s)\right)\right]$$

where,

$$K_{FR}(s) = K_{BR}(s) = \frac{1 - e^{-ST}}{1 + e^{-ST}}$$

The transformed resonator electrical impedance thus becomes,

$$\mathcal{Z}_{TR}(s) = \frac{1}{SC_o}\left[1 - \frac{2K^2}{ST}\left(\frac{1 - e^{-ST}}{1 + e^{-ST}}\right)\right] \qquad (2)$$

$$\therefore \quad \mathcal{Z}_{TR}(jw) = \frac{1}{jwC_o}\left[1 - \frac{2K^2}{jwT}\left(\frac{1 - e^{-jwT}}{1 + e^{-jwT}}\right)\right] \qquad (3)$$

$$= \frac{1}{jwC_o}\left[\, 1 - K^2 \tan \frac{(wT/2)}{(wT/2)} \,\right]$$

Plotting impedance amplitude and phase as functions of frequency yields the characteristics outlined in figures 5.3a and 5.3b. The nominal transducer parameters used in obtaining these curves are shown in table 5.1. A close study of the figures reveals the following three main aspects.

i) The phase angle of the impedance function is always equal to $\pm \pi/2$. That is, the impedance of a lossless, piezoelectric resonator always constitutes a pure reactance.

ii) The amplitude function contains impedance maxima which occur at odd multiples of a particular frequency. This frequency, denoted by f_2, is defined as the anit-resonant frequency, or the mechanical resonant frequency of the transducer.

iii) The amplitude function also contains impedance minima, which are not related by simple multiples of a fundamental frequency. For the lossless resonator, these correspond to points of zero impedance, with the first minimum occurring at the transducer resonant frequency, denoted by f_1. This is sometimes referred to as the electrical resonant frequency and is invariably lower than the frequency of mechanical resonance.

It should be noted that this theory applies only to an ideal, lossless resonator which behaves as a pure reactance and the characteristic frequencies f_1 and f_2 are well defined. In practice, mechanical and electrical dissipation present in real materials obscures the definition of these frequencies. For example, in a lossy resonator there are generally three frequencies of interest near the impedance maximum and three frequencies near the impedance minimum. These correspond to the frequency of max/min absolute impedance, the frequency of max/min resistance and the frequency of max/min reactance. They are extensively used in the determination of transducer parameters such as coupling coefficient and mechanical quality factor (16). However, for the purpose of the present analysis it is sufficient to consider a loss-free transducer.

In order to appreciate the nature of the impedance characteristics, consider the admittance block diagram of figure 5.4. The resonator impedance is thus given by the following Laplace equation.

$$Z_R(s) = (1 - A_T(s))/sC_o \qquad (4)$$

where

$$A_T(s) = \frac{2K^2}{ST} \frac{(1 - e^{-ST})}{(1 + e^{-ST})}$$

$$T = \frac{1}{2f_2}$$

f_2 is the frequency of mechanical resonance.

And,

$$A_T(jw) = \frac{2K^2}{jwT} \frac{(1 - e^{-jwT})}{(1 + e^{-jwT})}$$

$$\therefore \quad A_T(w) = \frac{2K^2}{wT} \tan (wT/2)$$

A_T represents the total amount of current feedback and is henceforth defined as the feedback factor. Figures 5.5a and 5.5b depict the amplitude and phase characteristics of A_T, as functions of frequency. In order to understand their significance, consider the behaviour of the resonator reverberation factor, which is the same for each face and is given by,

$$K_R(s) = \frac{(1 - e^{-ST})}{(1 + e^{-ST})}$$

The amplitude and phase characteristics of this function are shown in figures 5.6a and 5.6b. The value of K_R is infinite when,

$$e^{-ST} = -1$$

or,

$$wT = m\pi \qquad m = 1,3,5 \ldots$$

For m equal to unity,

$$f = \frac{1}{2T}$$

This corresponds to the frequency of mechanical resonance,

and at odd multiples of this frequency, the reverberation factor is infinite.

The value of K_R is equal to zero when,

$$e^{-ST} = 1 \qquad \text{or,}$$

$$wT = (m-1)\pi \qquad m = 1,3,5 \ldots$$

For m = 3,

$$f = \frac{1}{T}$$

This corresponds to twice the frequency of mechanical resonance. Consequently, the reverberation factor is equal to zero at even multiples of the mechanical resonance. The amplitude behaviour of the lossless resonator reverberation factor may readily be observed from figure 5.6a.

Phase characteristics of the reverberation factor are outlined in figure 5.6b, from which it is apparent that the phase is always $\pm \pi/2$ radians. This fact is readily apparent from,

$$\frac{(1 - e^{-jwT})}{(1 + e^{-jwT})} = K_R = j \tan (wT/2)$$

It is now possible to consider the behaviour of the feedback function, A_T. However, before doing so, it should be noted that the behaviour of K_R is somewhat analogous to that associated with a lossless open circuit transmission line. That is, conditions of maximum constructive interference (maximum amplitude)

and conditions of maximum destructive interference (zero amplitude) occur at odd and even multiples of the mechanical resonance respectively.

From figure 5.5a, it may be observed that the magnitude of the feedback function is a maximum at odd multiples of the mechanical resonance, while for even multiples the magnitude is zero. That is, at frequencies of $2f_2$, $4f_2$ etc., there is no feedback, while at f_2, $3f_2$ ..., there occurs maximum current feedback. This is to be expected from the behaviour of the reverberation factor. However, due to the 1/S multiplier in the feedback function, the magnitude at A_T has a finite value at low frequencies, and also demonstrates a general decrease with increasing frequency, although this may not be readily apparent at positions of impedance maxima in figure 5.5a.

Figure 5.5b indicates that the phase of the feedback factor changes by π radians at regular multiples of the mechanical resonant frequency. Again this is to be expected, since the 1/S multiplier corresponds to a constant phase shift of $-\pi/2$ radians. When added to the phase shift of K_R in figure 5.6b, the result shown in figure 5.5b is obtained. It is important to note that in terms of the feedback model, a phase shift of π radians in the feedback factor corresponds to a reversal in the type of feedback from positive to negative and vice versa.

From equation 4, the impedance of the transducer is

equal to zero when A_T is real and equal to unity. (Note that A_T is always real for the lossless resonator). That is, when:

$$\frac{wT}{2K^2} = \tan(wT/2) \qquad \text{or,}$$

$$\frac{X}{K^2} = \tan(X) \qquad \text{---------- (5)}$$

where $X = \pi fT$.

This equation has been used by Onoe et al (33) in order to determine the fundamental and overtone electrical resonant frequencies for different values of coupling coefficient. From this equation it is readily observed that the fundamental and overtone frequencies of electrical resonance are not related as simple integer multiples as in the case of mechanical resonance. This fact is verified by figures 5.3a,b and 5.5a,b; where it may be observed that the frequencies of electrical and mechanical resonance come closer together with increasing frequency. The reason for this will be shortly evident, in that electrical resonance is a feedback effect, which of course decreases with frequency.

It is now possible to study the resonator impedance characteristics with specific reference to the feedback model. In order to simplify the process, consider two separate frequency ranges, separated by the frequency of electrical resonance, f_1.

I. Impedance Characteristics Below Resonance

i.e. $0 \leqslant f < f_1$

With reference to figure 5.5a and 5.5b, the amplitude of the feedback function in this frequency range is less than unity and the corresponding phase shift is zero. Under these conditions, the feedback is positive in nature and for a fixed input voltage, total current through the transducer increases. Consequently, the effective electrical impedance is lower than that expected from the reactance of the static capacitance. This effect may readily be observed from figure 5.3a, where the amplitude of the impedance function steadily decreases with frequency, eventually becoming zero at the electrical resonance, f_1. At this particular frequency, the feedback factor is equal to unity. With reference to figure 5.3b, the phase angle of the impedance function within this frequency range remains constant at $-\pi/2$ radians. Consequently, the resonator impedance characteristics over the frequency range $0 \leqslant f < f_1$ are essentially those of a pure capacitance, modified by the effects of positive feedback.

Due to these secondary piezoelectric effects, the effective low frequency capacitance is larger than the static capacitance; which is measured under mechanically clamped conditions, when no feedback is possible. There are thus two capacitances associated with the piezoelectric transducer, which may be defined as

follows.

a. The free capacitance, denoted by C_T. This capacitance is measured for the piezoelectric resonator operating under low frequency conditions, usually in the region of 1 kHz.

b. The static capacitance, denoted by C_O. This is the actual bulk capacitance of the transducer material and is not modified by piezoelectric action. As a result, it is smaller in value than C_T.

At this stage, it is interesting to verify a unique relationship between the electromechanical coupling coefficient K, and the two transducer capacitances. Consider the feedback function, expressed in terms of frequency

$$A_T = \frac{2K^2}{WT} \tan (wT/2)$$

$$= \frac{K^2}{X} \tan (X)$$

$$\therefore \quad A_T = \frac{K^2}{X} \frac{\sin (X)}{\cos (X)} \qquad \text{where } X = \pi fT$$

For X very small,

$$\sin X \to X$$

$$\cos X \to 1$$

$$\therefore \quad A_T = K^2$$

That is, for very low values of frequency, the total

amount of secondary feedback is given by the square of the electromechanical coupling coefficient. The relationship between currents of the summary point in figure 5.4 may now be written as follows.

$$I(s) = K^2 I(s) + V(s)\, sC_o$$

Assuming V is held constant, the transform of I may be written as,

$$I(s) = S\, Q(s)$$

and at low frequencies,

$$Q(s) = C_T V(s)$$

$$\therefore \quad I(s) = S\, C_T V(s)$$

This yields,

$$C_T = K^2 C_T + C_o$$

$$\therefore \quad K^2 = \frac{C_T - C_o}{C_T} \qquad \text{---------- (6)}$$

This well known relationship would appear to present an ideal method of obtaining the value of K from known values of C_T and C_o. However, there are practical difficulties associated with accurate measurement of the transducer capacitances. The dielectric constant corresponding to C_o is ideally measured with both surfaces of the transducer rigidly clamped; which is extremely difficult because of the great stiffness of transducer materials. One method of overcoming this

problem is to measure the capacitance under high frequency conditions. That is, above all elastic resonances and their major harmonics,when inertia effectively blocks out the piezoelectric effect.

However, due to the imperfect nature of all dielectric materials, interfacial polarisation (uneven charge distribution) results in the effective dielectric constant having a certain degree of frequency dependence, which is independent of any piezoelectric action. For example, using quoted figures for PZT 5-A (59), the dielectric constants increase by 2.4% per decade over the frequency range 1 Hz to 1 kHz. For frequencies greater than 1 kHz and less than 20 MHz, the dielectric constants decrease by 2.4% per decade of frequency. Consequently, in order to minimise such errors, C_T and C_o should ideally be measured at the same frequency.

Yet another technique, mentioned by various authors such as Miller (31) and Kasai (17), recommends that the static capacitance be measured at a frequency corresponding to twice the mechanical resonance. At this frequency, the feedback factor is zero, and hence no feedback may occur. Although this method is theoretically sound, it does not consider the presence of other, unwanted modes corrupting the results. As will be evident at a later stage, the conditions under which this method is viable have to be very accurately defined.

II. Impedance Characteristics Above the Resonant Frequency

Once again referring to figure 5.5a, it is evident that the feedback factor increases in magnitude with frequency, eventually becoming greater than unity and reaching a maximum value at the mechanical resonance. For values of A_T greater than unity, the resonator impedance is negative, corresponding to a phase change of π radians. This occurs after the frequency of electrical resonance and may readily be observed from figure 5.3b. As the input voltage is assumed constant, the current phase has changed by π radians, effectively leading to a reversal in the type of feedback, from positive to negative.

Consequently, total current flowing through the transducer decreases, resulting in an effective increase in impedance. This process increases with frequency until the point of mechanical resonance is reached. At this frequency, the phase of the feedback factor undergoes a phase change of $-\pi$ radians, which may be seen from figure 5.5b. (As shown in figure 5.3b, the overall phase of the resonator impedance also changes by $-\pi$ radians). In consequence, the type of feedback once again undergoes reversal, from negative to positive, giving rise to an increase in current through the transducer. The effective impedance of the resonator thus starts to fall, as shown in figure 5.3a.

At a frequency equal to twice the mechanical resonance,

the magnitude of the feedback factor is equal to zero, and at this frequency the transducer behaves electrically as a capacitance of value C_o. By increasing frequency still further, the transducer impedance magnitude continues to fall until the first overtone of electrical resonance is reached, corresponding to the second root of equation 5. However, in this case the separation between electrical and mechanical resonant frequencies is not so great. This is not surprising, since the phenomenon of electrical resonance is a positive feedback effect and the total amount of current feedback tends to decrease with frequency. For example, consider figure 5.5a, where the fundamental electrical resonant frequency occurs at f_1. At this point, the magnitude of the feedback factor is equal to unity. The first overtone of electrical resonance occurs at the frequency denoted by f_{11}, where the magnitude of A_T is again unity. However, since the amount of feedback has been reduced by increasing frequency, f_{11} is relatively higher, and hence closer to its associated mechanical resonance, than f_1. As frequency continues to increase, the difference between electrical and mechanical resonances becomes smaller, until eventually they cannot be distinguished. At this point, no secondary piezoelectric action takes place, and the transducer impedance corresponds to that of the static capacitance, C_o. This reduction in the amount of positive feedback at higher frequencies may also be readily observed from

the resonator phase characteristics of figure 5.3b.

. Additional Points of Interest

As stated previously, the overall behaviour of the transducer impedance function is that of a pure capacitance, modified by the effects of positive feedback. Figure 5.7 shows a comparison between the impedance magnitudes of a pure capacitance equal to the static capacitance, C_o, and the transducer impedance magnitude. As expected, the curves intersect of frequencies corresponding to even multiples of the mechanical resonance. The effects of feedback are clearly demonstrated.

It should also be noted that the electrical impedance is purely capacitance if K is equal to zero. As indicated earlier, the amount of feedback, and hence the relationship between electrical and mechanical resonances, depends on the value of coupling coefficient. Figure 5.8 shows the impedance magnitude characteristics for three different values of K, corresponding to $K^2 = 0.75$, 0.5 and 0.25. Once again it maybe observed that the frequencies of electrical and mechanical resonance approach equality under conditions of minimum feedback. That is, at the lowest value of coupling coefficient.

At this stage it is worth noting an additional point which is given greater emphasis in chapter 7. Electrical resonance corresponds to a condition of maximum current flow through the transducer. Since this condition infers maximum charge on the transducer electrodes, it is reasonable to expect that a maximum stress is generated

at this frequency. This is corroberated by an analysis of the piezoelectric transmitter and explains why in many instances, maximum stress output does not coincide with the frequency of mechanical resonance. Consequently, any factors which affect the position of electrical resonance, must also determine the frequency of maximum stress output from the transducer.

As stated in section 5.2, the amount of feedback also depends upon the front and rear face loading conditions, with maximum current feedback occurring for the mechanically free resonator. This is to be expected, since, for the resonator all mechanical energy is reflected back into the device, resulting in maximum secondary piezoelectric action. Furthermore, it must be emphasised that the present analysis corresponds only to the ideal transducer. Internal dissipation also affects the amount of feedback as well as the mechanical resonance characteristics. Aspects of transducer losses are dealt with in chapters 6 and 9. The next section describes the transducer impedance characteristics when the device is loaded mechanically at each face.

5.3.ii Electrical Impedance of the Mechanically Loaded Transducer

When a transducer is mechanically loaded by materials possessing real acoustic impedances, the impedance characteristics are defined by equation 1. For the general situation, the transfer function cannot be

described by a single feedback loop and hence the complete admittance block diagrams of figures 5.1 and 5.2 must be used. The analysis is correspondingly more complex than in the case of a mechanically free transducer, or resonator.

With reference to figure 5.1, it may be observed that the transfer function consists of two feedback factors, corresponding to the front and rear faces of the transducer. The total amount of feedback, which is the sum of the front and rear face feedback factors, is thus given by the following Laplace equation.

$$A_T(s) = \frac{K^2}{ST} \left[K_F(s) \frac{Z_C}{Z_C+Z_1} + K_B(s) \frac{Z_C}{Z_C+Z_2} \right]$$

Where K_F and K_B are the front and rear face reverberation factors respectively.

In order to appreciate the nature of the loaded transducer characteristics, it is necessary first of all to study the behaviour of this function under different conditions of mechanical load. Three separate configurations are considered, corresponding to the following physical situations.

. The transducer is equally loaded at both faces by water. Since the acoustic impedance of water is 1.4 kg/m² s, this situation corresponds to light mechanical loading, or light damping.

. The transducer is assumed to be loaded at the rear face by a material having an acoustic impedance

equal to one half of the transducer acoustic impedance. This condition is henceforth referred to as, 'fifty percent matched backing'. The transducer is loaded at the front face by crown glass. Since the acoustic impedance of crown glass is 14.1 kg/m²-s, this solution corresponds to medium mechanical loading, or medium damping.

. The transducer is assumed to be loaded at the rear face by a material whose acoustic impedance is equal to that of the transducer. That is, a condition known as 'matched backing'. The device is loaded at the front face by crown glass. This situation corresponds to heavy mechanical loading, or heavy damping.

Consider firstly the frequency response characteristics of the reverberation factors K_F and K_B and K_B, as these yield considerable insight into the behaviour of the overall feedback factor, and hence impedance. As a result of their symmetry, it is sufficient to analyse only one, in this case K_F.

$$K_F(jw) = \frac{(1 - e^{-jwT})(1 - R_B\, e^{-jwT})}{(1 - R_F\, R_B\, e^{-j2wT})}$$

As in the case of the mechanically free transducer, this function is equal to zero when,

$$wT = (m-1)\pi, \qquad m = 1,3,5 \ldots$$

This situation occurs at even multiples of the mechanical resonance and is the same as the case for the

resonator. Note that the term $(1 - R_B e^{-jwT})$ may never equal zero as the reflection coefficient is always less than unity. In a similar manner, the amplitude of K_F is never infinite, as was the case of the mechanically free transducer. For example, this condition is only reached when,

$$R_F R_B e^{-2jwT} = 1$$

$$\therefore \quad \cos 2wT = \frac{1}{R_F R_B}$$

As the product $R_F R_B$ is always less than unity for the loaded transducer, the condition may never be realised and hence the amplitude of the reverberation factor is always finite. It should be noted also, that in practice the resonator reverberation factor is never infinite due to internal mechanical dissipation within the transducer.

Amplitude-frequency characteristics of K_F are shown in figure 5.9a, corresponding to the three different conditions of mechanical load. In each case, the magnitude reaches maximum and minimum values at odd and even multiples of the mechanical resonance respectively. The amplitude function also decreases with increasing mechanical load. That is, with increasing damping. This is to be expected, since more energy is effectively being transferred to the surrounding media.

Figure 5.9b depicts the phase characteristics of K_F under the same three conditions of mechanical load.

Unlike the resonator, the loaded phase function is no longer either $\pm \pi/2$ radians, but varies between $+\pi/2$ and $-\pi/2$ in a periodic manner over the frequency range. In consequence, a reverberation factor for the loaded transducer is no longer purely imaginary, but contains real components, the relative magnitudes of which increase with mechanical damping. This is clearly outlined in figure 5.9b, where the function is purely real at odd multiples of the mechanical resonance. This relative increase in real parts with damping may also be anticipated, since the effective dissipation increases with increasing loss to the surrounding media.

It is now possible to evaluate the significance of the total current feedback factor for a mechanically loaded transducer. This may be expressed in the frequency domain by the following equation:

$$A_T(jw) = \frac{K^2 \ (1-e^{-jwT}) \ \mathcal{Z}_C}{jwT(1-R_F R_B e^{-j2wT})} \left[\frac{(1-R_B e^{-jwT})}{\mathcal{Z}_C+\mathcal{Z}_1} + \frac{(1-R_F e^{-jwT})}{\mathcal{Z}_C+\mathcal{Z}_2} \right] \qquad (7)$$

The magnitude and phase of A_T are shown as functions of frequency in figures 5.10a and 5.10b respectively. The three cases of mechanical damping described previously were again considered. From figure 5.10a, it may be observed that the total amount of current feedback varies with the following parameters.

. The total amount of feedback decreases with increasing mechanical load. This effect is in

sympathy with the behaviour of the reverberation factors which also exhibit a decrease with increasing mechanical damping.

. Under conditions of light mechanical load, the total amount of current feedback is a maximum at odd multiples of the mechanical resonance. This effect may again be reconciled with the behaviour of the reverberation factors. However, as damping is increased, the distinct maxima demonstrate a significant decrease, eventually disappearing altogether. For conditions of heavy damping, the maximum amount of feedback occurs at lower frequencies, where it is limited by the square of the coupling coefficient. This effect is a combination of the reverberation factor characteristics and the $\frac{1}{jw}$ multiplier in the feedback factor.

. The total amount of current feedback decreases with increasing frequency. This is similar to the behaviour of the mechanically free transducer.

It is interesting to note that like the piezoelectric resonator, the amount of feedback at low frequencies is equal to K^2 and is independent of mechanical load. Although not readily apparent from equation 7, the validity of this statement may be demonstrated as follows.

From equation 7, and letting $wT = P$

$$A_T(jw) = \frac{K^2(1-\cos P+j\sin P)}{jP(1-R_FR_B\cos 2P+jR_FR_B\sin 2P)} \times$$

$$\left[(1-R_B\cos P+jR_B\sin P)\left(\frac{1+R_F}{2}\right)+(1-R_F\cos P+jR_F\sin P)\left(\frac{1+R_B}{2}\right)\right]$$

$$= \frac{K^2}{jP}(1-\cos P+j\sin P) \times$$

$$\left[\frac{(1-R_B\cos P+jR_B\sin P)\left(\frac{1+R_F}{2}\right)+(1-R_F\cos P+jR_F\sin P)\left(\frac{1+R_B}{2}\right)}{1-R_FR_B\cos^2 P+R_FR_B\sin^2 P+j2R_FR_B\sin P\cos P}\right]$$

For w very small,

$$\sin P \to P$$

$$\cos P \to 1$$

$$\therefore \quad A_T = \frac{K^2}{jP}(jP)\left[\frac{(1-R_B+jR_BP)\left(\frac{1+R_F}{2}\right)+(1-R_F+jR_FP)\left(\frac{1+R_B}{2}\right)}{1-R_FR_B+R_FR_BP^2+j2R_FR_BP}\right]$$

In the limit, as $P \to 0$

$$\underset{w\to 0}{A_T} = K^2\left[\frac{(1-R_B)(1-R_F)/2+(1-R_F)(1-R_B)/2}{1-R_FR_B}\right]$$

$$= \frac{K^2\ 2(1-R_FR_B)}{2(1-R_FR_B)}$$

$$= K^2$$

Consequently, it maybe concluded that as frequency tends to zero, the total amount of current feedback tends towards a limiting value of K^2 and is hence independent of mechanical load. Equation 6, which related K to the transducer capacitances, is thus valid under general

conditions.

Figure 5.10b outlines the phase of the total feedback factor under the same three conditions of mechanical loading. The form of these characteristics may readily be appreciated by noting that the $\frac{1}{jw}$ multiplier contained in A_T corresponds to a phase shift of $-\pi/2$ radians. Consequently, by adding $-\pi/2$ to the phase characteristics of each reverberation factor, the overall phase of the feedback factor is obtained. As in the case of the piezoelectric resonator, this phase characteristic effectively determines the nature of the feedback. That is, whether the currents at the summing point of the feedback model sum in a constructive or destructive manner.

From figure 5.10b it may be observed that for low values of frequency and mechanical damping, the feedback factor is almost totally real with small imaginiary parts. However, as frequency increases up to the vicinity of mechanical resonance, stronger imaginary components emerge. Furthermore, as the amount of damping increases, the feedback factor becomes increasingly complex, the phase eventually varying almost linearly between 0 and $-\pi$ over the frequency intervals 0 to $2f_1$, $2f_1$ to $4f_1$ etc. As shall be demonstrated, the increasingly complex nature of the feedback factor has a significant effect on the overall impedance function.

It is now possible to consider the transducer impedance characteristics shown in figures 5.11a and 5.11b, which

describe the magnitude and phase characteristics respectively. In a manner similar to that for the resonator, the loaded transducer impedance may be represented by the following Laplace equation

$$Z_T(s) = \frac{1}{SC_o} (1-A_T(s))$$

The admittance transfer function is also represented by the block diagram of figure 5.4. However, unlike the resonator, the feedback factor for the loaded transducer is not purely real, but instead becomes more complex with increased mechanical damping. As a result, the feedback current is rarely in phase (completely positive) or anti phase (completely negative) with respect to the input current. This effect, which increases with mechanical load, tends to obscure the well defined impedance maxima and minima which were obtained for the mechanically free transducer.

The electrical impedance is a minimum when, for frequencies below mechanical resonance,

$$|1 - A_T(jw)| \quad \text{is a minimum}$$

For the loaded transducer, A_T is nearly always complex, the degree of which depends on mechanical damping. As a result, the behaviour of this function never tends to zero at a particular frequency, as in the case of the resonator. Instead, an impedance minimum is evident, the extent and position of which depends on

the amount of mechanical load. This may be seen from figure 5.11a, where the extent and position of the impedance minima for light and medium damping are clearly different. As damping increases, the impedance minimum disappears altogether, as the transducer electrical behaviour starts to resemble that of a capacitance. This may also be observed from figure 5.11b, where the impedance phase angle tends towards $-\pi/2$ radians as damping is increased. In addition, as in the case of the resonator, there is no feedback at even multiples of the mechanical resonance, and the impedance corresponds to that of the clamped capacitance, C_o.

In order to appreciate some of these effects, consider the water backed and water loaded transducer, a situation which corresponds to light mechanical damping. At low frequencies, the feedback factor is real and possesses a magnitude equal to K^2. The feedback current is thus in phase with the input current and hence the impedance falls, behaving electrically like the capacitance C_T. With increasing frequency, the feedback factor becomes complex and starts to increase in magnitude. Consequently, the feedback current becomes increasingly anti phase with respect to the input current, giving rise to the first impedance minimum as shown in figure 5.11a. This degree of phase shift further increases with frequency, resulting in an increase in impedance which reaches a maximum at the mechanical resonance. At this point, the

feedback is almost entirely negative, and hence as the magnitude of the feedback factor falls, the resultant decrease in negative feedback corresponds to an increase in total current through the transducer, causing the impedance to fall.

The same process occurs for increased damping, except that the magnitude of the feedback factor is reduced and the phase is always complex. (Except at zero frequency). As a result, the impedance maximum and minimum are less well defined, eventually decreasing altogther. In addition, like the resonator the amount of feedback decreases with frequency, with the result that any impedance fluctuations around odd multiples of mechanical resonance disappear. A similar effect is observed with the impedance phase characterisitcs, which eventually approach those of a pure capacitance for conditions of high frequency and/or heavy damping.

It is interesting to consider the transducer impedance under conditions of maximum damping. That is, when the device is backed and loaded by a material possessing the same acoustic impedance as the transducer. For this condition the impedance transform is given by,

$$Z_T(s) = \frac{1}{SC_o}\left[1 - \frac{K^2}{ST}(1-e^{-sT})\right]$$

In this case, the impedance approximates to that of a capacitance, which at low frequencies tends towards the free capacitance C_T, and at higher frequencies

behaves like the damped transducer capacitance C_o. For example,

$$Z_T(jw) = \frac{1}{jwC_o}\left[1 - \frac{K^2}{jwT}(1-\cos wT+j\sin wT)\right]$$

For higher frequencies,

$$Z_T(jw) = \frac{1}{jwC_o}$$

which is the impedance of the damped capacitance.

While for low frequencies,

$$Z_T(jw) = \frac{1}{jwC_o}\left[1 - K^2\right]$$

And from equation six,

$$Z_T(jw) = \frac{1}{S\ C_T}$$

which is the impedance of the free capacitance.

These effects are clearly demonstrated in figure 5.12a, where the impedance magnitude characteristic of a heavily damped transducer is compared against the impedance behaviour of the two capacitances. It is interesting to note that the impedance approximates to the clamped capacitance at very much lower frequencies than for the mechanically free transducer; close correlation being obtained for frequencies above the mechanical resonance. This is even more pronounced for transducers of lower electromechanical coupling

coeffifient, due to the corresponding reduction in feedback. The effects of decreasing K are demonstrated in figure 5.12b where it may be readily observed that the impedance more closely approximates the clamped capacitance C_o.

5.3.iii Impedance Characteristics Under Conditions of Rigid or Semi Rigid Loading

In order to complete the section on transducer electrical impedance, it is worthwhile to consider the situation where the transducer is loaded at one or both faces by a material possessing a higher acoustic impedance than that of the transducer. For example, the term 'rigid loading' applied to either face implies that the transducer is loaded at that face by a material whose elastic stiffness is so high, that the particular face of the transducer is incapable of mechanical displacement. Since piezoelectric devices have high coefficients of stiffness, such a condition is impossible to achieve in practice. In addition, although some loading materials have higher acoustic impedances than the transducer material, a coupling medium (often water based) is invariably inserted between the device and the load surface. As a result, the physical situations described in this section are rarely encountered in practice, and consequently only the major effects are presented. The following conditions are described.

. The rigidly backed and rigidly loaded transducer.

For this highly theoretical case,

$$\mathcal{Z}_1 >> \mathcal{Z}_c, \quad \mathcal{Z}_2 >> \mathcal{Z}_c, \quad R_F = R_B = -1$$

T_F and T_B are zero and hence no secondary piezoelectric action may occur. The impedance is thus that of the clamped capacitance, C_o.

. The rigidly backed, air loaded transducer.

In this case,

$$\frac{T_B}{2} = 0, \quad \frac{T_F}{2} = 1, \quad R_F = 1, \quad R_B = -1$$

The transducer feedback factor is thus given by,

$$A_T(s) = \frac{K^2}{sT}\left[\frac{1 - e^{-2sT}}{1 + e^{-2sT}}\right]$$

$$\therefore \quad A_T(w) = \frac{K^2}{wT}\tan(wT)$$

This is similar to the feedback factor obtained when the transducer is mechanically free, except that wT/2 has been replaced by wT. Consequently, the impedance magnitude exhibits maxima at,

$$f = (2m+1)\frac{f_1}{2}, \quad m = 0,1,2,3 \ldots$$

Zero magnitude is expected when the following transcidental equation is satisfied.

$$\tan(wT) = \frac{wT}{K^2}$$

This equation behaves in a similar manner to that for the piezoelectric resonator. That is, the impedance

amplitude is zero at frequencies which are close to, but less than, the frequencies of maximum impedance. For the same reasons as before, the separation of impedance maxima and minima decreases with increasing frequency.

The amplitude and phase characteristics appropriate to this condition are shown in figures 5.13a and 5.13b respectively. The form of these characteristics may be explained in an identical manner to that adopted for the piezoelectric resonator, except that f_1 is replaced by $f_1/2$ in the analysis of the relevant feedback and reverberation factors.

It is interesting to note the analogy between reverberation factor behaviour and that of a lossless transmission line. For example, in the mechanically free transducer, reflection coefficients are equal to unity; that is, no phase change on reflection. This situation is analogous to the behaviour of a lossless open circuit transmission line. On the other hand, for the rigidly damped transducer, reflection coefficients are equal to - 1; a situation which corresponds to the lossless transmission line on electrical short circuit.

. Miscellaneous loading and backing configurations.

Figures 5.14a and 5.14b show the transducer magnitude and phase characteristics for the following conditions of mechanical damping.

The rigidly backed transducer operating directly into

a glass load (medium damping).

The air backed transducer operating into a steel load of acoustic impedance 47 Kg/m²-s. This is mechanically stiffer than the piezoelectric material, which is assumed to have a nominal acoustic impedance of 33.712 Kg/m² s. (medium damping).

The transducer with 50% matched backing and operating into a steel load (heavy damping).

From the figures it may be observed that the impedance characteristics demonstrate the expected maxima and minima under conditions of lighter mechanical damping. It should be noted that in this context, light damping implies that the magnitudes of the reflection coefficients are close to unity, hence maximising the effects of feedback.

The frequencies of minimum and maximum impedance for the two cases of medium damping are different, being governed by the mechanical loading conditions. For miscellaneous loading of the type discussed here, it is difficult to generalise on the positions of impedance fluctuation. However, it is possible to conclude that as the stiffness of the surrounding media decreases, the frequencies of maximum and minimum impedance tend to increase, although for an accurate indication, individual cases should be treated separately.

In these examples, the highest amount of mechanical damping occurs during the situation of 50% matched

backing and operation into a simulated steel load. As may be expected, the impedance characteristics start to resemble those of a capacitor although in this case the overall damping is not heavy enough for such an effective approximation.

5.4 Concluding Remarks

This chapter has demonstrated how a systems feedback approach may be adopted in order to describe operational impedance of a piezoelectric transducer. In the analysis, complex electro-mechanical phenomena which contribute to the impedance characteristics have been clearly identified over a wide range of external operating conditions. From the study, it is considered that the feedback model is superior to other, dynamic analogies in identifying and explaining the following aspects of transducer impedance.

(i) The phenomenon of electrical resonance is clearly shown to be a feedback effect and is due exclusively to secondary piezoelectric action.

(ii) The position and extent of impedance maxima and minima depend on external mechanical loading conditions as well as frequency and coupling coefficient..

(iii) The low frequency feedback factor, i.e. the relative amount of secondary piezo-

electric action; depends only on the coupling coefficient. This is valid under all conditions of mechanical load, apart from the rigidly clamped situation, where no mechanical displacement is possible. At very high frequencies, for example ten times mechanical resonance, secondary effects disappear.

CHAPTER VI

SIMULATION AND RESULTS PART I

6.1. INTRODUCTION

This chapter describes the simulation and experimental verification of a transducer voltage transfer function. The voltage transfer function is defined as the ratio of the measured voltage across the transducer terminals and the input source voltage.

Consider a transducer operating in the transmitting mode while subject to arbitrary conditions of electrical loading. This situation is described extensively in Appendix C, but for convenience the configuration is outlined in Figure 6.1.

From this figure, the Laplace Transform of the voltage transfer function may be expressed as follows.

$$\frac{Vo(s)}{e(s)} = \frac{ZT(s)\,ZE(s)}{Zo(s)\,ZT(s)+Zo(s)\,ZE(s)+ZT(s)\,ZE(s)} \qquad (1)$$

Where,
ZT is the electrical impedance of the transducer.
Zo and ZE are the electrical impedances corresponding to the voltage generator and external load respectively. The possible variations in these parameters are described in Appendix C. Zo may comprise a resistive, capacitive or inductive element (or the series combination of all three) while ZE may comprise the parallel combination of resistive and inductive loading elements.

Although the voltage transfer function is a relatively uncommon characteristic in transducer measurement studies, it provides considerable insight into many aspects of device performance; particularly for the transmission mode. For example, it will be demonstrated that the measured voltage response may be used to provide a clear indication of mechanical loading effects, and in some instances, important piezoelectric parameters. The technique is also considered to offer the following additional advantages.

(i) Experimental verification of the voltage response may be performed in both time and frequency domains with relative ease. As a result, a wide range of electrical source and loading conditions may be conveniently investigated. It is thus possible to verify simulation studies without recourse to more complex measurement techniques necessary for the transmission and reception modes.

(ii) It is possible for some transducer parameters, such as static capacitance, to vary considerably from the manufacturer's quoted figures. For example it is shown in Appendix D that this quantity may deviate by as much as 20% from its nominal value. By measuring the voltage response, variations in

device parameters are readily observed and steps may be taken to compensate for incorrect values.

(iii) The transducer model assumes loss free, single mode wave propagation within the device. However, in practice there is a finite loss coupled with radial mode disturbances. A study of the voltage response provides a clear indication of both these effects and as a result limitations of the model are readily observed. For example, internal losses are expected to have greatest influence on device operation under conditions of light damping, when most of the wave energy is reflected back into the transducer. Radial mode vibrations are expected to become more dominant as the diameter to thickness ratio decreases, eventually corrupting thickness mode resonances. By studying the nature of these effects, a range of operating conditions for the model may thus be clearly defined.

In addition, the voltage response technique permits relatively straightforward verification of the transducer impedance characteristics

discussed in Chapter 5. Consequently, it is considered appropriate at this stage to evaluate voltage response, and in the following chapter, present a more conventional investigation based on transducer transmission and reception. Two sets of simulations are performed, corresponding to CW and transient operation in both frequency and time domains.

6.2 CW OPERATION

This section investigates the transfer function described by equation 1, in the frequency domain. The voltage generator is assumed to be a continuous wave source possessing an output impedance which is real and equal to 50 Ω. Additional electrical components may be added either in parallel or in series with the transducer, depending on the particular application. This mode of operation and the various electrical loading configurations are fully described in appendices B and C.

A computer program describing transfer function behaviour in the frequency domain was developed in order to perform the simulations. The program is designed to cover all possible configurations of electrical

and mechanical loading and a complete BASIC listing is provided in Appendix E.

6.2i General Simulation Results

Before describing the experimental techniques and particular simulation studies it is worthwhile to briefly review the results of Chapter 5. This is done by considering the voltage transfer function under the same conditions of light, medium and heavy damping. That is, the transducer is subject to the following loading conditions:

Water Backed and Water Loaded (light damping)
50% Matched Backing and Glass load (medium damping)
Ideal Backing and Glass load (heavy damping)

Consequently, the voltage transfer function frequency response characteristics are expected to demonstrate marked fluctuations at electrical and mechanical resonance; for conditions of light damping. As the mechanical load increases, these fluctuations are expected to decrease, as the transducer impedance eventually tends towards that of its clamped capacitance.

Figure 6.2a shows the frequency response of the voltage transfer function for two values of source resistance, corresponding to 50Ω and 470 Ω. (The

nominal transducer parameters of Table 5.1 are used in this and the subsequent two simulation diagrams.) In this figure the transducer is lightly damped, and hence fluctuations caused by the transducer impedance function are clearly evident. Increasing source resistance produces the expected attentuation in the transfer characteristic, although feedback effects still dominate due to the light loading.

Figure 6.2b shows the effects of increasing damping for a source resistance of 50 Ω. Fluctuations in the transfer characteristic are reduced because of the diminished secondary action. Under conditions of heavy damping the transducer impedance tends towards that of the static capacitance, at all but the lowest of frequencies.

Figure 6.2c outlines the effect of introducing an inductance in series with the transducer, under the three conditions of mechanical load. The source resistance is 50Ω and the value of inductance is 20μH. This value was selected in order to produce a tuned resonant frequency of 1MHZ (the transducer mechanical resonance) with the static capacity Co. That is,

$$f = \frac{1}{2\pi\sqrt{Lo\ Co}}$$

From table 5.1, Co = 1.261nF

and for Lo = 20μH,

f = 0.999MHZ.

For conditions of light damping, the effects of feedback dominate the response, but as a result of tuned resonance, the peak output is substantially increased. As mechanical clamping is increased, the transducer impedance approaches a pure capacitive reactance. Consequently the transfer characteristics are dominated by the Lo-Co combination, which approaches that of a low pass filter.

The three simulation examples were selected in order to outline some general features of the voltage transfer function in the frequency domain. In subsequent sections, particular transducer devices are tested and experimental results compared with their corresponding computer simulations. Transducer parameter variations, unwanted vibrational modes and the effects of internal loss are investigated under different conditions of mechanical and electrical loading.

6.2ii CW Experimental Techniques

The experimental method for determining the voltage transfer function is outlined in figure 6.3, which depicts a transducer operating under mechancially free conditions.

A Dymar VHF (low distortion) signal generator was employed as the voltage source. The output impedance of the instrument is 50Ω and when checked over the frequency range 0 to 10MHZ, was found to deviate by ±2Ω from this value. Consequently, the output impedance was assumed to be 50Ω throughout the experimental period. Frequency measurements were performed using a Tektronix 7D15 225 MHZ Universal Counter and voltage measurements by means of a Hewlett Packard 3400 rms voltmeter. The latter instrument possesses an input impedance and bandwidth of 10MΩ and 10MHZ, respectively. The transducer was mounted in a special holder, designed to permit flexibility when changing devices and allow additional electrical components to be added with relative ease. All connecting leads were kept as short as possible.

The output voltage from the generator was adjusted to 200mV with the terminals open circuit i.e. no

transducer in the system. This voltage, denoted by Vo-c was maintained constant throughout the experiments. After inserting a transducer, frequency was slowly increased and the voltage across the device monitored on the rms voltmeter. This voltage is denoted by Vo and hence the voltage transfer function for the system shown in figure 6.3 may be expressed as follows. (From Equation 1)

$$\left|\frac{Vo}{Voc}\right| = \left|\frac{ZT}{50 + ZT}\right|$$ Where ZT is expressed in ohms

This magnitude was plotted as a function of frequency over the range 100KHZ to 10MHZ.

Four different transducers were tested. The transducer was Lead Zirconate Titanate (PZT5A) and the devices possessed electrical resonant frequencies of 0.5, 1, 2 and 5MHZ. Where possible, the physical dimensions and parameters of each transducer were carefully checked. Full details on each transducer and the individual measurements are described in Appendix D. All transducer data is provided in Tables D1 and D2, contained in this appendix.

Tests were initially conducted with each transducer in the mechanically free state. This situation of air backing and air loading corresponds to the resonator condition described in Chapter 5. Because of the electrical conductivity of water, this medium was not used to simulate conditions of light damping. Instead, transformer oil was employed. This material has an acoustic impedance similar to that of water (1.27Kg/m-s (Ensminger (9)) and is electrically non-conductive. In section 6.2iii a commercially available ultrasonic probe was used to demonstrate the effects of increased mechanical load. For later sections of the work, different backing materials were employed and a technique for measuring the acoustic impedances is described in section 6.3iii.

In addition, electrical loading conditions were also varied. This included varying source resistance and the incorporation of inductive matching elements, both in series and in parallel with the transducer. These components were easily attached to the transducer holder by simply inserting them in appropriate sockets.

6.2iii Results and Simulations

Graphs of transfer function magnitude versus frequency are presented for each case. The graphs were drawn by inserting data on a cassette tape and then using the 4051 graphics terminal to plot the results. For convenience, simulated response characteristics are shown on the same graph.

a) Mechanically Free Transducer Response

Consider firstly the response of a mechanically free transducer possessing the nominal electrical resonant frequency of 2MHZ. The device has a diameter/ thickness ratio of 21.16 and a mechanical resonance corresponding to 2.3MHZ. The theoretical value (provided by the manufacturer) of static capacitance is 2.4nF and this was used in the simulation diagram. Other relevant parameters are provided in Appendix D, tables D1 and D2.

Experimental and simulated transfer function responses are shown in figure 6.4a. It may be observed that the frequency of electrical resonance is slightly greater than 2MHZ. However, as described in Appendix D, each transducer has a 7% tolerance variation in electrical resonant frequency. The electrical resonance in this

case is within the tolerance range. In addition, the simulated plots were calculated from a basis of the mechanical resonant frequency, which defines the transit time, T. Transit time was calculated by dividing transducer thickness by the longitudinal wave velocity. Although thickness of each transducer was carefully measured, published values of velocity shown in Appendix D were used. Consequently, any variation in this quantity has a corresponding effect on transit time, and hence electrical and mechanical resonant frequencies.

From figure 6.4a, the following differences are evident between the practical and theoretical characteristics.

1. Radial mode vibrational effects may be readily observed at lower frequencies by the additional oscillations in the experimental transfer characteristic. They are caused by impedance fluctuations in the transducer as the diameter of the disc expands and contracts. These effects are clearly evident for frequencies up to the mechanical resonance (maximum transducer impedance) after which they tend to decay, having almost disappeared at twice mechanical resonance. Radial

- mode effects tend to obscure both frequencies of maximum and minimum transducer impedance, making exact measurement of these quantities extremely difficult.

2. Effects of internal dissipation within the transducer are also evident. This may be observed from the fact that the experimental transfer characteristic is neither zero nor unity at the electrical and mechanical resonant frequencies respectively. The impedance maxima also decrease with frequency, as indicated by a drop in the peak magnitude of the experimental graph at the first overtone of mechanical resonance. It may be noted that the effects of internal dissipation on the transducer impedance characteristic are similar to those described in chapter 5, when losses occur due to light mechanical loading. In fact Martin and Sigelman (27), in an attempt to include internal dissipation in their Thevenin Model, postulated a 'loading factor' on the transducer face. The acoustic impedance of the loading factor was selected to produce closest agreement between theoretical and practical measurements on transducer impedance.

The factors which contribute to transducer loss are complex functions, involving many parameters. For example, absorption of the mechanical wave occurs, resulting in attenuation in the piezoelectric material. This is generally frequency dependent, the amount of attenuation increasing with frequency. However, published data (Kossof (18)) on piezoceramic materials of the type considered here indicates that such mechanical dissipation is extremely small when compared to the total loss encountered when the transducer is mechanically loaded, even under conditions of light damping. Nevertheless, some transducer materials, notably Lead Metaniobate (Silk(44)) exhibit considerable attentuation and in such cases internal loss may not be neglected.

Another source of loss was revealed by Martin (26) and Hilke (14) who indicated that the piezoelectric parameter h is also frequency dependent, causing the electromechanical coupling factor to decrease with frequency. This serves to reduce secondary piezoelectric action even further at higher frequencies. However, it should be noted that very little published data on the frequency dependence of h is available for the transducer types under consideration.

3. Figure 6.4a also indicates that the experimental characteristic is generally of higher amplitude than the theoretical curve. That is, the theoretical value of transducer impedance is low, caused by too high a value of static capacitance. Consequently, the static capacitance was measured at twice the mechanical resonant frequency, where no piezoelectric action is assumed to take place. The method of measurement is fully described in Appendix D.

Some authors, for example Kikuchi [17], recommend this technique for measuring static capacitance. However, as shall be demonstrated, it is only valid for those situations where radial mode vibrations do not corrupt the results. That is, for those transducers possessing a sufficiently high diameter to thickness ratio. In the case of the 2MHZ crystal no radial modes are evident at twice mechanical resonance (4.6MHZ) and the measured value of static capacitance was found to be 1.87nF.

Figure 6.4b compares experimental and simulated responses for the new value of static capacitance. Apart from internal loss and radial mode effects, the two characteristics are in very close agreement.

Figure 6.4c shows the characteristics for a 4MHZ transducer which has a diameter/thickness ratio of 43.7. The static capacitance of this device was also measured at twice mechanical resonance and was found to be 3.77nF compared with its theoretical value of 4.88nF. The measured value was used in the simulation plot and again the characteristics are observed to be in good agreement. It should be noted that in this case, radial mode effects do not obscure the frequencies of minimum and maximum impedance.

Figures 6.4d and 6.4e compare experimental and theoretical characteristics for 1MHZ and 0.5MHZ transducers respectively. The diameter/thickness ratios are 10.7 and 5.33 respectively and all other relevant parameters are outlined in Appendix D. From the figures, the following points may be noted.

1. Measurement of static capacitance at twice mechanical resonance is extremely difficult due to radial mode effects occurring in the vicinity of this frequency. Even at four times mechanical resonance, radial modes are still evident, making accurate measurement almost impossible. In these instances, an estimate of static capacitance was

made on the basis of a 'closest fit' between experimental and theoretical curves. For the 1MHZ transducer, static capacitance was assumed to be 1.05nF (theoretical value of 1.22nF) while for the 0.5MHZ transducer a value of 0.57nF (theoretical value 0.61nF) was obtained. The estimated values were used in the simulation curves.

2. Differences between the two sets of overtone frequencies are observed to increase with frequency. This is caused partly by experimental inaccuracy, but is considered largely due to error in calculating the frequencies of mechanical resonance as described earlier. These two transducers are thicker than the 2MHZ and 4MHZ devices and hence any error in measuring transit time is compounded in the case of the lower frequency transducers. However, since the overtone frequencies are largely damped out, it was not considered worthwhile to repeat the experiment for different values of mechanical resonance.

b. Transducer Response Under Conditions of Mechanical Damping.

As stated earlier, the transducers are assumed loaded at both faces by transformer oil. The theoretical and simulated response characteristics corresponding to 1, 2 and 4MHZ transducers are shown in figures 6.5a, 6.5b and 6.5c respectively. From the graphs, the following main features emerge:

1. Radial and thickness mode impedance fluctuations are reduced by the increased mechanical damping. This may readily be verified by comparing the respective characteristics with those for the mechanically free transducers. Such behaviour is expected (for thickness mode resonances) from the transducer impedance characteristics discussed in Chapter 5.

2. The effects of internal loss are much less significant and for all three cases, excellent agreement is obtained between simulated and experimental results. However, in the case of the 1MHZ transducer, the overtone frequencies of electrical and mechanical resonance are not in complete agreement, primarily because of slight measurement error in the value of mechanical resonance.

Nevertheless, within the limits of experimental accuracy, the characteristics are in very close agreement. It may thus be concluded that for this type of transducer material, the effects of internal dissipation are negligible under finite conditions of mechanical load.

To complete the present section, figure 6.5d shows the measured response for a commercially available 1MHZ probe which is loaded at both faces by (unknown) solid materials. For such conditions of damping, transducer impedance fluctuations are expected to diminish and this is reflected in the characteristic shown in the figure. It should be noted that no corresponding simulation characteristic is outlined, due to the difficulty in obtaining values for the acoustic impedances of the loading media. However, the main features of increased damping are readily demonstrated.

c. Transducer Response Under Varying Conditions of Electrical Load

In this set of examples, a 2MHZ mechanically free transducer was tested under three different conditions of electrical load. That is, a resistive element in parallel with the transducer, an inductive element in

parallel with the transducer and an inductive element in series with the transducer.

Figure 6.6a demonstrates the attentuation introduced to the transfer characteristic when a resistor of 100Ω is connected across the device. The experimental and simulated results are shown to be in excellent agreement.

Figure 6.6b shows the transfer characteristics when a 2.2μH inductor is connected across the transducer electrodes. This value of inductance resonates with the transducer free capacitance (CT = 4.35nF) at approximately 1.6MHZ and with the clamped capacitance at approximately 2.5MHZ. At these frequencies, the transfer characteristic is expected to attain a maximum value of unity. Although this may readily be observed from the figure, secondary piezoelectric effects still dominate the response. Comparing this figure with figure 6.4b reveals that two impedance maxima are now evident on either side of the fundamental electrical resonance. The inductor has also served to increase slightly the position of the first mechanical resonance. Furthermore at low frequencies and hence small values of inductive reactance, the effects of radial mode vibrations have been extensively damped out. This feature of radial mode damping under light electrical load conditions is further emphasised in section 6.3.

Figure 6.6c shows the response when a 10μH inductor is connected in series with the transducer. This resonates with the transducer free and clamped capacitances at 0.76 and 1.16MHZ respectively. Once again secondary effects are observed to dominate the response although the amplitude of the transfer characteristic has been increased by the series-resonance of the inductance and the transducer capacitance. In this case radial mode vibration has not been suppressed, possibly because of the higher electrical loading. Excellent agreement is again obtained between the practical and theoretical characteristics.

6.3 TRANSIENT OPERATION

This section investigates the behaviour of the voltage response under transient conditions. That is, the transducer is assumed to be driven by the application of a negative going step or ramp function to a blocking capacitor. A complete description of this mode of operation is described in Appendix C which includes an analysis of the transmitting circuitry under a variety of electrical load conditions. Circuit configurations appropriate to transient operation are shown in Appendix C, figures C1 and C2.

From these figures, equation 1 may be expressed as follows,

$$\frac{Vo(s)}{e(s)} = \frac{ZT(s)\ ZE(s)}{Zo(s)\,[ZT(s) + ZE(s)] + ZT(s)\ ZE(s)}$$

where,

$$Zo(s) = Ro + \frac{1}{sC_B}$$

$$ZE(s) = RE||LE$$

Ro is the on resistance of the pulser or electronic switch.

CB is the blocking capacitor.

RE and LE are additional electrical loading elements which may be connected across the transducer.

In addition, if the pulser is a fast switching MOSFET as described in Appendix C, the measured voltage across the transducer electrodes may be expressed by the following transform equation.

$$Vo(s) = \frac{1}{s} \frac{ZT(s)\ ZE(s)}{(Ro + \frac{1}{sCB})\ (ZT(s)+ZE(s)) + ZT(s)ZE(s)} \quad (2)$$

This quantity was evaluated in both time and frequency domains, for a vareity of electrical and mechanical load conditions. Frequency response was obtained by substituting jw for s and plotting the magnitude of the output voltage as a function of frequency. Time domain response was obtained by evaluating the real and imaginary parts of equation 2, and after appropriate frequency sampling, performing an Inverse Fast Fourier Transform (IFFT). A complete listing and description of the software is provided in Appendix E.

6.3i General Simulation Results

As in the previous section, it is worthwhile to consider the results of some general simulation studies before commencing on experimental investigation. In these examples, a transducer with a resistive load is considered, since this is an extremely common transmitting configuration. An outline of the system is shown in figure 6.7.

This configuration is employed in many pulse excitation systems in order to approximate an impulse of voltage across the transducer. The pulser is assumed ideal, delivering a negative going step input to the blocking capacitor. Unless otherwise stated, the nominal transducer characteristics of Table 5.1. were used in the simulations.

Frequency spectra of the output voltage corresponding to three values of load resistance are shown in figure 6.8a. The transducer has a mechanical resonance of 1MHZ and is subject to conditions of light damping (water backed and water loaded).

For small values of load resistance (10Ω) the resultant spectrum is clearly wideband, although as expected, the amplitude is very low. This behaviour may be predicted, since the time constant CoRE is extremely small compared with the transducer transit time (12ns cf 500ns). Consequently, the measured voltage approximates closely to an impulse function, although small fluctuations induced by secondary piezoelectric effects may be observed.

Increasing load resistance to 100Ω reduces the overall bandwidth and the effects of feedback are more clearly visible. For a load resistance of 1kΩ , the spectrum is essentially narrowband, with the transducer impedance characteristics a dominant factor. It is evident that the value of load resistance must be kept small to obtain a wideband voltage response from this system. This was also observed by Brown and Weight (3) who proposed simple R-C shaping circuits in order to increase bandwidth. However, bandwidth may be varied by inserting a suitable value of inductance in parallel

with the load resistor. This is demonstrated in figure 6.8b, where a considerable change in the frequency response is observed. It should be noted however, that the spectrum still tends to be dominated by the effects of secondary action.

Voltage response in the time domain is shown in figure 6.9a, for the water loaded , water backed transducer with a resistive load of 100Ω connected across the electrodes. In this case, distoration imposed by secondary piezoelectric action is very evident. Apart from the first transit interval (0.5us), the exponential rise associated with a pulsed R-C system is barely recognisable. However, the reduction in secondary action through increased damping is readily seen from figure 6.9b which corresponds to a transducer with 50% matched backing and operating into a glass load (medium damping). However some secondary action is still evident as the pulse shape does not form a perfect exponential. This is because of the increase in transducer capacitance towards the end of the decay period. That is, at the low frequency end of the spectrum.

Considerable insight into the nature of the time response may be obtained by reducing the time domain to one transit interval of the transducer. Over this time interval, the reverberation factors associated with the transducer

impedance are unity, hence permitting considerable simplification of the voltage transfer function.

Consider the special case of a transducer free of any electrical loading and driven from a pulser/ generator via a coupling capacitor CB. The voltage source is assumed to possess zero output impedance and deliver an ideal, negative going step input to the coupling capacitor. As described in Appendix C, some FET switching devices approximate very closely this condition. The circuit configuration is shown in 6.10 and hence the voltage transfer function may now be expressed as follows.

$$\frac{Vo(s)}{e(s)} = \frac{ZT(s)}{Zo(s) + ZT(s)} \quad \text{where,}$$

$$ZT(s) = \left(1 - \frac{K^2}{ST}\left(KF(s)\frac{TF}{2} + KB(s)\frac{TB}{2}\right)\right)/SCo$$

$$Zo(s) = 1/SCB$$

$$e(s) = \frac{-u}{s}$$, where u is the amplitude of the step input.

Over one transit interval, KF and KB are unity and hence the transducer impedance becomes,

$$ZT(s) = \left(1 - \frac{K^2}{ST}\left(\frac{TF}{2} + \frac{TB}{2}\right)\right)/sCo \qquad o \leq t < T$$

$$= (s-a)/s^2Co$$

where $a = \frac{K^2}{2T}\,[TF + TB]$

Consequently, the transfer function may be expressed as follows,

$$\frac{Vo(s)}{e(s)} = \frac{\frac{CB}{Co+CB} \cdot (s-a)}{s - \frac{CB \cdot a}{Co + CB}} = \frac{K_1(s-a)}{s-K_1a}$$

Where $K_1 = CB/(Co+CB)$.

The Laplace Transform of the output voltage is thus given by,

$$Vo(s) = \frac{-K_1(s-a)u}{s(s-K_1a)}$$

This may be expanded by partial fractions to give,

$$Vo(s) = u\left(\frac{-1}{s} + \frac{(1-K_1)}{s-K_1a}\right)$$

The response in the time domain is obtained by inverse transforming this expression.

$$Vo(t)/u = -1 + (1-K_1)\exp(K_1 aT)$$

$$o \leq t < T$$

Substituting for K_1 and a gives,

$$\frac{Vo(t)}{u} = -1 + \frac{Co}{Co+CB} \cdot \exp\left[\frac{CB}{Co+CB} \cdot \frac{K^2}{2} \cdot (TF+TB)\frac{t}{T}\right] \quad \text{———3}$$

$$o \leq t < T$$

This function is plotted in figure 6.11, for a water loaded, water backed transducer. Three nominal values of transducer capacitance are shown, corresponding to CB/2, CB and 2CB. Otherwise, the transducer parameters of Table 5.1 were used in the graphs.(Unit step input)

At t=o, there is an initial jump in voltage which is given by the ratio $\frac{CB}{Co+CB}$, which is to be expected in any capacitive divider system. A steady exponential rise then occurs, determined by the term in square brackets in equation 3. This expression describes secondary piezoelectric action, which is shown to depend on the following quantities.

1. As expected, secondary action depends on mechanical load, becoming a maximum under light loading conditions. For example,

$$TF = \frac{2Zc}{Zc+Z_1}, \qquad TB = \frac{2Zc}{Zc+Z_2}$$

These quantities tend towards their maximum value when Z_1 and Z_2 are small i.e. conditions of light damping. This is may be predicted, on the basis of the discussion in Chapter 5.

2. The amount of secondary action increases with coupling coefficient. This is also to be expected from analyses performed in previous chapters.

3. Secondary action is dependent on the electrical loading conditions; increasing as the electrical load impedance decreases. This result is not apparent from the investigation of Chapter 5, although in both transmitter and receiver analyses, the amount of feedback was observed to increase as the external load impedance decreased.

Consequently, secondary action is maximised when K, CB, TF and TB are large.

It is interesting to note the form of equation 3 under mechanically free conditions. That is, when TF and TB are unity. The output voltage may be expressed as follows.

$$\frac{Vo}{u} = -1 + \frac{Co}{Co+CB} \cdot \exp\left[\frac{2K^2CB}{Co+CB} \cdot t/T\right] \quad o \leq t < T$$

For t just less than the transit interval, the measured voltage becomes,

$$\frac{Vo}{u} = -1 + \frac{Co}{Co+CB} \exp\left[\frac{2K^2CB}{Co+CB}\right]$$

$$\therefore K = \left[\frac{Co+CB}{2CB} \ln\left(\frac{Co+CB}{Co}\left(1+\frac{Vo}{u}\right)\right)\right]^{1/2} \qquad (4)$$

$$= \left[\tfrac{1}{2}\left(1+\frac{CB}{Co}\right) \ln\left(\left(1+\frac{CB}{Co}\right)\left(1+\frac{Vo}{u}\right)\right)\right]^{1/2}$$

This provides a method of measuring electromechanical coupling coefficient for the thickness mode transducer, providing the static capacitance of the transducer is accurately known. In a similar manner, equation 3 may be manipulated to provide information on the acoustic impedance of external loading media, provided that Co and K are accurately known. Application of these equations to practical measurement are discussed extensively in the following results section.

6.3ii Experimental Techniques

A schematic diagram of the apparatus used in determining the transient response is shown in figure 6.12.

A complete circuit diagram of the electronic pulser is provided in Appendix C, figure C4. The switching device used was an International Rectifier IRF830. switching mosfet. This device has an 'on' resistance of 1.35Ω and a turn on time of less than 30ns. The input (U), comprised a negative step function of voltage which could be varied between 1v and 500v via a Brandenburg D.C. power supply. Pulse repetition frequency was adjusted to approximately 50 pulses per second by means of a Hewlett-Packard pulse generator. A Tektronix 7000 series storage oscilloscope was used to display the voltage waveforms appearing across the transducer electrodes. It should be noted that after firing, the pulser was maintained in a conducting state for 50μs. However, provision was made to adjust this period from 100ns to 50μs, although the feature was not necessary for the present set of experiments.

The same set of four transducers employed in section 6.2 were again tested. That is, the devices possessed electrical resonant frequencies of 0.5, 1, 2 and 4MHZ.

However, the majority of experiments were performed on the 1MHZ transducer since this device, with a low diameter to thickness ratio of 10.9, should provide an excellent indication of the model limitations with respect to pure thickness mode wave propagation.

In this section, all experimental results and simulation diagrams are shown in the time domain; although frequency response may readily be investigated by replacing the oscilloscope with a spectrum analyser.

6.3iii Results and Simulations

Figure 6.13a compares the theoretical and simulated response characteristics for the 1MHZ transducer. A resistor of 120Ω was connected across the transducer electrodes and a step input of 50v applied to the 100pf blocking capacitor. The transducer was immersed in an oil bath in order to provide conditions of light mechanical damping. It is readily apparent that both figures are in extremely close agreement, even after several transducer transit intervals. No radial mode effects are apparent, despite the relatively small diameter/thickness ratio (10.92). This would appear to substantiate observations made in section 6.2, that radial mode vibrational effects are considerably diminished under conditions of low impedance electrical loading.

Figure 6.13b compares the response characteristics for the same configuration, except that the blocking capacitor has been increased to 2.2nF. Once again the theoretical and experimental curves are in very close agreement. The increase in secondary action due to the increased voltage across the transducer becomes apparent when the voltage scales in figures 6.13a and 6.13b are compared. No radial mode effects are again apparent in the latter figure.

Figure 6.13c shows the response of a commercially available, 1MHZ probe louded at each face by solid media. The blocking capacitor was 100pf and a 50v step input was applied to the network. A resistor of 120 Ω was connected across the transducer electrodes. The effects of increased damping become readily apparent when figures 6.13a and 6.13c are compared. The extra mechanical loading has considerably reduced secondary piezoelectric action; which has almost disappeared after a few transit intervals. In fact, the behaviour indicated in figure 6.13c resembles that shown in figure 6.9b; although the damping is probably less in the former figure.

Figure 6.14a compares the theoretical and experimental response characteristics when a 4.7μH inductance is

connected in parallel with a 120Ω resistance across the 1MHZ transducer. In this case a 50v step input was applied to a blocking capacitor of 2.2nF. The transducer assembly was immersed in an oil bath to provide conditions of light damping. Again it may be readily observed that the two curves are in extremely close agreement, and no radial modes are apparent.

It is interesting to note the distortion of the waveshape due to secondary action in this latter figure. Figure 6.14b compares the transient response of the configuration with and without feedback. That is, K = 0.486 and K = 0 respectively. For K = 0, the transducer impedance is that of a pure capacitance, of value equal to Co. Consequently, the smooth decaying oscillatory waveform shown in figure 6.14b is achieved. (A full description of this type of waveform is presented in Appendix C). However, for K =0.486, considerable distortion is introduced, resulting in a longer decay time and different frequency of oscillation.

Figure 6.15 shows the transient responses corresponding to the 1MHZ and 4MHZ transducers. Each device is mechanically free and no resistive or inductive elements areconnected across the electrodes. In both

photographs the waveforms demonstrate a slow rise over which is superimposed an almost triangular wave pattern. The slow rise is caused by radial mode oscillation and this is particularly evident in the 1MHZ transducer, which has a much lower diameter/thickness ratio. It is interesting to note the influence of radial mode vibration under such conditions of high impedance electrical loading.

After application of the initial voltage step, both waveshapes show an exponential rise until the peak of the first triangle is reached. This corresponds to one transit interval, as described in section 6.3ii. The measured voltage at this point is denoted by Vo and this is related to the coupling coefficient by equation 4 i.e.

$$K = \left[\frac{Co+CB}{2CB} \ln\left(\frac{Co+CB}{Co}\left(\frac{1+Vo}{u}\right)\right)\right]^{1/2}$$

$$= \left[\tfrac{1}{2}\left(1+\frac{CB}{Co}\right) \ln\left(\left(1+\frac{CB}{Co}\right)\left(1+\frac{Vo}{u}\right)\right)\right]^{1/2}$$

where U is the amplitude of the applied step function of voltage.

Consequently, if Co, CB, Vo and u are accurately known, then the thickness mode coupling coefficient may be evaluated.

This was done for each transducer in turn by applying a step input of voltage to the blocking capacitor. It should be noted that CB must not be too large, or the measured secondary response becomes very small and is difficult to determine. This is readily observed from equation 3 where,

$$\frac{Vo}{u} \longrightarrow -1 \qquad \text{If } CB >> Co$$

i.e. the voltage induced by secondary action is completely damped out.

Consequently a blocking capacitance of 100pf was selected in each case. The value of capacitance was checked on a Wayne-Kerr Bridge in order to minimise experimental and measurement error. The following results were obtained.

a. 4MHZ transducer (see figure 6.15).

u = 150V

CB = 100pf Gives,

Co = 3.7723nF K = 0.484.

Vo = -2.1v (measured from the oscilloscope trace)

Diam/thickness = 43.7:1.

b. 2MHZ transducer.

u = 50v

Co = 1.87nF Gives,

Vo =-1.4v K = 0.483.

Diam/thickness = 21.16.

c. 1MHZ Transducer (see figure 6.15)

u = 50v

Co = 1.05nF Gives,

Vo =-2.42v K = 0.4876.

Diam/thickness = 10.7

d. 0.5MHZ Transducer

u = 50v

Co = 0.57nF Gives,

Vo =-4.22v K = 0.496

Diam/thickness = 5.33

These values are in very close agreement with the theoretical value of thickness mode coupling coefficient of 0.486. Even at the lowest diameter/thickness ratio, the percentage error is only 2%. Conventional measurement techniques (15) involve measuring the frequencies of electrical and mechanical resonance. This is extremely difficult for those transducers which possess

diameter/thickness ratios of less than 20. As demonstrated in Section 6.2iii, radial mode vibrations make accurate determination of the resonance frequencies extremely difficult due to multiple oscillations around these points. Although radial mode effects may be readily observed using the transient response technique, their effect over the first transit interval is very slight, hence allowing accurate measurements to be made over the entire transducer range.

This technique is very straightforward and easy to use, requiring only a fast, gate controlled electronic switch of low on resistance, a known value of blocking capacitance and an oscilloscope. However, the value of transducer static capacitance must also be accurately known and if possible, measured, as described in section 6.2iii.

It is also possible to predict acoustic impedance values by means of this technique. For example, the following expression which relates mechanical quantities to measured voltage may be obtained from equation 3.

$$TF + TB = \frac{2(Co+CB)}{CBK^2} \ln\left[\frac{Co+CB}{Co}\left(1+\frac{V_o}{u}\right)\right] \qquad \text{——— 5}$$

$$\therefore \quad \frac{Z_3}{Z_3+Z_1} + \frac{Z_2}{Z_3+Z_2} = \frac{Co+CB}{CBK^2}\left[\ln\left(\frac{Co+CB}{Co}\left(1+\frac{Vo}{u}\right)\right)\right]$$

$$= x \quad \text{say,}$$

Consequently, if K, Co, Vo and Z_3 are accurately known, then it is possible to estimate Z_1 or Z_2. For example, consider a transducer backed by a material of unknown acoustic impedance and loaded at the opposite face by air or a vacuum i.e.

$\frac{Z_2}{Z_3+Z_2} = x - 1$, Z_3 is the acoustic impedance of the transducer material

$$\therefore \quad Z_2 = (2-x)Z_3/(x-1) \qquad \text{——— 6}$$

To test the theory, it was decided to measure the acoustic impedance of a lead based compound which is used commercially as a transducer backing material. This substance (Devcon L) consists of lead (94%) and a plasticiser (6%). When mixed with suitable quantities of hardner, the material solidifies in a time which is proportional to the amount of hardning agent used in the process.

A transducer of electrical resonant frequency equal to 1MHZ was selected. The static capacitance was carefully measured and as described in section 6.2ii found to be 1.16nF. Figure 6.16 shows the transducer assembly after backing with the lead based compound.

The following data was used in the experiment:

$u = 50v$

$CB = 100pf$

$Z_3 = 33.712\ kg/m^2\text{-}s$

This produced a measured voltage of -2.4v across the transducer electrodes. Substituting these values into equations 5 and 6 produced the following value for the acoustic impedance of the backing material.

$Z_2 = 9.11 \times 10^6\ kg/m^2\text{-}s$

Figure 6.17 compares the experimental and theoretical voltages across the backed transducer, when a resistive load of 100Ω is connected in parallel with the device. The small resistive load damps out radial mode oscillations, permitting the study of thickness mode behaviour over several transit intervals. Once again, a 50v step input was applied to a blocking capacitor of 100pf. From the figure it may be observed that the two characteristics are in very close agreement, hence

corroborating the accuracy of the acoustic impedance measurement. Damping introduced by the backing material is readily seen from the increased decay of secondary piezoelectric action.

Although more experimental verification may be necessary, the transient technique appears extremely promising for the measurement of thickness mode coupling coefficient and acoustic impedance. Other authors such as Steutzer (55) and Kasai (17) have also reported on the use of transient response methods for determining piezoelectric properties.

In the analysis of Steutzer, in step function of charge was deposited on the transducer electrodes by means of a mechanical switch and a charged capacitor of very small value. The capacitor value had to be small in order to present a high reactance, thus isolating the transducer arrangement from associated supply electronics. Consequently, the method is only an approximation, being valid for these specified conditions. In addition, the high electrical impedance conditions result in strong radial mode disturbances. This method may only be applied to those devices possessing diameter to thickness ratios of greater than 20:1.

It is interesting to note that the results of Steutzer may be obtained from a limiting case of the present, more general transient response analysis. For a positive step function of charge, Steutzer obtained the following expression for measured voltage across the transducer electrodes (after one transit interval). The transducer is assumed equally loaded at both faces by a material of acoustic impedance Z_L.

$$Vo = \frac{Qo}{Co}\left[1-K^2\left(\frac{2Z_s}{Z_s+Z_L}\right)\right]$$

Where Qo = UCB is the applied charge function corresponding to a voltage of u volts.

$$Vo = \frac{UCB}{Co}\left[1-K^2.\frac{2Z_s}{Z_s+Z_L}\right] \qquad \text{————7}$$

From equation 3, for a negative going step input of voltage.

$$Vo = U\left(-1 + \frac{Co}{Co+CB}\exp\left[\frac{CB}{Co+CB}\,K^2\left(\frac{TF+TB}{2}\right)t/_T\right]\right)$$

From very small values of CB i.e.

CB<<Co, and using Maclaurin's Series Expansion,

exp [ ] ⟶ 1 + [ ]

$$\therefore Vo = U\left(-1 + \frac{Co}{Co+CB}\left[1 + \frac{CB}{Co+CB}K^2\left(\frac{TF+TB}{2}\right)\right]\right)$$ for t just less than T.

$$\therefore Vo = \frac{UCB}{Co+CB}\left(-1 + \frac{Co}{Co+CB}K^2\left(\frac{TF+TB}{2}\right)\right)$$

For CB<<Co and $TF = TB = \frac{2Z_s}{Z_s+Z_L}$, this expression becomes,

$$Vo = -\frac{UCB}{Co}\left(1 - K^2\frac{2Z_s}{Z_s+Z_L}\right) \qquad \text{——————8}$$

This is equivalent to equation 7, except that the input is a negative step function of voltage. In this analysis, the approximate method of Steutzer has been improved and extended to a more general situation, where almost any value of blocking capacitance may be used. However, the value of blocking capacitor must not exceed the transducer static capacitance by a large amount, otherwise secondary action is damped out, as described previously.

Furthermore, the method may be applied to a much wider range of transducers and excellent results were obtained for diameter/thickness ratios as low as 5. The improvement in accuracy is believed to arise because of two factors:

1) The method is exact, no longer requiring an approximation.

2) In the analysis of Steutzer, the transducer is effectively on electrical open circuit. Consequently, radial mode effects are at a maximum, leading to measurement difficulties in the case of low frequency transducers. However, in the present method, the transducer is electrically loaded by an impedance which is equivalent to the reactance of the blocking capacitor. This is apparently sufficient to reduce radial mode effects over the first transit interval, hence improving measurement accuracy. However, further investigation into this aspect will have to be performed, in order that radial mode effects can be predicted.

In the analysis of Kasai, a voltage step was applied to the transducer from a generator of internal resistance R_s. By measuring total current flow through the transducer, a series of curves were obtained, for which the thickness coupling coefficient was evaluated. It should be noted that the current quantity of interest (ie. that quantity proportional to K^2) is the feedback current described in chapter five. In cases where K is small, this current is correspondingly reduced and becomes difficult to measure. For example, it will be shown in the next

chapter that the feedback current depends also on the value of source resistance, becoming less as source resistance is increased. Consequently, this method may only be applied to those situations of low electrical source resistance.

In addition, the analysis of Kasai is applicable only for mechanically free transducers and the measurement of acoustic impedance cannot be made using this technique.

6.4. CONCLUDING REMARKS

In this chapter, operational impedance characteristics were used to determine a transducer voltage transfer function which relates source voltage to the measured voltage across the device. The theory was experimentally verified in both time and frequency domains for CW and transient modes of excitation. A variety of electrical and mechanical loading conditions were studied for a wide range of transducer dimensions and frequencies. The governing physical dimension was the transducer diameter/thickness ratio and this varied from approximately 5(0.5MH device) to 43(4MHZ device).

From the simulation, experimental and analytical results, the following main conclusions were drawn.

The CW investigation presented in section 6.2 showed experimental verification of the main transducer impedance characteristics under different mechanical loading conditions. A reduction in the amount of secondary piezoelectric action with increased mechanical loading was readily observed. In addition, the following features also emerged.

a. It is possible for substantial variations in some piezoelectric parameters to occur, particularly in the transducer dielectric constants. Unless otherwise corrected, this may cause considerable distortion in simulation and measurement studies.

b. The nature and extent of unwanted vibrational modes were clearly demonstrated. These effects were shown to complicate and influence transducer measurements, particularly at low values of diameter/thickness ratio.

c. The effects of internal dissipation on the behaviour of a mechanically free transducer were readily observed. However, under conditions of finite damping, it was shown that such losses may effectively be neglected for the type of transducer under consideration.

The transient analysis presented in section 6.3 demonstrated excellent agreement between simulation and experimental results. This not only verified some aspects of the transducer model, but provided a clear indication that the response characteristics of such a pulser-transducer configuration may be accurately predicted.

A method was also proposed for the measurement of thickness mode coupling coefficient and/or the acoustic impedance of solid loading media. This technique is considered an improvement over existing methods, as it enables fast, reliable measurements to be made on the transducer types under evaluation. The method possesses

the following additional advantages:

a. It is applicable over a wide range of transducer frequencies and dimensions.

b. It is simple and easy to use, requiring only a pulser, blocking capacitor and oscilloscope.

CHAPTER VII

SIMULATION AND RESULTS PART II

7.1. INTRODUCTION

This chapter presents a theoretical and experimental investigation of the transducer transfer functions described in chapters 3 and 4. Chapter 3 described the receiving transfer function for which a relationship between input force (stress) and output voltage was established in the S-domain. Chapter 4 outlined the derivation of the transmitting transfer function which relates input voltage to output force; again in the S-domain.

In subsequent sections, both transfer functions are investigated over a wide range of mechanical and electrical loading conditions. As in the previous chapter, transient and CW (or gated CW) modes of operation are considered separately, with essential simulation features being presented prior to the experimental results.

Particular emphasis is placed on the role of feedback in the simulation analysis and where possible the block diagram approach is used to explain transducer characteristics. Also, to maintain continuity with chapter 5, the investigation of both transfer functions involves current as the feedback quantity. Consequently, many of the simulation diagrams presented in chapter 5 are directly applicable to the present investigation, particularly for the transmitting mode.

The transfer functions are used to predict transducer response characteristics over a wide range of external loading conditions. Mechanical loading conditions of light, medium and heavy damping are considered in order to provide a representative cross section of practical operating situations. Electrical loading conditions are however more complex, depending upon the particular application. A generalised electrical load configuration is described extensively in Appendices B and C. This may be applied, (for both transmission and reception), to both transient and CW modes of operation.

Where possible, the transducers calibrated in the previous chapter were employed in the experimental sections of the work. The characteristics of each transducer are presented in Appendix D.

7.2. THE PIEZOELECTRIC TRANSMITTER TRANSFER FUNCTION

7.2(i) General Characteristics

A generalised transfer function relating input voltage to output force was obtained in chapter 4 with the corresponding block diagram shown in figure 4.8. For the present analysis, the block diagram may be rearranged as shown in figure 7.1, which indicates the summation of current quantities at the input summing point. By treating the

transmitting model in this manner, much of the analysis contained in chapter 5 may be directly applied to the feedback model. This not only maintains continuity, but also avoids unnecessary duplication of the simulation diagrams.

From figure 7.1, the voltage force transfer function may be expressed as follows:

$$\frac{F_F(S)}{e(S)} = \frac{-h\, C_o\, Z_I(S)\, K_F(S)\, A_F/2}{1 - \frac{K^2}{ST}\, Z_F(S)\, [K_F(S)\, T_F/2 + K_B(S)\, T_B/2]} \qquad \text{——— 1}$$

where

$$Z_I(S) = \frac{Z_E}{Z_o + Z_E + Z_o Z_E\, SC_o}$$

$$Z_F(S) = \frac{Z_E + Z_o}{Z_o + Z_E + Z_o Z_E\, SC_o}$$

Z_o represents the output impedance characteristics of the voltage generator or driving circuit, while Z_E is the impedance of any external electrical load connected directly across the transducer. The generalised form of these impedances is shown in figure 7.2 and a more detailed discussion is presented in Appendix B.

Adopting the notation used in chapter 5, equation 1 may be expressed in terms of a feedback factor, A_T

$$\frac{F_F(S)}{e(S)} = \frac{-hC_o\ Z_I(S)\ K_F(S)\ A_F/2}{1 - Z_F(S)\ A_T(S)}$$

where

$$A_T(S) = \frac{K^2}{ST}\left\{K_F(S)\ \frac{Z_C}{Z_C + Z_1} + K_B(S)\ \frac{Z_C}{Z_C + Z_2}\right\}$$

The functions A_T, K_F and K_B have been extensively investigated in chapter 5. They may readily be applied to an investigation of the piezoelectric transmitter provided that the electrical loading conditions are also known. Figure 7.1 reveals that the output stress wave is strongly dependent on both electrical and mechanical loading factors as a result of the constraints which they impose on both primary and secondary piezoelectric action. For example, the following parameters directly influence the forward path, ie primary piezoelectric action.

(i) The electrical load directly influences the nature of the output force or pressure waveform through the forward loop parameter Z_I. The extent of this influence depends on the form of Z_E and Z_o and although it is difficult to generalise, it should be noted that conditions which correspond to zero output force (Z_E zero, Z_o infinite) are unlikely to be encountered in practical situations.

(ii) The reverberation factor K_F also has a direct influence on the output pressure waveform, as a result of the external mechanical load conditions. Consequently, zero output is expected to occur at even multiples of mechanical resonance and in the absence of feedback, a maximum is expected at odd multiples of this resonance.

(iii) Zero output force occurs if the block $\frac{A_F}{2}$ is equal to zero, ie

$$\frac{Z_1}{Z_C + Z_1} = 0$$

Consequently, this condition only arises when the transducer operates in the mechanically free state ($Z_1 = 0$), or resonator mode. Such operating conditions do not apply to this chapter.

Secondary piezoelectric action is determined by the two feedback loops in the transmitter block diagram. The following factors are shown to influence the total amount of current feedback.

(i) Maximum current feedback is expected to occur under conditions of light mechanical loading. That is, for larger values of T_F, T_B, K_F and K_B. These conditions were discussed extensively in chapter 5 in relation to feedback effects on

transducer operational impedance.

(ii) The amount of secondary piezoelectric action is directly proportional to the square of the coupling coefficient.

(iii) Electrical load conditions also determine the amount of current feedback. Both feedback loops contain the factor Z_F and hence secondary piezoelectric action is expected to increase for low values of Z_E or Z_o, when maximum current may flow out of the transducer. In addition, the block Z_F will in general introduce a phase shift to the feedback loops. As indicated in chapter 5, such phase shifts can play a major role in determining the effects of secondary piezoelectric action. It is interesting to note that the impedance characteristics discussed in chapter 5 were actually derived from a limiting case of this general configuration. That is, no external electrical loading connected across the transducer and Z_o set to zero. Z_F is thus equal to unity and the total amount of current feedback is determined by A_T.

(iv) As in the case of electrical impedance, the current feedback is inversely proportional to frequency.

In the following section, the main characteristics of the voltage force transfer function are presented in both time and frequency domains. Computer simulation was performed on the 4051 graphics terminal and a complete listing of the program is described in Appendix E. It was thus possible to study the transmitting response over a wide variety of electrical load conditions, mechanical load conditions and electrical input stimuli. As demonstrated in the present section, a block diagram approach greatly enhances the identification of those elements which have a major influence on system performance.

7.2ii Investigation of the Transmission Transfer Function Using Simulation Techniques

This section investigates the response characteristics of the transmission transfer function. The set of mechanical load conditions described in the previous two chapters are again considered. That is, light damping (water loaded and water backed), medium damping (50 per cent matched backing and a glass load) and heavy damping (ideal backing, glass load). Unless otherwise stated, the nominal transducer parameters shown in Table 5.1 are used in the simulation diagrams. The value of piezoelectric constant, h, was taken to be 21.5×10^8 v/m (Vernitron). The section covers both CW and transient modes of operation, over a variety of electrical load conditions.

7.2iii CW Operation

1. The Electrically Free Transducer Driven by an Ideal Voltage Generator

This is an idealised situation where the transducer is on electrical open circuit and is driven via a sinusoidal voltage generator possessing zero output impedance, ie

$$Z_o = 0$$
$$Z_E = \infty$$

It should be noted that for Z_o equal to zero, then the resultant voltage force transfer function is actually independent of Z_E, ie Z_I and Z_F are both equal to unity. The electrical driving conditions thus correspond to those described in the analysis of the mechanically loaded impedance transfer function. Consequently, the amount of current feedback is the same and the voltage force transfer function may be expressed as follows:

$$\frac{F_F(S)}{e(S)} = \frac{-hC_o\ K_F(S)\ A_F/2}{1 - A_T(S)}$$

I_T is the total current flowing through the transducer and its Laplace transform is described by the following equation:

$$I_T(S) = \frac{SC_o}{1 - A_T(S)}$$

therefore

$$\frac{F_F(S)}{e(S)} = -I_T(S)\ h/S\ K_F(S)\ A_F/2$$

I_T is equivalent to the reciprocal of the transducer electrical impedance, Z_T, under conditions of unit applied voltage. Consequently, current minima and maxima are expected to occur, the position and extent of which are determined by the amount of feedback. The process is clearly illustrated in figure 7.3 which shows the total current (I_T) as a function of frequency for the three specified conditions of mechanical damping. As expected, maximum current fluctuation occurs under conditions of light damping, when secondary piezoelectric effects are a maximum. The current characteristic starts to smooth out as damping is increased, indicating a reduction in the amount of feedback. The dotted line in figure 7.3 indicates current flow through a capacitance of value equal to C_o, the transducer static capacitance. That is, the total current flow under conditions of zero feedback.

Transducer current is not the only quantity which influences the voltage force transfer function. The transfer function may be expressed as follows:

$$\frac{F_F(S)}{e(S)} = -\ I_T(S)\ \frac{h}{S}\ K_F(S)\ A_F/2$$

$$= -I_T(S)\ F_P(S) \qquad \text{2}$$

On a physical basis, the term h/S represents a conversion factor from current to force, while K_F and A_F are the reverberation and transmission factors defined in chapter 4, Section 4.5. F_P is defined as the forward path transmission parameter and its frequency response characteristics are shown in figure 7.4, for the three conditions of mechanical load. From this figure it is evident that mechanical damping has a considerable influence on the response, particularly at lower frequencies. It should also be noted that the parameter F_P is simply proportional to the time integral of the reverberation factor K_F. Consequently, a finite (non-zero) response occurs at zero frequency, which is given by the following expression.

$$\lim_{\omega \to o} F_P = \frac{hA_F}{2}\, T \left(\frac{1 - R_B}{1 - R_F R_B} \right)$$

$$= \frac{hT}{Z_C} \left(\frac{Z_1 Z_2}{Z_1 + Z_2} \right)$$

The low frequency magnitude of F_P is large when both impedances Z_1 and Z_2 are relatively high, ie under conditions of heavy damping. This may readily be observed from figure 7.4 for frequencies up to the fundamental mechanical resonance, denoted by f2. For frequencies above f2, the amplitude response of F_P generally decreases as a result

of the 1/S multiplier contained in the function. However, the main characteristics inherent in K_F remain evident, for example, the increase in bandwidth under higher damping conditions.

The voltage force transfer function frequency response may now be obtained by multiplying the total current response by the forward path transmission parameter response, as described in equation 2. This is shown in figure 7.5 for the same three conditions of mechanical load. It is evident from the figure that considerable variations occur in bandwidth as the damping changes.

In addition, the position of the first centre frequency is also observed to decrease under conditions of heavy damping. This occurs directly as a result of the low frequency characteristics of F_p, which tends to reduce the centre frequency under conditions of heavy damping.

The differences in bandwidth are mainly attributed to the nature of the reverberation factor K_F; bandwidth increasing in proportion to the degree of damping. The position of the first centre frequency is lower than the frequency of mechanical resonance in each case and this is primarily influenced by the amount of feedback for conditions of light and medium damping. Also, as the amount of feedback

decreases with frequency, the frequencies of maximum output eventually approach the harmonic frequencies of mechanical resonance. A similar shift in the frequency of maximum output is also observed wth a decrease in coupling coefficient. Figure 7.6 shows the transfer function response for two values of K, corresponding to 0.7 and zero. The latter value is equivalent to zero feedback.

It should be noted in figure 7.5 that no general decrease in output force takes place as frequency is increased. However, it must be remembered that this is an idealised situation which assumes an ideal voltage generator and the transducer to be mechanically loss free. In practice, there is a decrease in the amplitude response with frequency.

To summarise, the following conclusions may be drawn concerning the output force frequency characteristics when the transducer is electrically driven via an ideal voltage generator:

a) The response is independent of any electrical load connected across the transducer.

b) Under conditions of light mechanical loading, the frequency of peak output force is dominated by the effects of current feedback. The system is essentially narrow-band and the first centre frequency approximates closely to the electrical resonant frequency of the transducer.

c) Under conditions of heavy damping, the effective bandwidth is increased and the peak output frequency (first centre frequency) decreases to below the electrical resonance.

2. The Electrically Loaded Transducer Driven from a Non-Ideal Generator

For the electrically loaded transducer, the voltage force transfer function is still defined by equation 2, ie

$$\frac{F_F(S)}{e(S)} = -I_T(S)\ F_P(S)$$

The function F_P is independent of electrical load conditions. However, the total current flowing through the transducer must now be expressed as follows:

$$I_T`(S) = \frac{SC_o\ Z_I(S)}{1 - Z_F(S)\ A_T(S)}$$

The feedback factor for the electrically unloaded transducer is given by A_T. Denoting the feedback factor under electrically loaded conditions by $A_T`$ yields,

$$A_T`(S) = A_T(S)\ Z_F(S)$$

therefore

$$\left|A_T`(\omega)\right| = \left|A_T(\omega)\right|\left|Z_F(\omega)\right|$$

$$\angle A_T`(\omega) = \angle A_T(\omega) + \angle Z_F(\omega) \qquad \text{——————} \quad 3$$

Consequently the amplitude and phase of the feedback factor is modified by the presence of the feedback impedance Z_F.

In addition, the total input current to the transducer under electrically free conditions is given by (for unit applied voltage),

$$I(S) = SC_o$$

Consequently, the input current under electrically loaded conditions may be expressed as:

$$I`(S) = SC_o \, Z_I(S) = I(S) \, Z_I(S)$$

therefore $$\left|I_T`(\omega)\right| = \left|I(\omega)\right| \left|Z_I(\omega)\right|$$

In the following examples, a wide range of electrical loading conditions are considered. Amplitude and phase characteristics relating to input current and feedback impedance are shown in figures 7.7-7.9b for the following conditions of electrical load:

- Generator output resistance of 50Ω
- Inductances of 2.2 μH (L_o) in series with 50Ω generator resistance
- Inductances of 2.2 μH (L_M) in parallel with the transducer. The generator resistance is 50Ω.

Consider firstly, the situation of a non-ideal voltage generator driving the transducer. This configuration is shown in figure 7.10, where the generator is assumed to possess an output resistance equal to R_o ohms.

In this case,

$$\left|I\hat{}(\omega)\right| = \omega C_o/(1 + \omega^2 R_o^2 C_o^2)^{\frac{1}{2}}$$

This quantity is shown in figure 7.7, for R_o equal to 50 ohms. For unit input voltage, the maximum value of input current is now limited to $1/R_o$.

The magnitude and phase of the feedback factor are now given by:

$$\left|A_T\hat{}(\omega)\right| = \left|A_T(\omega)\right|/(1 + \omega^2 R_o^2 C_o^2)^{\frac{1}{2}}$$

$$\angle A_T\hat{}(\omega) = \angle A_T(\omega) - \tan^{-1}(\omega R_o C_o) \qquad \text{——————} 4$$

The magnitude of the feedback current thus demonstrates an additional, frequency dependent decrease which is governed by the time constant $R_o C_o$. Feedback current, and hence secondary piezoelectric action is thus reduced for larger values of R_o. This is readily shown in figure 7.11 which shows the variation in feedback factor for three values of source resistance, corresponding to 0, 50 and 470 ohms. The reduction in secondary action for higher values of source resistance (and frequency) may readily be observed.

Phase angle of the feedback factor is also modified by the finite value of source resistance, the phase shift increasing with frequency as a result of equation 4. The degree of phase shift, for a source resistance of 50Ω, is shown in figure 7.9a. This has important consequences under conditions of light damping, where the type of feedback has a considerable influence on the nature of the total output current. The nature of these effects may be illustrated as follows.

Figure 7.12 depicts the total current response for a source resistance of 50Ω and the three stated conditions of mechanical load. For conditions of light damping, a comparison with figure 7.3 indicates that the 50Ω source resistance has reduced the total current, especially at the positions of current maxima. However, at frequencies below mechanical resonance (f2), attenuation introduced by the source resistance is very small. For example, figure 7.8 shows that the feedback impedance is approximately unity within this frequency range, resulting in almost zero attenuation of feedback current. This is reflected in figure 7.11 which shows that the magnitude of the feedback factor is almost unchanged by the introduction of a 50Ω source resistance. As a result, secondary action within this frequency range should not show the reduction indicated in figure 7.12.

However, a close study of figure 7.9a reveals a phase shift in the feedback factor of approximately 20^{o} at the frequency of mechanical resonance. This phase shift in the feedback loop saves to reduce the amount of positive feedback in a manner analogous to that described in chapter V, for the mechanically loaded transducer. As a result, the first current maximum in figure 7.12 has been substantially reduced, indicating a reduction in the effects of secondary action.

The overall current attenuation and phase shift increases with frequency, leading to greater reductions in current fluctuation. Eventually feedback effects disappear and the total current tends towards $1/R_{o}$.

The amount of feedback is also significantly reduced under conditions of increased damping. This occurs as a result of additional phase shifts in the feedback loop which smooth out current fluctuations. Consequently, amplitude and phase changes in the feedback factor which arise directly from a finite value of source resistance have proportionally less effect under conditions of heavier damping. However, as may be observed from figure 7.12, the source resistance serves to further minimise feedback induced current fluctuations.

The output force characteristics are readily obtained from the product of $I_{T}`(\omega)$ and $F_{p}(\omega)$. These are shown for two

values of source resistance, 50Ω and 470Ω in figures 7.13a (light damping), 7.13b (medium damping) and 7.13c (heavy damping). From these graphs, the following main features are apparent:

a) Increasing source resistance reduces the peak amplitude of the frequency response characteristic. This is to be expected, as a result of the relative attenuation in input current. For the same reason, the responses exhibit a general decrease with frequency.

b) The amount of feedback decreases with source resistance and frequency. This is verified by a general shift in centre frequency towards mechanical resonance and its harmonics.

c) Overall system bandwidth demonstrates a general increase with increased mechanical loading.

It should also be noted that under conditions of light damping, relatively small values of source resistance have a considerable effect on the frequency response characteristics. This is readily verified by comparing figures 7.13a and 7.5 for the water backed and water loaded transducer. The response under lightly damped conditions is dominated by secondary piezoelectric action and hence any changes in the feedback loop caused by electrical loading are readily observed in the output force characteristic.

This effect is not so marked under conditions of increased damping, where electrical loading has relatively less influence.

Before concluding this section, it is interesting to compare the output response under conditions of zero feedback. Figures 7.14(a-c) show the output force characteristics under open loop conditions for source resistances of 50Ω and 470Ω. From the graphs it may be observed that for higher damping and source resistance a close approximation to the closed loop responses of figures 7.13(b and c) is obtained. However, in the lightly damped situation, a close approximation occurs only at higher frequencies, where feedback effects are reduced. It should also be noted that an increase in -3db bandwidth occurs under closed loop conditions. This may readily be observed by comparing figures 7.13a and 7.14a, for a source resistance of 50Ω. The increase in -3db bandwidth under closed loop conditions is discussed again in later sections.

To summarise, the following main features emerge concerning the influence of generator resistance on the output force response.

i Increasing source resistance serves to decrease the input current to the transducer, especially at higher frequencies. The output force response thus generally demonstrates a decrease with frequency.

ii Increasing source resistance decreases the amount of secondary action, feedback effects becoming almost negligible for high values of source resistance.

iii Relatively small values of source resistance may have considerable effects on the output force characteristics under conditions of light damping. Phase shifts in the feedback loop are responsible for this phenomenon by causing a reduction in the amount of positive feedback.

The investigation of inductive loading follows in a similar manner. Figure 7.15 shows two possible configurations where the inductor is placed in series or in parallel with the transducer. In each case the generator has an output resistance of R_o ohms.

Consider firstly an inductive element placed in series with the transducer configuration, as shown in figure 7.15a. The Laplace transform of the input current is thus given by,

$$I(S) = SC_o Z_I(S)$$

$$= \frac{SC_o}{S^2 L_o C_o + SC_o R_o + 1}, \text{ and}$$

$$Z_F(S) = \frac{1}{S^2 L_o C_o + SC_o R_o + 1}$$

For an inductive element placed in parallel with the transducer, as shown in figure 7.15b, the input current and

feedback impedance may be expressed by the following transform equations:

$$I^{\wedge}(S) = \frac{S^2 C_o L_M}{R_o(1 + S^2 L_M C_o) + SL_M}$$

$$Z_F(S) = \frac{R_o + SL_M}{R_o(1 + S^2 L_M C_o) + SL_M}$$

Under both series and parallel loading conditions, the inductive elements resonate electrically with the transducer static capacitance at a frequency given by,

$$f_{res} = \frac{1}{2\pi (LC_o)^{\frac{1}{2}}}$$

The magnitude and phase of input current and feedback impedance are shown in figures 7.7 through to 7.9b for both series and parallel inductive loading. Values of inductance selected for the diagrams were 2.2 μH and 20 μH, corresponding to tuned resonant frequencies of 3 MHz and 1 MHz respectively.

From the figures, it is apparent that inductive loading may exert a considerable influence on the input and feedback current characteristics of the piezoelectric transmitter. As a result changes in bandwidth and centre frequency may readily be achieved by the appropriate choice of inductive matching element. This is demonstrated in figures 7.16

and 7.17 which show the frequency response characteristics for both types of inductive matching under mechanical load conditions corresponding to light, medium and heavy damping.

Figure 7.16 outlines the response when a 2.2 μH inductor is connected in parallel with the transducer. As a result, the centre frequency is increased to approximately 3 MHz for each mechanical load configuration. This shift in centre frequency may be attributed directly to the relatively low level of input current at lower frequencies, as indicated in figure 7.7.

Figure 7.17 shows the frequency response characteristics when an inductance of 20 μH is placed in series with the transducer element. In this example, the overtone frequencies of mechanical resonance have been suppressed and the -3db bandwidth about the fundamental resonance has been increased. A study of the input current characteristic in figure 7.7 indicates a sharp peak about tuned resonance, followed by a rapid decay as frequency increases. Consequently, the output force contribution at higher frequencies is substantially reduced.

Also, from figure 7.17, it is interesting to note the twin peaks on either side of mechanical resonance. This is most evident under conditions of light damping and is due mainly to the influence of secondary piezoelectric action. It is evident from figures 7.8 and 7.9a that the series

inductance has considerable influence on the magnitude and phase characteristics of the feedback current. Consequently, the well defined maximum occurring near electrical resonance is no longer apparent and the complex characteristic of figure 7.17 is formed as a result.

In summary, the following main conclusions may be drawn concerning the effects of inductive loading on the output force frequency response.

a) Bandwidth and centre frequency may be selected by the appropriate choice of inductive matching element. The inductance may be placed in series or in parallel with the transducer. A series element usually enhances low frequency response while a parallel element usually enhances high frequency response.

b) The response is most easily predicted under conditions of heavy damping, when secondary action is a minimum. Under lightly damped conditions, the effects of secondary action are difficult to predict, because of complex magnitude and phase changes within the feedback loop. In such instances, the complete transmission model must be used to accurately determine frequency response.

7.2iv Transient Operation

This section investigates transmission behaviour under transient conditions, in both time and frequency domains. The

transducer is driven by the application of a negative going step function to a blocking capacitor via a fast electronic pulser. A complete description of this mode of operation is provided in Appendix C. As a result, the output force may be expressed by the following Laplace equation:

$$F_F(S) = \frac{1}{S} \quad \frac{hC_o \, Z_I(S) \, K_F(S) \, A_F/2}{1 - Z_F(S) \, A_T(S)} \qquad \text{5}$$

This equation was evaluated in both time and frequency domains for a variety of electrical and mechanical load conditions. A description and listing of the software is presented in Appendix F.

Consider firstly, the transducer to be free of any parallel electrical loading as shown in figure 7.18. This is equivalent to applying a step input of voltage across the transducer electrodes. The pulser is assumed to possess an extremely low value of internal resistance (<5Ω) and consequently,

$$Z_o(S) = \frac{1}{SC_B}$$

$$Z_I = \frac{C_B}{C_o + C_B} = Z_F$$

Z_I and Z_F are thus reduced for lower values of blocking capacitance. Frequency spectra of the output force are shown in figures 7.19(a and b) for two values of C_B, corresponding to 2 nF and 0.1 nF respectively. Transducer static capacitance was 1.261 nF, as indicated in Table 5.1. Mechanical load conditions of light, medium and heavy damping are shown. The following main features are apparent from the figures.

a) The peak amplitudes are substantially reduced for the lower value of blocking capacitor. This is to be expected from the corresponding reduction in Z_I.

b) Secondary action is reduced for the lower value of blocking capacitance. This is evident from the shift in centre frequency towards mechanical resonance (1 MHz), under conditions of light damping. The reduction in secondary action may be attributed to the decrease in Z_F, the feedback impedance. This is not apparent under increased damping, where the effects of secondary action are reduced.

c) The bandwidth increases under conditions of increased mechanical load. Under lightly damped conditions, the spectrum is narrow band, centred between electrical and mechanical resonance, depending on the value of blocking capacitance.

In conclusion, it is possible to eliminate secondary action in such a transmitting system by selecting a low value of blocking capacitance. This is of course equivalent to increasing source impedance, hence preventing current flow out of the transducer. Secondary action is thus inhibited, as described in Section 7.2iii.

Some authors, for example Filipczynski (11) have employed this technique in order to model transducer transient response. However, as indicated in figure 7.19b, secondary action is by no means eliminated under conditions of light damping, even for C_B equal to 100 pf. Consequently, for transducers of high coupling coefficient ($K > \cdot 5$) and low damping, such an approximation is only valid if the blocking capacitance is very small ($C_B < 5$ pf); resulting in an extremely inefficient transmission system.

The corresponding time domain responses are shown in figures 7.20(a and b) for the large and small values of blocking capacitance respectively. Both wave forms are observed to comprise a train of positive exponential functions, alternatively in sign at integral multiples of the transducer transit time. The exponential slope is greater for the higher value of blocking capacitance, although in this case, the signal tends towards sinusoidal behaviour after a few transit intervals. Considerable distortion is also evident.

Excellent insight into the nature of these responses may be achieved by truncating the time domain to a single transit interval, ie $0 < t < T$. During this time interval, the reverberation factors K_F and K_B are unity and hence equation 5 may be expressed as follows:

$$F_F(S) = \frac{\frac{1}{S} hC_o \cdot A_F/2 \cdot Z_I(S)}{1 - \frac{K^2}{ST} Z_F(S) \left\{\frac{T_B}{2} + \frac{T_F}{2}\right\}}$$

$$= \frac{Z_I K_1}{S - K_2 Z_F}$$

$$= \frac{CK_1}{S - CK_2}$$

where,

$$C = \frac{C_B}{C_o + C_B}, \quad K_1 = \frac{hC_o A_F}{2}, \quad K_2 = \frac{K^2}{T} \left\{\frac{T_B}{2} + \frac{T_F}{2}\right\}$$

This function has an inverse haplace transform given by,

$$F_F(t) = CK_1 e^{K_2 C t} \qquad 0 < t < T$$

therefore

$$F_F(t) = \frac{C_B}{C_o + C_B} \frac{hC_o A_F}{2} \exp\left[\frac{C_B}{C_o + C_B} K^2 \left\{\frac{T_F}{2} + \frac{T_B}{2}\right\} t/T\right] \qquad \text{——6}$$

$$0 < t < T$$

Under conditions of no feedback (for example, K = 0) the output force over this time interval is a step function of amplitude $[C_B/(C_o + C_B)].hC_o A_F/2$. The exponential term in equation 6 describes secondary piezoelectric action. As expected, secondary effects depend on coupling coefficient, mechanical damping and electrical loading conditions. This may readily be observed by comparing figures 7.20(a and b). Over the truncated time interval, the exponential rise is greater in the former figure, indicating enhanced secondary action.

It is evident from these figures that secondary action may introduce considerable distortion to the output force waveform. Under conditions of zero feedback, the time domain response consists of a train of decaying step functions, the rate of decay being proportional to the amount of mechanical damping. As secondary action increases, an exponential rise is associated with each step function, as observed in figure 7.20b. When feedback is further increased, the exponential characteristics become difficult to distinguish after a few transit intervals. The waveshape demonstrates a series of sharp spikes which eventually approximate towards sinusoidal behaviour. This latter phenomenon was also observed by Steutzer (54) in his analysis of transducer current behaviour under short circuit conditions. Under these conditions, current feedback is of course a maximum.

As a second example of transient time-domain response, consider the transducer to be loaded by a resistive element connected across the electrodes. This configuration is shown in figure 7.21.

Time domain waveforms were simulated under two conditions of mechanical load, corresponding to medium and heavy damping. The following system characteristics were used in the simulation diagrams.

$$C_B = 2.2 \text{ nF}$$

$$C_o = 1.261 \text{ nF}$$

$$K = 0.5$$

$$R_E = 100\Omega$$

Mechanical Resonance = 1 MHz

Figures 7.22(a and b) outline the responses under conditions of medium and heavy damping respectively. From these diagrams, the following main features are apparent:

a) Signal bandwidth is increased under heavily damped conditions. The effective pulse length is reduced to little more than two transit intervals plus a low amplitude exponential 'tail'. This latter feature is proportional to the exponentially decaying driving voltage, which has an effective time constant of $(C + C_B)R_M$, where C is the value of transducer capacitance. Features of the driving voltage under such conditions were discussed in

chapter VI. For heavy damping (matched backing), no reflections occur from the transducer rear face, as all energy is transmitted to the backing material. Consequently reverberation within the transducer is eliminated, giving rise to the waveshape shown in figure 7.22b.

b) For both conditions of mechanical load, there is little evidence of the positive exponential behaviour previously associated with secondary action. This may be attributed firstly to the reduction in positive feedback with increased damping. Secondly, charge generated by secondary action may now decay through the load resistance, ie the negative exponential nature of the driving waveform serves to suppress the effects of secondary action. This is evident under conditions of medium damping, as shown in figure 7.22a. The exponential nature of the waveform is a combination of a positive exponential function (secondary action) and a negative exponential (driving voltage). The net result is a flattening of the waveshape, although in this instance, driving voltage is the dominant factor. However, after two transit intervals, the driving voltage has decayed sufficiently to be in turn, overcome by secondary effects. This is evident during the third transit interval in figure 7.22a, where a positive exponential is observed.

Under conditions of heavy damping (figure 7.22b), little secondary action is evident, as indicated by the negative exponential characteristics of the waveform.

In summary, the following conclusions may be drawn concerning the nature of transient time-domain behaviour for the piezoelectric transmitter:

i) Over the first transit interval, the waveform of force is similar to the driving voltage. This is repeated with alternate sign reversals, at multiples of the transit interval. There is an overall amplitude decay with time, the rate of which is proportional to mechanical damping. Increasing damping reduces the number of internal reflections, hence increasing signal bandwidth.

ii) Secondary effects are reduced under conditions of high source impedance, low mechanical coupling and high mechanical damping.

iii) Secondary action may introduce considerable distortion to the time domain waveshape. This is particularly evident under conditions of light mechanical load.

A further investigation of transient time-domain behaviour is performed in Section 7.4 where comparisons are made between simulation theory and practical measurement.

7.3 THE PIEZOELECTRIC RECEIVER TRANSFER FUNCTION

7.3i General Characteristics

A transfer function describing the behaviour of a piezoelectric receiver was obtained in Chapter III. The subsequent block-diagram relating force to voltage is shown in figure 3.14, which clearly illustrates the various physical processes involved. This transfer function may be expressed as follows:

$$\frac{V_o(S)}{F_F(S)} = \frac{-T_F\, U(S)\, K_F(S)\, \frac{h}{SZ_C}}{1 - U(S)\, \frac{h}{SZ_C} \left\{ \frac{hY_E}{S} \left[K_F(S)\, \frac{T_F}{2} + K_B(S)\, \frac{T_B}{2} \right] \right\}}$$

Where V_o is the output voltage observed across the transducer electrodes when a wave of force F_F is incident on the front face of the device. An arbitrary electrical load of impedance Z_E is assumed to be connected across the electrodes. Other factors in the transfer function are:

$$U(S) = \frac{SC_o\, Z_E(S)}{1 + SC_o\, Z_E(S)}$$

This is the voltage attenuation factor introduced by the external electrical load.

$$Y_E = \frac{1}{Z_E}$$

is defined as the feedback admittance.

Substituting for U(S) and noting that,

$$\frac{h^2 C_o}{Z_C} = \frac{K^2}{T}$$

the transfer function may be expressed as follows:

$$\frac{V_o(S)}{F_F(S)} = \frac{-T_F\ K_F(S)\ \frac{h}{SZ_C}\ \frac{SC_o\ Z_E(S)}{\{1 + SC_o\ Z_E(S)\}}}{1 - \frac{1}{\{1 + SC_o\ Z_E(S)\}}\ \frac{K^2}{ST}\left[K_F(S)\ \frac{T_F}{2} + K_B(S)\ \frac{T_B}{2}\right]}$$

$$= \frac{-T_F\ K_F(S)\ \frac{h}{SZ_C}\ U(S)}{1 - Z_{FR}(S)\ A_T(S)} \qquad \text{——————————} \quad 7$$

where

$$Z_{FR}(S) = \frac{1}{1 + SC_o\ Z_E(S)}$$

This quantity is defined as the feedback impedance for the transducer operating in the receiving mode. Consequently, an investigation of equation 7 may proceed by adopting similar techniques to those employed for the piezoelectric transmitter. For example, the influence of secondary piezoelectric effects may be investigated by considering the known characteristics of the feedback factor A_T to be modified in both amplitude and phase, by

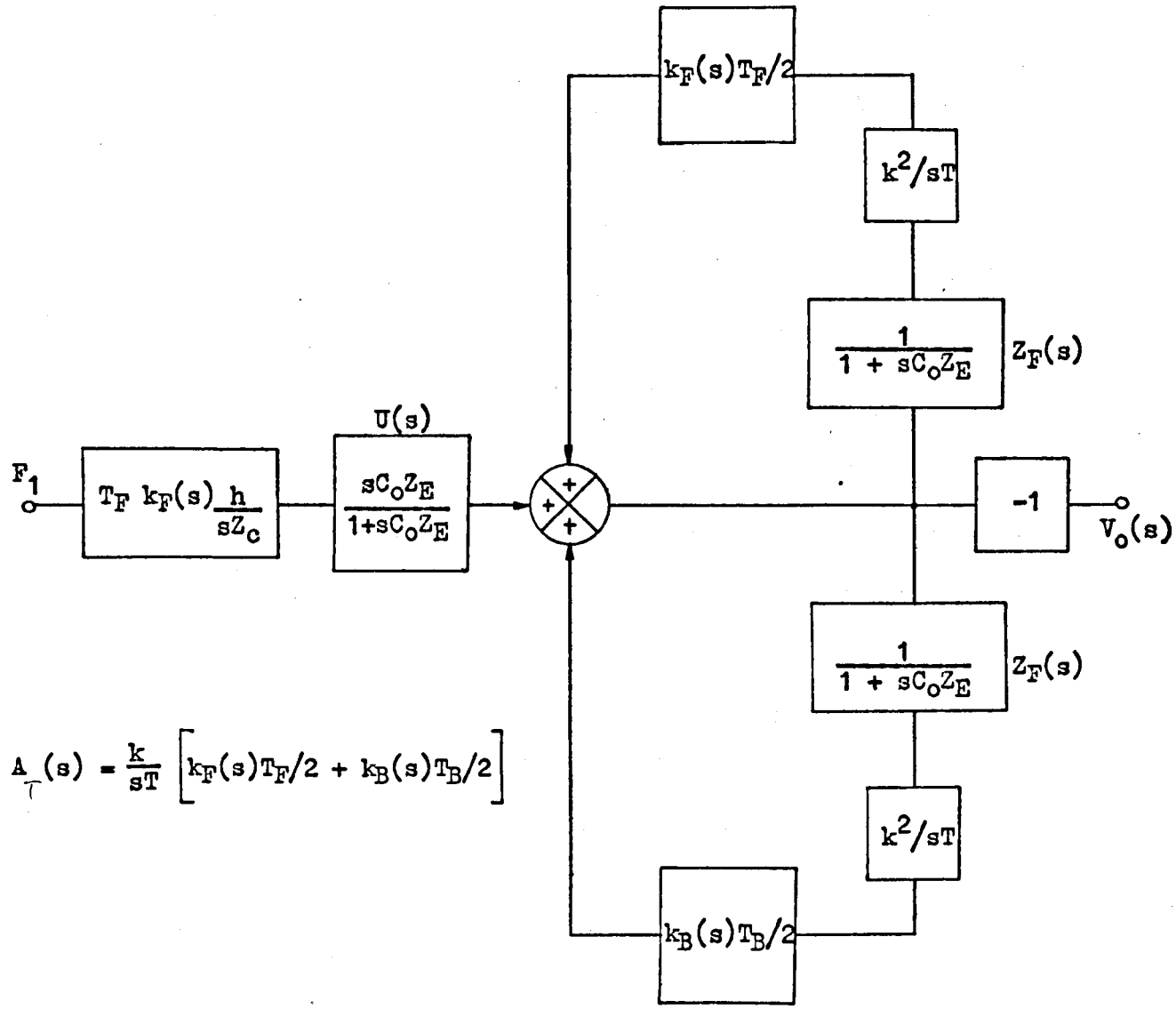

Fig. 7.23. Simplified Block Diagram of a Piezoelectric Transducer in the Receiving Mode

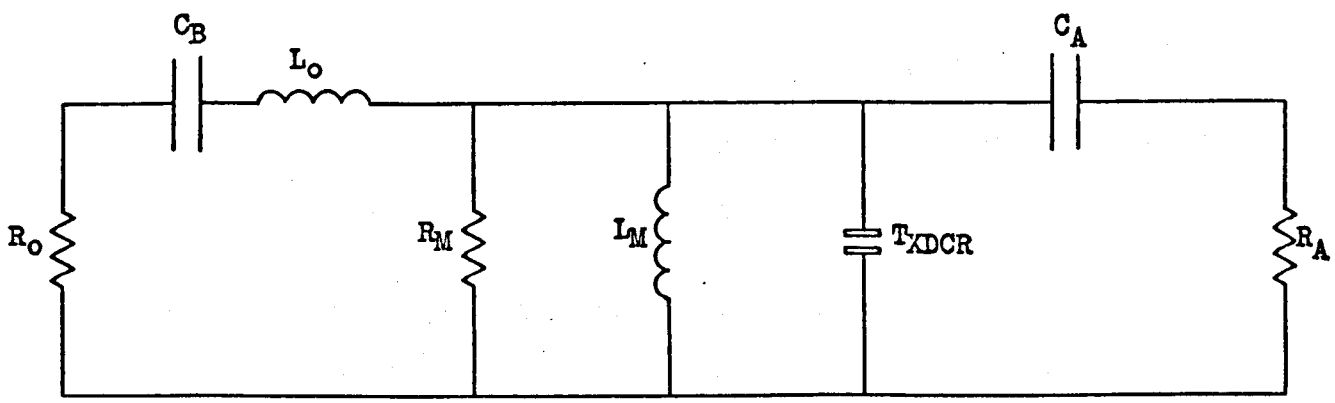

Fig. 7.24. General Electrical Loading Conditions for the Pulse-Echo Receiver

a contribution from Z_{FR}. In a similar manner, the effects of electrical loading on the forward path may be considered by an appropriate investigation of the attenuation factor U. A block diagram corresponding to equation 7 is shown in figure 7.23 where voltage quantities are combined at the input summing point.

From this diagram it is apparent that no secondary action may occur if the transducer is electrically open circuit. That is, no external electrical loading elements are connected across the device. In this situation, the transfer function is open loop and the response is proportional to the time integral of the reverberation factor K_F. The maximum amount of secondary action occurs under short circuit conditions, when the output voltage is of course zero.

The amount of secondary action is also dependent on the feedback factor A_T, and hence is expected to decrease with increased frequency and external mechanical loading. In subsequent sections the receiving response is investigated under a variety of loading conditions and by means of the feedback model, those factors having a significant influence on the response are readily isolated.

As in the case of the transmitter, a computer program was developed in order to investigate the receiver transfer function in both time and frequency domains. A complete

listing of this program is provided in Appendix F. Electrical loading conditions were generalised so that system analysis could be made over a wide, practical range of operating conditions. A complete discussion on electrical loading of the receiving transducer is given in Appendix B. Figure 7.24 outlines the general electrical loading conditions for the pulse-echo receiver. In this figure, the branch R_O-C_B-L_O represents the output characteristics of the transmitting circuit and R_M-L_M the impedance network of any matching or pulse shaping circuit. The branch C_A-R_A is chosen to represent amplifier coupling and input impedance characteristics respectively.

7.3ii Investigation of the Reception Transfer Function Using Simulation Techniques

This section investigates the frequency response characteristics of the receiver transfer function under the following conditions of mechanical load:

light damping (water loaded and water backed)
medium damping (50% matched backing, glass load)
heavy damping (ideal backing, glass load)

In addition, the following electrical load conditions are also investigated:

a. The transducer is electrically isolated. That is, all external loading components are assumed to possess such

large values of impedance that the device may be considered on electrical open circuit. Such a situation may arise under transient conditions when the input impedance of any pre-amplifying stage is large (approximately 50 kΩ or greater).

b. The transducer is loaded by a resistive element connected across the electrodes. This component may correspond to a pulse shaping element in pulse echo mode, or to the input resistance of any successive stage.

c. An inductive element is connected across the transducer. Again this may form part of a matching or pulse shaping network.

i) Consider firstly an electrically isolated receiver. In this situation no current may flow out of the transducer and hence secondary piezoelectric action is completely inhibited. The transfer function is thus open loop and may be expressed as follows:

$$\frac{V_o(S)}{F_F(S)} = -T_F \frac{K_F(S)}{S} \frac{h}{Z_C}$$

On a physical basis, T_F is the transmission coefficient for waves of force entering the transducer, $1/SZ_C$ is a conversion factor relating force to particle displacement and K_F is a reverberation factor describing the difference

in particle displacement between opposite faces of the device. The piezoelectric constant, h, relates particle displacement to voltage. By substituting for h/Z_c, the transfer function may be expressed as follows:

$$\frac{V_o(S)}{F_F(S)} = \frac{-T_F}{hC_o} \frac{K^2}{T} \frac{K_F(S)}{S}$$

It is evident from this equation that the output voltage is proportional to the time integral of the input force. Consequently, the behaviour of the function is similar to that of the forward path transmission factor (F_p), described in Section 7.2ii. That is, the frequency response generally has a finite value at zero frequency (d.c.) which is a function of the mechanical load conditions.

Figure 7.25 shows the open-circuit receiver frequency response for the three stated conditions of mechanical load. The following main features are evident from the figure.

i.i) Maximum response occurs under conditions of light damping. Since there is no secondary action, peak output occurs at the fundamental mechanical resonance. Other peaks are evident at overtones of this frequency, but they are of much lower amplitude. The system is essentially narrow band.

i.ii) As damping is increased, the peak response is considerably reduced, with maximum response occurring at

frequencies below mechanical resonance. The frequency of maximum output is dependent upon the degree of damping.

i.iii) In all three cases there is a finite response at zero frequency, the magnitude of which depends on the amount of mechanical loading. Under such conditions, the transfer function may be expressed as follows:

$$\frac{V_o}{F_F}_{\omega \to o} = -T_F \frac{h}{Z_C} T \frac{(1 - R_B)}{(1 - R_F R_B)}$$

$$= \frac{-T_F K^2}{hC_o} \frac{(1 - R_B)}{(1 - R_F R_B)}$$

$$= \frac{-2 K^2}{hC_o} \frac{Z_2}{Z_1 + Z_2} \qquad \text{8}$$

For example, when the transducer is equally loaded at both faces, the magnitude of the transfer function is equivalent to K^2/hC_o. Consequently, for the water loaded, water backed transducer, $hC_o = 2.7$ and $K = 0.7$, the transfer function has a magnitude of 0.18 at zero frequency. This may readily be observed from figure 7.25.

In conclusion, the open circuit receiver response is greatly influenced by mechanical loading with maximum output occurring under lightly damped conditions at the fundamental frequency of mechanical resonance. The response indicates a

general decrease with frequency under all conditions of mechanical load. It should be noted that the output voltage is proportional to the time integral of the input wave of force.

ii) Under finite conditions of resistive loading, the voltage attenuation factor is no longer unity, ie

$$U(S) = \frac{SC_oR}{1 + SC_oR}$$

$$\text{therefore} \quad \left|U(\omega)\right| = \frac{\omega C_oR}{(1 + \omega^2 C_o{}^2R^2)^{\frac{1}{2}}}$$

This function increases from zero with frequency, eventually reaching a maximum value of unity. The rate of increase is dependent on the product C_oR. As a result, the output voltage will generally be lowest for small values of load resistance, over the frequency range of interest.

In addition, the amplitude and phase of the feedback loop is also modified by the factor Z_{FR}.

$$Z_{FR}(S) = \frac{1}{1 + SC_oR}$$

$$\text{therefore} \quad \left|Z_{FR}(\omega)\right| = \frac{1}{(1 + \omega^2 C_o{}^2R^2)^{\frac{1}{2}}}$$

$$\underline{/Z_{FR}(\omega)} = -\tan^{-1} \omega C_oR$$

As a result, the magnitude of this function decreases from unity at zero frequency, eventually becoming zero. Consequently, the influence of secondary piezoelectric action is expected to be greatest at low frequences and under conditions of light mechanical load. It should be noted that the resistive element introduces a phase shift into the feedback loop, which serves to further reduce the effects of secondary action. This condition is identical to that discussed in Section 7.2ii, for the resistively loaded transmitter.

Figure 7.26 shows the frequency response of a 1 MHz (mechanical resonance) receiver under the following conditions of resistive load. The transducer is subject to conditions of light mechanical damping.

a. R = 10, C_oR = 12.61 ns K = 0.7

b. R = 100, C_oR = 126.1 ns

c. R = 470, C_oR = 592.7 ns

d. R = 1 K, C_oR = 1.261 μs

e. R = 1 M, C_oR = 1.261 ms

From the figure the following main features are apparent:

i. For low values of load resistance, the magnitude of the frequency response characteristic is very small. Secondary effects are clearly evident from the reduction in centre frequency to positions below mechanical resonance.

For example, a resistive load of 10Ω gives,

$$Z_{FR} \simeq 1, \quad Z_{FR} = -4.5^{\circ}, \quad U = 0.08 \text{ (at 1 MHz)}$$

Consequently, the feedback factor is very nearly equal to A_T, and hence the frequency of maximum output is close to the electrical resonance of the transducer. However, because of the attenuation introduced by U, the response magnitude is relatively low.

ii. As the load resistance is increased, secondary effects are reduced and the frequency of maximum output shifts towards mechanical resonance. The magnitude of the response also increases.

For example, with a resistive load of 1 KΩ and frequency equal to 1 MHz,

$$Z_{FR} = 0.125$$

$$Z_{FR} = -82.8^{\circ}$$

$$U = 0.992$$

The factor, U, is almost unity and hence attenuation in the forward path may be neglected. However, the amount of feedback and the associated phase shift are sufficient to reduce the peak output below the maximum value; which occurs under open circuit conditions.

A resistive load of 1 MΩ approximates very closely to open circuit conditions. In this instance,

$$Z_{FR} = 1.26 \times 10^{-4} \quad (f = 1\ \text{MHz})$$

$$Z_{FR} \simeq 90^{\circ}$$

$$U \simeq 1$$

Consequently, the transfer function may be considered open loop. In general, the effects of feedback may be neglected at a particular frequency if,

$$\omega C_o R \geq 100$$

However, it should be noted that this criterion is by no means rigid, as it may be substantially reduced for lower values of coupling coefficient and/or increased mechanical damping.

The receiving response under conditions of inductive loading is shown in figures 7.27(a and b) which correspond to parallel inductive loads of 20 μH and 2.2 μH respectively. The inductance values were selected to resonate with the transducer static capacitance at frequencies of 1 MHz (20 μH) and 3 MHz (2.2 μH). Mechanical load conditions corresponding to light, medium and heavy damping were considered.

Under such conditions of electrical load, the attenuation and feedback impedance parameters may be expressed as follows:

$$\left|U\right| = \frac{\omega^2 L_M C_o}{(1 - \omega^2 L_M C_o)}$$

$$\left|Z_{FR}\right| = \frac{1}{(1 - \omega^2 L_M C_o)}$$

$$\underline{/Z_{FR}} = 0$$

The feedback and input attenuation factors are thus a maximum at the frequency of tuned resonance. Consequently, it may be expected that the receiver response is maximised at this particular frequency. However, a study of figures 7.27(a and b) reveals that maxima occur on either side of tuned resonance. These fluctuations are especially prominant under conditions of light damping.

The response minima in the vicinity of tuned resonance arises directly from secondary piezoelectric action and as such, may be attributed to phase changes within the feedback loop. Consequently, the type of feedback changes from positive to negative and vice versa as frequency is increased. The expected maxima at tuned resonance do not occur due to the strong influence of negative feedback in this region. As damping increases, the distinct peaks are reduced, eventually being eliminated under heavily damped conditions.

It is also evident from figures 7.27(a and b) that bandwidth and centre frequency may be selected by the appropriate

choice of inductive tuning element, although care must be taken when operating under conditions of light mechanical load. In general, inductive matching of this type produces a narrowband spectrum, which is most easily predicted under conditions of high mechanical damping.

It was stated earlier that the response in the time domain for an open circuit piezoelectric receiver is proportional to the integral of the input wave of force. However, since the input force waveform is very rarely an ideal step or sinusoidal function, time domain response of the piezoelectric receiver is not included in the present section. Instead, the simulated time domain response of a complete transmit-receive system (loop response) is presented in Section 7.4 for a variety of electrical and mechanical load conditions. Simulation accuracy is also discussed by comparing the theoretical characteristics with experimentally measured results.

7.4 COMPARISON OF EXPERIMENTAL AND SIMULATION RESULTS

This section describes experimental techniques employed for verification of transducer behaviour in both transmitting and receiving modes. The experimental work is based on time domain performance under pulsed, transient conditions; hence permitting a wide range of external loading factors to be studied with relative ease. A comparison with the

appropriate simulation response is readily achieved from an oscilloscope wave trace.

Furthermore, a close study of experimental and theoretical time domain waveshapes yields considerable insight into some practical limitations of the transducer model. In particular, diffraction and edge wave effects which occur in the transmission mode are observed without difficulty.

Experimental testing in the frequency domain may also be performed by replacing the oscilloscope with a suitable spectrum analyser. It should be noted that most analysers possess an input impedance of 50Ω and great care must be taken to ensure that electrical loading of the transducer does not occur. A high frequency (minimum 20 MHz bandwidth), high input impedance (minimum of 10 kΩ over the frequency range) buffer amplifier must therefore be inserted. However, for the present purpose, it is considered that more information on transducer behaviour is available from a study of the time domain.

In addition, an investigation of the transmission system also verifies the accuracy of the electronic pulser model. (This was also achieved, to some extent in chapter VI). This has important consequences for transducer calibration studies in such areas as medical ultrasonics and non-destructive testing. It has been indicated by Carson (5)

and Erikson [10] that a requirement exists for defining a standard ultrasonic generator to evaluate and calibrate piezoelectric devices. Such a generator must produce a short duration voltage 'spike' similar to that employed in most commercial scanning systems. The type of pulser modelled in Appendix C conforms to this requirement and may readily be characterised by turn on time and on resistance.

Where possible, all experiments were conducted using the piezoelectric transducers studied in chapter VI. Full details on the physical characteristics of these devices are presented in Appendix D.

7.4i Experimental and Measurement Techniques

A diagram of the experimental system employed to investigate the generation and reception of acoustic transients is shown in figure 7.28.

In order to minimise diffraction effects a separate transmit-receive configuration was used. It is also possible to study pulse-echo operation by placing a suitable reflector in front of the transmitting transducer. However, accurate measurement of the acoustic pressure wave profile is extremely difficult because of diffraction and interference effects.

Water was selected as the transmission medium because of its relatively low attenuation characteristics and well defined acoustic properties. In addition, effective acoustic coupling to solid media is best achieved by means of a thin liquid layer between transducer and load. This intermediate layer may introduce considerable distortion and attenuation to the transmitted and received waveforms. (See for example, Redwood and Lamb (39)).

It should be noted that the relative positions of transmitting and receiving elements may be extremely important in the determination of accurate wave profiles. In general, the distance between transducers was maintained at a minimum to reduce attenuation losses; diffraction effects and possible distortion induced by non-linear propagation characteristics of the transmission medium.

Measuring systems of the type described are extensively used in transducer calibration studies where time averaged output power or peak power are the measured parameters. However, quantitative measurements of the spatial and temporal distributions of acoustic pressure are much more difficult as a result of diffraction effects in the transmitted wave and physical limitations of the detecting transducer.

The most widely accepted method of quantifying acoustic wave distributions is the use of a miniature piezoelectric

hydrophone probe. This device comprises a thickness mode piezoelectric ceramic mounted at the end of a rod or cone; the latter providing acoustic backing and mechanical support. A typical hydrophone is shown in figure 7.29. For the purpose of accurate wave measurement, the piezoceramic hydrophone suffers from the following severe limitations.

a. To achieve adequate spatial resolution and directivity characteristics, a small diameter disc must be employed. The disc diameter should not exceed 1-2 mm in order to fulfil these requirements. However, such a small diameter leads to a fundamental radial mode resonance in the 1 MHz region. The radial mode greatly influences the measured characteristics, making accurate representation of the acoustic field profile almost impossible.

b. For accurate reproduction of an acoustic waveform, the hydrophone must possess a flat frequency response characteristic which extends well beyond the centre frequency of the incident ultrasonic signal. The type of transducer under consideration (5-4 MHz) thus requires a minimum hydrophone bandwidth of 25 MHz. Consequently, for thickness mode operation, a detector thickness of 0.05 mm or less is required to obtain the desired frequency response.

However, physical constraints imposed in the construction of the hydrophone make the manufacture of such a receiver

extremely difficult. Electrode mounting and the positioning of protective layers and backing materials generally ensure that commercially available hydrophones demonstrate extremely uneven frequency characteristics.

c. The high acoustic impedance of piezoceramic materials (33×10^6 kg/m^{2}s) compared with water (1.4×10^6 kg/m^{2}s) gives rise to considerable acoustic reflection at the hydrophone face. This perturbs the very acoustic field which the device is required to measure.

In addition, to achieve a good broadband response, the hydrophone configuration should possess matched backing. Materials possessing the same value of acoustic impedance as the transducer are difficult to manufacture and moreover, reliable bonding to the transducer is not always guaranteed.

Another measuring technique, adopted by various authors like Carome (5) and Ying (64) involves the use of a thick piezoelectric transducer as the receiving element. By employing a receiving device sufficiently thick that the transit time is greater than the pulse length of the incident acoustic wave, reverberation within the receiving element may be ignored. That is, only those displacement contributions from the receiver front face are included in the response. Although this technique eliminates uneveness in the frequency response caused by the reverberation factors, it also suffers from the following disadvantages:

i. A significant perturbation of the incident acoustic field takes place as a result of acoustic mismatch and relatively large surface area of the detecting device.

ii. Such a device does not possess good directional characteristics. This may distort the receiving response if the incident acoustic wavefront is non-planar.

iii. Although radial mode effects are confined to lower frequencies (1-5 MHz), considerable distortion may be incurred, especially under conditions of high impedance electrical loading.

iv. When operating into a high impedance electrical load, the detector output is proportional to the time integral of the incident acoustic force. Some authors, for example Carome (5), utilised a differentiating network, positioned at the receiver output to achieve a more accurate representation of the incident acoustic wave. Great care has to be exercised in order that the differentiator does not electrically load the receiving element.

However, recent developments in hydrophone technology have led to the concept of an entirely different type of receiving device. The polyvinylidene membrane hydrophone (pvdf) described by Shotton (43) and others (65) has eliminated many of the disadvantages associated with piezoceramic receiving elements.

PVDF is a piezoelectric plastic polymer which is used as a thin, acoustically transparent membrane, stretched over an annular frame large enough to allow the entire ultrasonic beam to pass through the central aperture. A small central region of the membrane is coated on both surfaces with metal film electrodes and is polled to induce piezoelectric properties only within that region. The device may be regarded as a small sensing element suspended freely in the ultrasonic field, which responds to the local pressure fluctuations associated with the passage of ultrasonic waves. This type of detector is considered to offer the following important advantages:

a. The pvdf may be fabricated as a film, with thicknesses down to a few microns. Such devices thus possess fundamental thickness mode resonances far above the range of interest.

b. Radial mode frequencies are related to the diameter of the entire membrane, rather than that of the active element. Radial mode resonances are thus reduced to a few kHz.

c. The acoustic impedance of pvdf (4.1×10^6 kg/m^{2}s) is more closely matched to that of water than is the impedance of ceramic materials. Consequently, the acoustic reflection coefficient at the membrane surface is relatively low, hence reducing perturbation of the acoustic field and

ensuring that the hydrophone frequency response is essentially broadband. When immersed in water, membrane hydrophones thus possess a broad, flat frequency response, free from the effects of reverberation associated with conventional backing and mounting configurations. In addition, the piezoelectric properties of pvdf (see Table 7.1) are such that the sensitivity of the device is comparable with piezoceramic receiving elements.

A disadvantage of pvdf is the low value of dielectric constant (<12), resulting in a transducer static capacitance of only a few pf. Consequently, the output voltage signal from the hydrophone is reduced by lead, cable and amplifier input capacitances.

Another possible drawback results from the thin film leads being exposed to the water surface. Unless distilled water is used, the finite water resistance constitutes an electrical load across the active element. In addition, electrical pick-up and interference may result because of the water conductivity.

However, the latter limitation has been largely overcome with the recent introduction of the bilaminar shielded membrane hydrophone (43) in which the thin film conducting leads are electrically isolated from the water surface by a thin layer of insulating material. Although membrane thickness is slightly increased as a result, no adverse

effects on device performance have yet been reported.

While pvdf membrane hydrophones of this type are not yet commercially available in large quantities, a prototype bilaminar device was obtained from Marconi Research Laboratories for the purpose of experimental evaluation. The particular device has an active area of 1 mm^2 and a fundamental mechanical resonant frequency of 44 MHz. Other relevant details of the hydrophone parameters (supplied from the manufacturer) are outlined in Table 7.1. It must be emphasised that in the course of the experimental work, the performance of the prototype hydrophone was also under investigation, as evaluation of the devices has never been reported under similar conditions.

Simulated frequency response characteristics for this hydrophone are shown in figure 7.30, for two values of cable capacitance, corresponding to 50 pf and 140 pf. Attenuation as a result of the larger value of cable capacitance is readily observed. Both characteristics exhibit flat frequency responses up to approximately 10 MHz, after which they steadily rise to the mechanical resonance of 44 MHz. Note that for this type of transducer, water loading is equivalent to medium conditions of mechanical damping. It should be noted also that both characteristics correspond to electrical loading equivalent to 1 MΩ across the transducer. The cable capacitance was assumed to act in parallel

with this resistive element.

Figure 7.31 shows the frequency response characteristics of a resistively loaded hydrophone. Resistive loads of 1 kΩ and 10 kΩ are considered, along with a cable capacitance of 140 pf. (140 pf is the manufacturer's stated value for the cable capacitance of the prototype hydrophone). In both cases, the response is no longer flat over the important frequency range of 1-10 mHz, and the hydrophone will thus distort the ultrasonic wave characteristics. For this reason, all experimental work was performed with the hydrophone connected directly into the oscilloscope amplifier, which constitutes an electrical load of 1 MΩ in parallel with 20 pf. However, the problem of cable attenuation remains, and this is expected to considerably reduce the amplitude of the hydrophone response, but not appreciably distort the received voltage waveshape.

The latter statement may be explained by considering the transfer function for the piezoelectric receiver. For the low value of coupling coefficient ($k^2 = 0.0225$) and relatively high mechanical loading conditions, it is safe to ignore the effects of secondary action and hence the transfer function may be expressed as follows:

$$\frac{V_o(S)}{F_F(S)} = -T_F\, U(S)\, \frac{K_F(S)}{S}\, \frac{K^2}{ThC_o}$$

The total cable capacitance, C_p, is considered to act in parallel with the transducer. Consequently, the attenuation factor U, may be written as follows:

$$U(S) = \frac{SC_o}{SC_p} \left[1 + \frac{SC_o}{C_p} \right]$$

therefore $$U = C_o/(C_o + C_p)$$

The receiver transfer function is thus reduced in magnitude by the cable capacitance, but the phase response remains unaffected. Magnitude reduction is readily observed from figure 7.30. For a transducer static capacitance of 2.22 pf and cable capacitances of 50 pf and 140 pf, a magnitude reduction factor of 2.70 is evident between the respective characteristics.

This type of membrane hydrophone is thus expected to faithfully reproduce the acoustic waveform for the range of transducers described in Appendix D. That is, piezoceramic transmitters, with electrical resonant frequencies from 0.5-4 MHz.

Operating characteristics of the receiving device are not the only conditions which must be considered when attempting to quantify the ultrasonic waveform. The transducer model predicts that a plane wave is emitted from the front face of the piezoelectric transmitting element. In practice, diffraction effects result in two separate wave components generated at the front face. A plane wave component, as

predicted by the model, and a diffracted edge wave component emanating from the perimeter of the device.

The concept of a direct plane wave, which travels in the geometrical beam region straight ahead of the transducer, and diffracted edge waves which travel in all directions from the edge of the transducer, was first reported by Kozina and Makarov (19). This later received experimental confirmation by Carome (4) and subsequent theoretical investigations were performed by Stephanishen and Robinson (41). More recent work by Weight and Hayman (60) demonstrated the presence of plane and edge wave components in a water medium by means of schlieren visualisation. Photoelastic studies made by the present author (as yet unpublished) have confirmed the existence of both longitudinal and shear edge-wave components in solid media.

Typical edge and plane wave formations for the transducer near field are shown in figure 7.32, where interaction between the two components may be clearly observed.

The transducer near field is defined (10) as that region in front of the transducer which is given by,

$$x < \frac{d^2}{4\lambda}$$

where x is the distance in front of the transmitting element (m)

d is the transducer diameter (m), and

λ is the wavelength of the acoustic wave in the transmission medium (m).

In the axial far-field of the transducer (ie $x > d^2/4\lambda$), diffraction theory (41) predicts that the plane and edge-waves combine to produce a waveform which decays inversely with distance from the source. For a 1 MHz, 20 mm diameter transducer, the far field commences approximately 70 mm in front of the transducer face.

The present feedback model assumes only plane-wave propagation from the transmitting device. Consequently, the model cannot produce a totally accurate representation of the ultrasonic wave profile in either the near or far fields.

However, experimental verification of the plane-wave characteristics (as predicted by the model) is possible by careful positioning of a suitable receiving element within the transducer near field. Ideally, the detecting device should be placed as close as possible to the transmitter face, without incurring unwanted reverberation between transmitter and receiver. Although edge-wave distortion is considerably reduced towards the near-field/far-field interface, (the edge-waves decay in proportion to 1/x, plane waves theoretically remain unattenuated within the near field) this

area should not be used for accurate measurement of the plane-wave component. As discussed previously, the transmitted plane-wave characteristics often incorporate high frequency components in the form of spikes and other rapid discontinuities. Such features are likely to be obscured as a result of attenuation and frequency selective absorption induced by a relatively long water column.

Consider a detector situated on the axis and close to the transmitting device. A study of figure 7.32 indicates that several plane-wave cycles may be received before edge-wave interference starts to take place. The number of undistorted plane-wave cycles which can be measured in this manner increases as the transducer diameter increases in relation to the fundamental wavelength. That is, axial near-field diffraction effects are reduced for transducers of large diameter to thickness ratio.

It should be noted that measurements of this nature may only be performed using a small detecting device which causes minimum perturbation of the acoustic field. The pvdf hydrophone is ideally suited to this purpose. Measurement of the plane-wave component within the near field by means of a detector of dimensions compatable to the transmitting element is extremely difficult, due to edge-wave distortion and field perturbation.

Recently published work by Ying (65) has reported on transducer near-field behaviour using a thick, disc transducer as the detecting device. Experimental results were shown to be in close agreement with computer simulations based on Mason's model. This is surprising in view of the expected distortion associated with this type of detecting transducer.

7.4ii Experimental Results

This sub-section presents a representative set of experimental results, which may be conveniently grouped into two parts. Firstly, various acoustic field profiles for a 1 MHz (electrical resonance) piezoelectric transmitter are considered. The device was backed at its rear face by the lead based epoxy, Devcon L; described in chapter VI. The transducer front face operated directly into the water column. Different electrical driving conditions were considered, representing various methods of transient excitation. In each case the detecting element was the pvdf membrane hydrophone, positioned 15 mm in front of and axially with respect to the transmitter face.

Secondly, the loop response characteristics for a transmit-receive system incorporating two circular disc, piezoceramic devices are considered. In this case, the receiving element consisted of an air backed, water loaded transducer with an electrical resonant frequency of 1 MHz. The transmitting

element was the same transducer employed in the previous experiments, ie the 1 MHz, lead epoxy backed, water loaded device. Consequently, a comparison could be made between the known plane-wave profile and the actual output from a detecting transducer. The driving conditions were maintained constant, while the detecting response was investigated under a variety of electrical load conditions.

In order to minimise edge-wave interference, the receiving element was placed axially at a distance of 70 mm from the transmitter. This corresponds to the end of the near field. Although some frequency smoothing of the acoustic wave is expected in such a long water column, integration effects in the receiver are expected to dominate and hence the measured characteristic should compare favourably with the predicted receiver response. Accurate measurement of the acoustic wave profile is thus not possible using this technique.

Consider firstly the transducer-hydrophone configuration. Figure 7.33 compares experimental and simulated results for the loop response of the system. That is, the responses correspond to the hydrophone output. The electronic driving network is also shown corresponding to a 300 V step input from the FET pulser. Excellent agreement is observed between the two waveforms, with secondary effects clearly evident from the positive exponentials contained in the characteristics.

Figure 7.34 outlines the simulated plane wave of force expected under the same driving conditions. Apart from the inversion (introduced by the receiving element) and amplitude scaling factors, the theoretical response characteristics of figures 7.33 and 7.34 are almost identical; demonstrating that the membrane hydrophone accurately represents the incident ultrasonic wave profile.

Figure 7.35 shows the simulated and experimental response profiles for a driving system incorporating a lower value of blocking capacitance (100 pf).

In this case, the almost square-wave nature of the characteristics indicates a reduction in secondary action, as discussed in Section 7.2iv. Once again, excellent agreement is obtained between experimental and theoretical waveforms.

Figure 7.36 indicates the response of a resistively loaded transmitter (100Ω). Experimental results are shown for two different time scales corresponding to 5 μs (A) and 1 μs (B) per division. Photograph B clearly demonstrates the edge-wave, which occurs after the plane wave component. The edge-wave is of course not predicted by the model. A close study of the figures reveals negative exponential behaviour over the first wave cycle, thereafter positive exponentials exist as a result of secondary piezoelectric action. This phenomenon was also described in Section 7.2iv.

The final configuration studied was that of an inductively loaded transmitter, as shown in figures 7.37(a and b), corresponding to inductance values of 4.7 μH and 2.2 μH respectively. In each case, a load resistance of 100Ω was also connected in parallel with the transducer. This type of configuration is common in some non-destructive testing applications (10) where the electrical load impedance is used to shape the driving pulse.

From the figures it is evident that the system response varies considerably as the inductance value changes. A much higher output is achieved for the larger value of inductance and in both cases, considerable waveform distortion is evident. Favourable agreement between simulated and experimental response characteristics is again achieved. However, there is some disparity, particularly in figure 7.37b, where the sharp discontinuities observed in the theoretical trace tend to be smoothed out under practical conditions. This is thought to be caused by frequency dependent attenuation in the transducer material and water column. In addition, the inductance values may not be completely accurate over this range of frequencies, since they were only specified up to 100 kHz.

For all of the characteristics shown in figures 7.33 through to 7.37b, excellent agreement was obtained between simulated and practical response measurements. The membrane hydrophone was shown to perform extremely well in providing

accurate information concerning the ultrasonic wave profile. As expected from Section 7.2, the nature of this wave profile varied enormously under different conditions of electrical load. Such variations are not always apparent when using conventional hydrophone detecting techniques. It should be noted, that to obtain an accurate description of the entire acoustic field, diffraction effects must be considered. The present feedback model thus requires further work in order to overcome this limitation.

The second set of experiments involved an investigation of the loop response characteristics of a separate piezoceramic transmit-receive system. In each case, the transmitter configuration remained constant, corresponding to step excitation as shown in figure 7.33. Various electrical loading conditions for the receiving element were studied.

Figure 7.38 compares practical and simulated response characteristics for the 1 MHz, air backed, water loaded receiving element looking directly into the oscilloscope. In this mode, the receiver may be considered open circuit, ie no secondary action may occur within the device. The integrating action of the receiving transducer may readily be observed from the triangular nature of the waveshape. In addition, the light damping produces a narrowband response. Excellent agreement is obtained between practical and theoretical results.

Figure 7.39 shows the system response when a 100Ω resistor is connected across the receiving element. In this situation, secondary action has a considerable influence on receiver behaviour. This is indicated by the relative waveform distortion and bandwidth increase when compared with figure 7.38. Once again, close agreement is obtained between experimental and simulation results.

The final configuration to be investigated was that of the inductively loaded receiver, as shown in figures 7.40 (a and b) respectively. Inductance values of 2.2 μH and 20 μH were considered and in both cases a 100Ω shaping resistor was connected in parallel with the inductive element. In figure 7.40a, the low value of inductance tends to dominate the response, resulting in considerable distortion and amplitude reduction. This is to be expected, from the discussion in Section 7.3ii. As the inductance value is increased, the influence of the component diminishes and the resistive element tends to dominate the response. This is readily observed by noting the similarity between figures 7.40b and 7.39.

7.5 CONCLUDING REMARKS

Piezoceramic transducer behaviour has been investigated over a wide range of electrical and mechanical load conditions. Where possible, feedback systems theory was used to describe operating characteristics for both transmitting and receiving

modes. The theoretical investigation was experimentally verified for transducer operation in the time domain. Experimental results were found to be in close agreement with simulated response characteristics within the limitations of the feedback models. A pvdf hydrophone was shown to be successful in verifying ultrasonic plane-wave profiles. The major results concerning transmitter and receiver operation may be summarised as follows:

i. For the piezoelectric transmitter, the frequency of maximum output is generally lower than the frequency of mechanical resonance. Under conditions of light mechanical damping, peak output occurs close to the frequency of electrical resonance. For low values of coupling coefficient, secondary action is reduced and maximum output tends towards the frequency of mechanical resonance. Under conditions of light damping, secondary piezoelectric action serves to increase the -3db bandwidth of the output signal.

ii. The generator source impedance plays an important role in determining the output force characteristics. For voltage sources of very low output impedance (<5Ω), secondary effects are maximised and in addition, transmitting response is independent of any external electrical load (for example, matching elements) connected across the device. As source impedance increases, secondary effects are reduced along with the amplitude of the output wave of force. Under conditions of heavy damping and high values of source resistance

the transmitter model may be considered open loop. Variations in source impedance have most influence under conditions of light damping.

iii. The receiver model may be considered open loop if the receiving transducer operates under high impedance electrical loading conditions. In this case, the response is proportional to the time integral of the incident wave of force. Under such conditions, peak output occurs at the frequency of mechanical resonance, for the majority of mechanical load configurations. However, for conditions of heavy damping, maximum output may occur below this frequency.

iv. When the receiving element is electrically loaded by a finite impedance, secondary effects are introduced. These are maximised for small values of load impedance and may lead to considerable distortion of the output voltage; especially under conditions of light damping. The voltage response also suffers attenuation with decreasing electrical load impedance.

v. For both transmitting and receiving elements, inductive matching may be employed to optimise bandwidth and centre frequency. Such responses are most easily predicted under conditions of heavy mechanical damping. Considerable distortion (ie the presence of rapid discontinuities) of the output waveshape may also occur under some conditions of inductive loading.

vi. Both transmitting and receiving configurations demonstrate an increase in bandwidth with increased mechanical loading. In addition, the effects of secondary action diminish with frequency and increased mechanical damping.

During the course of the experimental investigation, it was emphasised that the present feedback model is unable to cater for diffraction effects. This limitation must be overcome if the techniques employed in this chapter are to be employed in the accurate determination of transducer field characteristics. Further discussion on this aspect is presented in chapter IX, under the section 'suggestions for further work'.

CHAPTER VIII

DIRECT EVALUATION OF TIME DOMAIN RESPONSE

8.1 INTRODUCTION

This chapter describes a method for obtaining detailed predictions of the time domain response for piezoelectric transducers operating in both transmitting and receiving modes. The technique makes use of the Z-transform to determine the behaviour of the reverberation factors K_F and K_B. By means of the substitution $Z = e^{ST}$, a direct description of these functions is readily obtained in the Z-domain and after suitable sampling of the input waveform, a wide variety of system responses may be conveniently investigated.

Time domain response is achieved with a minimum of computational effort and the need to transform from frequency to time is eliminated. As a result, the sampling and IFFT processes described in the previous chapters are excluded, providing considerable memory and time saving.

However, it must be stressed that the advantages in computational effort are only offered if both transmitting and receiving transfer functions are considered open loop, permitting the transformation from the S to Z domain to be performed with relative ease. Although various transform techniques are available to aid the S to Z transformation for a closed loop system, the resultant mathematical complexity offers no significant advantages in computational effort, over the techniques described in chapter VII.

Consequently, the modelling techniques described in this chapter are only applicable to situations where secondary piezoelectric action may be neglected. It will be recalled from previous chapters that this assumption is valid under one or more of the following operating conditions:

i. Low value of electromechanical coupling coefficient ($K < 0.15$),

ii. Under conditions of high mechanical loading (heavy damping), and

iii. When the associated electrical load impedances are high. In the case of the transmitting mode, this may occur as a result of high source resistance, or in the receiving mode if the transducer is electrically free as a result of high load impedances.

Conditions (ii) and (iii) are not uncommon in practice, especially in acoustic imaging and non-destructive testing wideband applications where heavily damped transducers are frequently employed. By means of the methods outlined in this chapter, excellent approximations to the time domain response of such systems may be obtained. If required, the frequency response may also be obtained, either from an FFT routine, or by appropriate substitution for the delay operator Z. The next section describes the application of the Z-transform to the transmitter and receiver

transfer functions and how the resultant model may be conveniently implemented on a digital computer.

8.2 REPRESENTATION OF THE OPEN LOOP TRANSFER FUNCTIONS IN THE Z-DOMAIN

8.2i The Open Loop Transfer Functions

The open loop transfer function relating input voltage to force leaving the transducer front face may be expressed as follows for the transmitting mode:

$$\frac{F_1(S)}{e(S)} = -\left(\frac{Z_E}{Z_o + Z_E + Z_o Z_E S C_o}\right) K_F(S)\ hC_o \frac{A_F}{2}$$

$$= -Z_I(S)\ K_F(S)\ hC_o\ \frac{A_F}{2} \qquad \text{——————————} \quad 1$$

$Z_I(S)$ is a transfer function which relates the signal generator voltage ($e(S)$) to the voltage across the transducer static capacitance, C_o under general conditions of electrical load. That is,

$$VC_o\ (S) = e(S) Z_I(S) \qquad \text{——————————} \quad 2$$

where VC_o (S) is the voltage appearing across the static capacitance of the transducer. The relationships between VC_o, e and the various electrical loading elements is illustrated in figure 8.1. The output force is now described by the following transform equation, where VC_o is regarded as the input voltage to the system.

$$F_1(S) = -VC_o(S)\ K_F(S)\ hC_o \frac{A_F}{2} \qquad \text{3}$$

Similarly, the open loop transfer function for the piezoelectric receiver may be expressed by the following equation:

$$\frac{V_o(S)}{F_1(S)} = -K_F(S)\ T_F \frac{K^2}{SThC_o}$$

therefore

$$V_o(S) = -F_1(S)\ K_F(S)\ T_F\ K^2/SThC_o \qquad \text{4}$$

It should be noted that this relationship is valid for a receiving transducer which is free of any external electrical loading, or where the load impedances are so high that they may safely be neglected. As such, the equation is exact and valid over all conditions of mechanical load. However, for the transmitting transfer function, secondary piezoelectric action is assumed negligible because of low coupling factor, heavy damping or high electrical loading. It is therefore an approximation, valid under one or more of these operating conditions.

The quantities V_{Co} and F_1 contained in equations 3 and 4 may be regarded as system inputs for transmission or reception respectively. In the subsequent analysis, they are represented by a set of samples; each sample approximating to a weighted impulse and separated in time by the appropriate

sample spacing. However, first it is necessary to manipulate the transfer functions into forms suitable for direct analysis in the time domain.

8.2ii The Open Loop Z-Transfer Functions

The reverberation factor K_F, which occurs in both transmitter and receiver open loop transfer functions, may be expressed in the S-domain by the following equation:

$$K_F(S) = \frac{(1 - e^{-ST})(1 - R_B\, e^{-ST})}{1 - R_F R_B\, e^{-2ST}} \qquad \text{5}$$

It was also shown in chapter III, Section 3.4 that the time domain representation of K_F may be considered as a train of weighted impulse functions, alternately changing in sign and separated by the transducer transit interval, T. That is, the impulse response of K_F is described by the following weighting sequence:

$$K_F(t) = \delta t - (1 + R_B)\,\delta(t - T) + R_B(1 + R_F)\,\delta(t - 2T)$$
$$+ R_F R_B(1 + R_B)\,\delta(t - 3T) + R_F R_B^2(1 + R_F)\,\delta(1 - 4T)$$
$$- R_F^2 R_B^2(1 + R_B)\,\delta(t - 5T) + R_F^2 R_B^3(1 + R_F)\,\delta(t - 6T)\_\_\_$$

where δ is the Dirac Delta Function,

therefore

$$K_F(t) = \delta t - (1 + R_B)\left[\sum_{n=0}^{\infty} (R_F R_B)^n \, \delta(t - \{2n + 1\}T)\right] +$$

$$+ R_B(1 + R_F)\left[\sum_{n=0}^{\infty} (R_F R_B)^n \, \delta(t - 2\{n + 1\}T)\right] \text{ ——— } 6$$

Now consider the input to the transducer (in either transmitting or receiving modes) to be represented by the time varying sequence x(t). By sampling x(t), the input may be considered as a train of weighted impulses, defined by the following equation for n samples:

$$x_s(t) = \sum_{\ell=0}^{n} x(\ell\Delta t) \, \delta(t - \ell\Delta t) \text{ ——— } 7$$

where Δt is the sampling period and $x(\ell\Delta t)$ represents the pulse train.

A convenient method for dealing with such sampled data is the Z-transform, which is defined as follows:

$$x(Z) = \sum_{\ell=0}^{\infty} x(\ell\Delta t) \, Z^{-\ell}$$

where $Z = e^{S\Delta t}$.

Hence $Z^{-\ell}$ simply represents a delay of ℓ samples.

Furthermore, it may be shown that if a sampled data input $x_s(t)$ is applied to a linear system possessing a weighting sequence $h(\ell\Delta t)$, then the output is defined in the Z-domain by the following relationship:

$$Y(Z) = X(Z)\ H(Z) \qquad \text{——————————} \quad 8$$

The Z-transfer function of K_F may be obtained by substituting for e^{-ST} in equation 5. However, additional insight into the nature of the process and selection of an appropriate sampling interval is obtained if the Z-transform is derived directly from the weighting sequence defined by equation 6.

Let the sampling period be an integer multiple of the transducer transit time. That is,

$$T = m\Delta t$$

This is a necessary condition in order to obtain the Z-transfer function of the transducer weighting sequence. For example, a delay of one transit interval is represented in the S-domain by the delay operator e^{-ST}. In order that this may be represented in the Z-domain by an integer number of samples, the following relationship must be satisfied:

$$e^{-ST} = Z^{-m}$$

$$= e^{-Sm\Delta t}$$

ie $$T = m\Delta t$$

Another constraint on the sampling process is that the sampling frequency must be greater than twice the highest frequency component in the system, in order to prevent aliasing in the frequency domain. In the case of the piezoelectric transducer, this is readily satisfied if m >10.

Equation 6 may now be written as follows:

$$K_F(t) = \delta(t) + R_B(1 + R_F)\left[\sum_{n=o}^{\infty} (R_F R_B)^n \, \delta(t - 2\{n + 1\}m\Delta t)\right]$$

$$- (1 + R_B)\left[\sum_{n=o}^{\infty} (R_F R_B)^n \, \delta(t - \{2n + 1\}m\Delta t)\right]$$

therefore

$$K_F(\ell\Delta t) = \delta(\ell\Delta t) + R_B(1 + R_F)\left[\sum_{n=o}^{\infty} (R_F R_B)^n \, \delta(\ell\Delta t - 2 \times \{n + 1\}m\Delta t)\right] - (1 + R_B)\left[\sum_{n=o}^{\infty} (R_F R_B)^n \, \delta(\ell\Delta t - \{2n + 1\}m\Delta t)\right]$$

therefore $$K_F(Z) = \sum_{\ell=o}^{\infty} \delta(\ell\Delta t) Z^{-\ell}$$

$$+ R_B(1 + R_F)\left[\sum_{n=0}^{\infty}\sum_{\ell=0}^{\infty}(R_FR_B)^n\,\delta(\ell\Delta t - 2\{n+1\}m\Delta t)z^{-\ell}\right]$$

$$- (1 + R_B)\left[\sum_{n=0}^{\infty}\sum_{\ell=0}^{\infty}(R_FR_B)^n\,\delta(\ell\Delta t - \{2n+1\}m\Delta t)z^{-\ell}\right]$$

$$= 1 + R_B(1 + R_F)\sum_{n=0}^{\infty}(R_FR_B)^n\,z^{-2\{n+1\}m}$$

$$- (1 + R_B)\sum_{n=0}^{\infty}(R_FR_B)^n\,z^{-\{2n+1\}m}$$

$$= 1 + R_B(1 + R_F)z^{-2m}\sum_{n=0}^{\infty}\{R_FR_Bz^{-2m}\}^n$$

$$- (1 + R_B)z^{-m}\sum_{n=0}^{\infty}\{R_FR_Bz^{-2m}\}^n$$

therefore

$$K_F(Z) = 1 + \sum_{n=0}^{\infty}\{R_FR_Bz^{-2m}\}^n\{R_B(1 + R_F)z^{-2m} - (1 + R_B)z^{-m}\}$$

Taking the sum to infinity for the geometric progression results in the following expression for $K_F(Z)$:

$$K_F(Z) = \frac{1 - Z^{-m}(1 + R_B) + R_B Z^{-2m}}{1 - R_F R_B Z^{-2m}} = \frac{Y(Z)}{X(Z)} \quad \text{——————} \quad 9$$

where $Y(Z)$ and $X(Z)$ are the notional output and input functions respectively, of the system represented by $K_F(Z)$.

Therefore

$$Y(Z) - Y(Z)R_F R_B Z^{-2m} = X(Z) - X(Z)Z^{-m}(1 + R_B) + X(Z)R_B Z^{-2m}$$

Inverse transforming this expression results in the following recursive equation describing the output sequence $y(n)$.

$$y(n) = x(n) - (1 + R_B)\, x(n - m) + R_B\, x(n - 2m) + R_F R_B\, y(n - 2m) \quad \text{————} \quad 10$$

Consider firstly the piezoelectric transmitter transfer function,

$$x(n) = V_{Co}\ (n)$$

and

$$F_1(n) = -y(n)\, \frac{hC_o\, A_F}{2}$$

Consequently, the transmitter may be modelled by the recursive network outlined in figure 8.2.

This model may be ideally implemented on a digital computer. By sampling the input voltage, an approximation to the output wave of force may be obtained for a variety of mechanical loading conditions. In addition, a wide variety of input

voltages may be accommodated, provided they are compatible with the constraints imposed by electrical loading in a practical system.

In a similar manner, the open loop receiver transfer function, described in equation 4, may be implemented by the recursive model shown in figure 8.3.

It should be noted that the integrator in figure 8.3 could have been replaced by the Z-transfer function $Z/Z - 1$ and a new recursive equation developed. However, in terms of programming effort, a single subroutine was used to simulate the recursive equation (10) for both transmitting and receiving modes. Consequently, it was found more convenient to simply integrate the sampled data by means of the trapezoidal rule, in order to obtain the receiver response.

The frequency response may be obtained by performing an FFT on the output data samples or by replacing Z with e^{jwt} in equation 9. From this, direct equivalence between equations 9 and 5 may readily be observed.

8.3 COMPUTER SIMULATION

A computer program was written to simulate transducer response in both transmitting and receiving modes. In addition, the loop response in a transmit-receive configuration was also evaluated. A general flow chart describing the package is shown in figure 8.4, and a complete listing is given in Appendix E.

The input samples $x(n)$ are generated by sampling a known time function which corresponds to either input force or input voltage. The samples are therefore assumed to be impulse functions with amplitudes equal to the values of the input time waveform at the sampling instants. A variety of input pulse shapes is incorporated in the program, including the unit step, rectangular pulse of varying width and gated CW of varying frequency, consisting of one half cycle up to 50 cycles. In addition, the voltage input from a capacitive discharge pulsed system (as described in Appendix C) is also included. The consequences of varying matching and pulse shaping elements are thus readily observed from the response curves. Some of the results obtained are presented in the following section, along with a comparison with those obtained from the exact (feedback) model.

8.4 RESULTS OF COMPUTER SIMULATION

In order to illustrate the main features of the modelling technique, two sets of simulations were performed for different conditions of electrical and mechanical loading. Medium damping (50 per cent matched backing, glass load) and heavy damping (ideal backing, glass load) were considered, while the transducer was electrically driven under the following pulsed conditions:

a. Capacitive discharge, with a resistor (R_E) connected across the transducer,

b. Capacitive discharge, with the parallel combination of a resistor (R_E) and inductor (L_E) connected across the transducer.

A general equation describing the transient input voltage is derived in Appendix C and from this, the sampled input voltage waveform may be expressed as follows:

$$V_{Co}(\ell\Delta t) = \frac{-V_m\, e^{-\alpha(\ell\Delta t)}}{toa\omega} \{\sin \omega\ell\Delta t - e^{-\alpha to} \sin \omega(\ell\Delta t - to)\}$$

where to is the turn on time of the pulser,

V_m is the magnitude of the applied voltage ramp function,

$$\alpha = \frac{1}{2R_E(C_o + C_B)}$$

$$\omega = \left[\frac{1}{L_E(C_o + C_B)} - \frac{1}{4R_E^2(C_o + C_B)^2}\right]^{\frac{1}{2}}$$

C_o, C_B are the transducer static capacitance and blocking capacitance respectively, and

$$a = \frac{C_o + C_B}{C_B}$$

In each case, the output wave of force was obtained and compared with the theoretical waveshape obtained under closed

loop conditions by means of the IFFT. This latter technique, which includes secondary piezoelectric effects was described in chapter VII and corresponds to an exact solution. As a result, waveshapes obtained using this technique are labelled 'exact solution' in some of the simulation diagrams. For completeness, the response of an identical piezoelectric receiver was also calculated. The receiving transducer was assumed to be on electrical open circuit and subject to the same mechanical loading conditions as the transmitter.

Consider firstly the situation where the transmitter is electrically loaded by a resistive element connected across the electrodes. The following nominal values were assumed:

$$to = 10 \text{ ns}$$
$$C_B = 2.2 \text{ nF}$$
$$C_o = 1.26 \text{ nF}$$
$$K = 0.48$$
$$R_E = 100\Omega$$
$$V_m = \text{Unity}$$

The simulation results are shown in figures 8.5(a-c) and 8.6(a-c) which correspond to conditions of medium and heavy damping respectively. A close examination of figures 8.5(a and b) reveals that the form of the output wave of force is similar in each case. However, the effects of secondary action are evident in the latter figure and are

recognisable by a reduction in the slope of the exponential parts of the function. This flattening of the waveshape is to be expected from the analysis performed in chapter VII, which considered the first transit interval. It was demonstrated that during this time interval, secondary piezoelectric action introduced an exponential increase to the waveshape (positive feedback). However in this case, the input voltage corresponds to a negative exponential function which acts in opposition to the secondary effect, hence flattening the waveshape.

Figures 8.6(a and b) show the corresponding waves of force under conditions of heavy damping. In this instance, secondary action has been further inhibited by the increased mechanical loading and the two figures demonstrate a very close correlation, although a slight amount of flattening may be observed in the latter figure.

The transmit-receive (loop) response characteristics for both systems are outlined in figures 8.5c and 8.6c; corresponding to medium and heavy damping respectively. The expected increase in output bandwidth with damping is readily apparent, as indicated by a reduction in the number of cycles in figure 8.6c. Integration due to the open circuit receiver may readily be observed.

The second set of simulation results correspond to the piezoelectric transmitter loaded electrically by the

parallel combination of a resistor and inductor. The following nominal component values were employed:

$$\begin{aligned} ton &= 10 \text{ ns} \\ C_B &= 10 \text{ nF} \\ C_o &= 1.26 \text{ nF} \\ K &= 0.48 \\ R_E &= 100\Omega \\ L_E &= 2.4 \ \mu H \end{aligned}$$

The form of the voltage observed across the transducer static capacitance V_{Co}, is shown in Appendix C, figure C3, where the effects of underdamping may readily be observed. Values of L_E, C_E and R_E were selected in order that the oscillation frequency was as close as possible to that of the mechanical resonance ($\omega = 2\pi \times 0.9655$ rads/sec).

Simulated waveforms are shown in figures 8.7(a-c) and 8.8(a-c); once again corresponding to medium and heavy damping respectively. A close study of figures 8.7(a and b) and 8.8(a and b) reveals excellent agreement between the open loop approximation and the exact (closed loop) solution. The amplitude is higher in the case of medium damping due to the constructive effect of the applied voltage and the mechanical oscillations within the transducer. Under such conditions, an inductor may be used to increase the output energy, although it must be noted that a narrowband output ensues. These effects are also

evident from the received voltage waveforms shown in figures 8.7c and 8.8c; where the number of cycles has been substantially increased in comparison to the previous situation of only resistive loading. It should be noted that the amplitude increase in figures 8.7 and 8.8 is due to a combination of inductive matching and an increase in the blocking capacitor C_B. Increasing C_B from 2.2 nF to 10 nF increases the initial deposition of charge to the transducer system.

It was stated in Section 8.1 that this modelling technique is valid only if secondary piezoelectric effects may be eliminated from the transfer function. Although such a stipulation implies that conditions of light damping are automatically invalid due to enhanced secondary action, it is interesting to compare the approximate model response under these conditions of mechanical load.

Simulated responses for the output waves of force are shown in figures 8.9(a and b), corresponding to a water loaded, water backed transducer. It is immediately apparent that under such conditions, the approximate model breaks down. The open loop response of figure 8.9a indicates excessive ringing which corresponds to an extremely narrow-band signal. In figure 8.9b however, secondary piezoelectric action has reduced the ringing as well as introducing considerable distortion to the output waveshape.

This reduction in the number of cycles (ie an increase in overall bandwidth) is to be expected from the simulation studies performed in chapter VII, where it was demonstrated that the effects of feedback in a lightly damped transmitting system were;

i. a reduction in the centre frequency from mechanical resonance, and

ii. an increase in the system bandwidth.

As a result of (i) the frequency of the driving voltage is no longer close to the frequency of maximum output force and hence the effect of secondary action is to reduce the amplitude and increase distortion in the output force waveform. This may readily be observed by comparing figures 8.9(a and b). As a consequence of (ii), the number of cycles is reduced.

8.5 CONCLUDING REMARKS

The validity of using Z-transform techniques to model piezoelectric transducer behaviour directly in the time domain has been demonstrated. Transducer response to a wide variety of input waveshapes may be obtained with a minimum of computational effort for both transmitting and receiving modes. The model has been shown to approximate very closely to the exact transmitter response under conditions of medium and heavy damping. However, the method should not

be used under conditions of light damping. That is, when both faces of the transducer are subject to light mechanical loading.

In many practical instances, the transducer is subject to a considerable amount of external damping. This is often deliberate, as in the case of wideband applications where heavy damping serves to increase bandwidth; or may arise directly as a result of probe construction. An example of the latter effect is the perspex 'wear plate' incorporated in many non-destructive testing probes. This is designed to protect the crystal face from damage and as a result, mechanical damping is increased. The Z-transform technique is extremely useful for predicting transducer response under such conditions.

Furthermore, a value of electromechanical coupling coefficient equal to 0.486 was used in the simulations; corresponding to the ceramic material PZT5-A (lead zirconate - titanate). For materials possessing lower values of coupling coefficient, secondary effects are diminished and the open loop approximation becomes valid over a wider range of mechanical load conditions.

CHAPTER IX

CONCLUSIONS AND SUGGESTIONS FOR FURTHER WORK

9.1 CONCLUDING SUMMARY

A systems approach has been applied to the study of thickness mode, piezoelectric transducer behaviour. Based on this theory, systematic, detailed investigations of reception, transmission and device operational impedance characteristics were conducted. A wide range of electrical and mechanical boundary conditions were included, for both CW and transient modes of operation.

Considerable emphasis was placed on the effects of electrical loading on transducer performance; as this has been an area subject to some neglect in previous work, particularly under transient conditions. Techniques for modelling transient piezoelectric systems were proposed, and these were shown to be successful under experimental conditions.

By deriving the transduction equations in a feedback systems manner, the resultant model is considered to overcome many of the inherent limitations of current transducer models. The model and the modelling technique, described in chapters III, IV and V, possess the following main advantages.

1 The model utilises realisable elements involving feedback mechanisms which clearly illustrate the physical phenomena involved.

2 The modelling involves basic concepts which do not require advanced knowledge of electric circuit topology.

It is thus easy to use and implement.

3 The model is truly wideband, suitable for the analysis of transient and CW applications; under a wide variety of electrical and mechanical loading conditions.

4 All piezoelectric, mechanical and electrical parameters which influence transducer behaviour are readily identified and may conveniently be evaluated for design considerations.

5 The thesis highlights the importance of secondary piezoelectric action on transducer behaviour. This is clearly modelled as a feedback effect, with current, charge, force or particle displacement as the feedback quantities. Illustrated in this manner, the complex mechanism of secondary action is considerably clarified and moreover, factors influencing secondary action, such as electro-mechanical coupling, frequency, mechanical damping and electrical loading, are readily identified.

Techniques for measuring such transducer parameters as thickness mode coupling coefficient, static capacitance, acoustic impedance ratios and mechanical bond integrity were also proposed. Although the preliminary results were very encouraging, it must be emphasised that further work is required, particularly to encompass a wider range of transducer frequencies and specimen geometries. It is hoped

that the measurement techniques described in chapter VI will provide a basis for further work in the design of single-element ultrasonic proves and multi-element transducer arrays.

In the course of the experimental work, a prototype pvdf membrane hydrophone was employed to accurately monitor ultrasonic pressure wave profiles in a water tank. From the results presented in chapter VII, it is considered that this device performs considerably better than other, commercially available hydrophone probes. As a result of this work, there is a possibility of further collaboration with the hydrophone manufacturer in the area of hydrophone simulation and calibration.

In conclusion, it is considered that the work presented in this thesis provides enhanced understanding of piezoelectric transducer systems behaviour and it provides a comprehensive basis for further investigation of such systems. The following section indicates some of the more important areas which would benefit from further investigation and analysis.

9.2 SUGGESTIONS FOR FURTHER WORK

The feedback model was developed with two principal aims in mind. Firstly, an improved understanding of piezoelectric transduction and the various factors which influence that process in thickness-mode transducers. Secondly, that the model forms part of an overall system concept which may be

used to aid the design of single element piezoelectric probes, multiple element transducer arrays and the electro-mechanical boundary conditions which affect the operation of such equipments.

Towards the latter aim especially, much additional work remains to be done, and the following pages present a brief summary of what are considered to be the more significant areas requiring further research.

9.21 Transducer Vibrations Other Than in the Thickness Direction

One of the fundamental assumptions made in the development of the present transducer model is that of single mode wave propagation in the thickness direction. However, in the course of the present work, radial mode vibrations were clearly evident and that under certain conditions they had a significant effect on transducer response. For example, radial mode effects were shown to have greatest influence on transducers of low diameter/thickness ratio under conditions of electrical open circuit. This behaviour is not predicted by the feedback model and in particular, the latter phenomenon is not fully understood. Consequently, further investigation into lateral vibration in a disc or plate transducer is required.

Lateral mode vibration is of particular importance in the development of multi-element transducer arrays for ultrasonic beam steering, scanning and focussing. Individual transducers within such phased arrays are subject to spacing and size restrictions which result in lateral modes comparable in frequency with the thickness vibration. As a result, accurate design of the beam profile output from ultrasonic phased arrays, is extremely difficult.

Since it is intended to extend the present model to aid the design of ultrasonic arrays, much further work is necessary to investigate the characteristics of lateral modes in order that effective methods of reducing their contribution may be achieved.

At the present moment it is doubtful whether there exists an exact mathematical solution describing the coupling between thickness and lateral vibration in either circular disc or rectangular plate transducers. Or, for that matter whether the solution may be incorporated within a suitable model.

Some approximate methods have been attempted, largely without success. For example Smith (52) extended Mason's model by including an extra transmission line, describing the radial mode. However, the approach was not rigorous and no meaningful results were achieved. As an extension to the present model, a feasibility study into lateral mode

vibration and the possibility of incorporating it within a feedback systems concept is currently being investigated.

9.2ii Mechanical Boundary Conditions Possessing Finite Thickness (Layers)

Development of the feedback model assumed that all mechanical loading media extended indefinitely away from the transducer. However, in practical probe designs, the load and backing materials often constitute layers of finite thickness. This may be deliberate; for example quarter wave matching to improve transmission characteristics or the incorporation of a protective 'wear plate' in some ndt probes. In addition, poor bonding between transducer and electrodes, transducer and backing, transducer and wear plate etc, may produce additional layers which can significantly distort the transducer waveshape.

Consequently, in order to apply the present work to the design of such probes provision must be made for extending the model to include layered media at both faces. Although this is technically feasible, the overall complexity of the transmission and reception block diagrams increases with the number of layers, obscuring much of the clarity contained in the original model. This is one of the reasons why layered media were not included in the development of the transducer model. In addition, as described in chapter II, much work has already been performed in the investigation of layered

load and backing media.

9.2iii State - Space Representation of Transducer Behaviour

It has been demonstrated that the feedback model offers considerable insight into piezoelectric transducer behaviour. However, it should be noted that there exists an alternative strategy to the block diagram, transfer function approach described in the thesis. This alternative strategy may well prove attractive for the modelling of multi-mode, multi-layered transducer systems.

The analysis of transducer behaviour may also be approached by means of the state space concept; in which the device is characterised by a set of first order differential (or difference) equations which describe the state variables of the system. It may thus be possible to define an optimum set of state variables in the sense that all quantities are of clear physical significance to the transducer system. Transducer performance is then evaluated by solving a set of first order equations, rather than a single higher order equation.

The viability of this approach to electro-acoustic systems has been confirmed by Ashley (1) who applied state variable theory to aid the design of an electrodynamic loudspeaker. Although a complete investigation has yet to be performed, the state variable concept may well prove attractive for

the study and modelling of piezoelectric transducer systems.

9.2iv Diffraction and Transducer Beam Characterisation

As indicated in chapter VII, there exists no provision within the present transducer model to accommodate diffraction effects in the ultrasonic sound field. Although the model accurately describes a plane wave component leaving the transducer face, the diffracted edge wave component is not included. The presence of an edge wave influences not only the shape of a transmitted acoustic pulse, but also transducer beam profile characteristics.

Figure 9.1 shows the instantaneous sound field characteristics of a 1 MHz transducer operating into a crown glass load via a thin film of water based couplant. The transducer is air backed and electrically driven under transient conditions. The photograph was taken by means of a photoelastic technique using apparatus specially constructed for the investigation of transient ultrasonic stress pulses in transparent solid media.

In the photograph, the main longitudinal wave component may readily be identified along with trailing shear waves arising directly from edge-wave diffraction. As well as shear mode edge-waves, longitudinal edge-waves also exist, although these are not readily apparent from the figure. The photograph was taken at a particular instant in time to illustrate far-field conditions.

Figure 9.2 shows the sound pressure output from the same transducer, but viewed at an earlier instant, in order to demonstrate near field conditions. Once again, plane and edge wave components may clearly be resolved.

It is evident from figures 9.1 and 9.2 that the transient sound field is extremely complex, and particularly so for solid media. Some simplification may be achieved with liquid loading, due to the absence of shear components. It is however, considered possible to accurately predict wave and sound field profiles using the feedback model.

This method involves the translation of each pressure pulse leaving the transducer into its CW components by means of an FFT. Each CW component is then allowed to propagate to the field point of interest using diffraction theory. The components are then assembled in the correct phase using an IFFT and the pressure amplitude calculated.

This technique may be employed to calculate the pressure wave profile in both near and far-fields; that is, the actual pressure wave incident on a receiving transducer. It may also be used to calculate the directivity and beam spreading characteristics of the transmitting device.

It must be emphasised that this method employs the actual pressure wave produced by the transmitting device to calculate field characteristics. Other analyses for example that of

Weyns (61) assume decaying exponential pulses or gaussian modulated sine pulses to be produced at the front face of the transducer (in addition to neglecting the edge wave). However, these are based on the output of a similar piezoelectric receiver and as such, may bear little or no resemblance to the actual acoustic pressure wave. This has important consequences in determining the operating characteristics of a transient sound field.

It was apparent in chapter VII that both electrical and mechanical load conditions influence the shape of the transmitted pressure and received voltage waveforms. Although the effects of mechanical loading have undergone considerable investigation, apart from the present work, no systematic study of electrical loading conditions has yet been undertaken. (See for example Mason and Thurston (19)).

In chapter VII it was shown that electrical loading has considerable influence on the output wave of force from the transmitting device. As a result, it is possible to assume that such factors also influence the transducer beam characteristics. This is in fact, confirmed by the sequence of photographs shown in figures 9.3(a-c).

The photographs, taken at the same instant of time, depict the beam characteristics of a 1 MHz transducer, operating into a glass load. In each case, a different value of inductance is connected across the device, with the rest

of the transmitting circuitry remaining constant. The transducer remained stationary while the inductance values were altered (by means of a switch in the driving unit), ensuring uniformity of the couplant layer. Marked changes in the beam characteristics are evident.

Apart from visualisation studies, some tentative work has already commenced on measuring beam profile characteristics in a water tank. Early results have indicated appreciable changes in beam characteristics as the electrical driving conditions are altered.

As a result, it is suggested that the feedback model should be used to form the basis of a simulation study of transient beam characteristics. This study is considered extremely important in defining operation standards for ultrasonic probes and arrays. The quality of medical diagnostic and ndt equipment depends strongly on uniformly and continuity in the field characteristics of the transducers employed.

9.2v Transducer Mechanical Loss

Development of the feedback model included the assumption that the transducer and all surrounding media are mechanically loss free. This approach has been experimentally justified for lead zirconate titanate piezoceramic devices under conditions of water loading. However, for more general ultrasonic system applications, the present model requires further

extension to include mechanical wave absorption in both the transducer element and propagating channel.

When an ultrasonic wave propagates through a medium, the intensity decreases exponentially with the distance travelled; energy dissipated in the form of heat. Silk (44) attempted to compensate for such loss by introducing an exponentially decaying attenuation factor into the transmission line model of Krimholtz et al. However, it should be emphasised that such losses are normally frequency dependent, attenuation increasing with frequency. In an attempt to overcome this problem, Dotti (8) recommended the insertion of a time spread into the transmission line section of his model.

It is similarly possible to approximate for frequency dependent absorption within the transducer by introducing a time spread into the reverberation section of the feedback model. As a result, the impulse response of each reverberation factor is no longer a train of weighted impulse functions, but instead comprises a train of pulses possessing finite width and shape. This technique may readily be applied by considering the following reverberation transfer function.

$$K_{FL}(S) = \frac{G(S)(1 - e^{-ST})(1 - R_B e^{-ST})}{(1 - R_F R_B e^{-2ST})}$$

Where G(S) is the transfer function of a spreading function intended to model frequency dependent attenuation. For

example, as a first order approximation, G(t) may be considered as a rectangular pulse of width Δt, ie

$$G(S) = \frac{1}{S} (1 - e^{-S\Delta t}) \qquad \Delta t < T$$

Consequently, the impulse response of KFL is a train of rectangular pulses, alternating in sign, the magnitudes of which are controlled by the values of R_F and R_B. Similarly, as a second order approximation, G(t) may be considered as a triangular pulse of width Δt, ie

$$G(S) = \frac{1}{S^2} (e^{-S\Delta t/2} - 1)^2$$

From which the attenuation with frequency is readily apparent. For transducer materials possessing high mechanical loss, the overall attenuation with distance may be modelled by including a loss factor, α, which is independent of frequency. As a result, the overall lossy, reverberation factor is given by,

$$K_{FL}(S) = \frac{G(S)(1 - e^{-ST}\, e^{-\alpha L})(1 - R_B e^{-ST}\, e^{-\alpha L})}{(1 - R_F R_B e^{-2ST}\, e^{-2\alpha L})}$$

where L is the transducer thickness.

This approach, although by no means rigorous, has provided encouraging results with the low-loss type of device under consideration. However, it must be emphasised that much

further investigation is required for the accurate modelling of lossy devices.

9.2vi Ultrasonic Channel Considerations

Characterisation of the propagating channel provides a similar, but often more difficult problem to that of internal mechanical dissipation within the transducer element. Attenuation mechanisms in various media range from granular scattering in metals, viscosity in liquids, to reflections at the layered interfaces of reinforced fibre composite materials. In addition, all media exhibit dispersion, whereby the acoustic velocity is also a function of frequency. This results in spreading and distortion of the ultrasonic wave as it propagates along the channel.

Although much work has been performed in the study of acoustic wave propagation (see for example, Gooberman (13)), current research involving ultrasonic materials evaluation has highlighted the need for more accurate characterisation in the following areas;

a the characterisation of various metallic media for ndt,

b the characterisation of human tissue for non-invasive medical diagnosis, and

c the characterisation of layered composite fibre materials.

Accurate modelling of the acoustic channel is extremely important where ultrasonic techniques are employed to identity abnormalities and discontinuities in the propagating medium. For example, it is possible to obtain a transfer function relating to such 'flaws' using ultrasonic spectral analysis techniques. Such a transfer function may be obtained from the following frequency domain equation.

$$F(\omega) = \frac{Y(\omega)}{X(\omega)\ T(\omega)\ C(\omega)\ R(\omega)}$$

where X describes the input voltage to the transmitter system,

T is the complete transfer function of the piezo-electric transmitter system, including diffraction effects,

R is the complete transfer function of the piezo-electric receiver system, and

Y is the measured characteristic of the received voltage.

In order to completely identify $F(\omega)$, each transfer function within this equation must be accurately known. While the feedback model may yield sufficient insight into the transduction process, the problem of channel characterisation still remains. This is viewed as a considerable challenge which must be overcome if further progress involving such techniques is to be made.

ACKNOWLEDGEMENTS

The author wishes to express gratitude to the SERC Marine Technology Directorate who funded the research program from which the present thesis developed.

Thanks is also due to the following personnel within the Department of Electronic Science and Telecommunications.

The Head of Department, Professor A M Rosie, for providing some of the facilities required to carry out this project.

Special thanks to my two colleagues, Dr C J MacLeod (Reader) and Dr T S Durrani (Senior Lecturer) who both supervised the present work. The author is grateful for the many hours of helpful discussion and encouragement which they provided throughout the duration of the project.

REFERENCES

1 ASHLEY, R. J., CILETTI, M. D. and WIATROWSKI, C. A., Signal flow graphs for electro-acoustic transducers (or modelling made easy) simulation, Vol 27, No 5, November 1976.

2 BLITZ, J., Fundamentals of ultrasonics, Butterworths (1963).

3 BROWN, A. F. and WEIGHT, J. P., Generation and reception of wideband ultrasound, Ultrasonics, July 1974, pp 161-167.

4 CAROME, E. F., PARKS, P. E. and MRAZ, S. J., Propagation of acoustic transients in water. Journal of the Acoustical Society of America, Vol 36, May 1964, pp 946-952.

5 CARSON, P. L., What a hospital physicist needs in a transducer characterisation standard: are tissue equivalent test objects necessary? IEEE Trans. on sonics and ultrasonics, January 1979, pp 1-6.

6 COOK, E. G., Transient and steady state response of ultrasonic piezoelectric transducers, IRE Convention Record, Vol 4, 1956, pp 61-69.

7 DESILLETS, C. S., FRASER, J. D. and KINO, G. S., The design of efficient broad-band piezoelectric transducers, IEEE Trans. on sonics and ultrasonics, May 1978, pp 115-125.

8 DOTTI, D., A new model of a piezoelectric transducer for direct impulse response evaluation. IEEE Trans. on sonics and ultrasonics, May 1975, pp 202-205.

9 ENSMINGER, D., Ultrasonics, the low and high intensity applications, Dekker, New York, 1973.

10 ERIKSON, K., Tone burst testing of pulse-echo transducers. IEEE Trans. on sonics and ultrasonics, January 1979, pp 7-14.

11 FILIPCZNSKI, L., Transients, equivalent circuit and negative capacitance of a piezoelectric transducer. Journal of Technical Physics, Vol 16, 1975, pp 121-134.

12 FOSTER, F. S. and HUNT, J. W., The design and characterisation of short pulse ultrasound transducers. Ultrasonics, May 1978, pp 116-122.

13 GOOBERMAN, G. L., Ultrasonics theory and application. English Universities Press Ltd, 1968.

14 HILKE, H. J., Piezoelectric transducer vibrations in a one-dimensional approximation. Applied physics, June 1973, pp 317-329.

15 IEEE Standard on piezoelectricity, STD 197611978.

16 IRE Standard on piezoelectric crystals: measurements of piezoelectric ceramics, 1961.

17 KIKUCHI, Y. and KASAI, C., A method for measuring the electromechanical coupling factor of piezoelectric materials by means of transient response. Ultrasonics, September 1975, pp 208-212.

18 KOSSOF, G., The effects of backing and matching on the performance of piezoelectric ceramic transducers. IEEE Trans. on sonics and ultrasonics, March 1966, p 20.

19 KOZINA, O. G. and MAKAVOV, G. I., Transient processes in the acoustic fields generated by a piston membrane of arbitrary shape. Soviet Physics Acoustics, Vol 7, (1961) pp 39-43.

20 KRAUTKRAMER, J., Ultrasonic testing of materials (1977), Springer.

21 LEEDOM, D. A., KRIMHOLTZ, R. and MATTHEI, G. L., Equivalent circuits for transducers having arbitrary even-or-odd symmetry piezoelectric excitation. IEEE Trans. on sonics and ultrasonics, July 1971, pp 128-141.

22 LEEDOM et al, New equivalent circuits for elementary piezoelectric transducers. Electronics letters, 25 June 1970, Vol 6, No 13.

23 LEWIS, G. K., A matrix technique for analysing the performance of multi-layered front matched and backed piezoelectric ceramic transducers. Journal of the Acoustical Society of America, pp 395-416, 1980.

24 LOW, G. C., A simple computer method for predicting the transient response of ultrasonic NDT probes (unpublished). Dept. Nat. Phil., University of Aberdeen.

25 LUKOSEVICUS, A. and KAZYS, R., Optimisation of the piezoelectric transducer response by means of electrical correcting circuits. Ultrasonics, May 1977, pp 111-116.

26 MARTIN, G. E., Dielectric, elastic and piezoelectric losses in piezoelectric materials. Proceedings of the 19th Ultrasonics Symposium, 1974, pp 613-617.

27 MARTIN, R. W. and SIGELMANN, R. A., Force and electrical thevenin equivalent circuits and simulations for thickness mode piezoelectric transducers. Journal of the Acoustical Society of America, August 1975, pp 475-489.

28 MASON, W. P., Electromechanical transducers and wave filters (2nd Edit), Van Nostrand Co Inc., New York, 1948.

29 MASON, W. P. and THURSTON, R. N., Physical acoustics Vol XIV, Academic Press, p 294.

30 MEEKER, T. R., Thickness mode piezoelectric transducers. Ultrasonics, January 1972, pp 26-36.

31 MILLER, E. B. and EITZEN, D. G., Ultrasonic transducer characterisation at the NBS. IEEE Trans. on sonics and ultrasonics, January 1979, pp 28-36.

32 OLSON, H. F., Solutions of engineering problems by dynamical analogies (2nd Edit), Van Nostrand, Princeton, New Jersey.

33 ONOE, M., TEIRSTEN, H. F. and MEITZLER, A. H., Shift in the location of resonant frequencies caused by large electromechanical coupling in thickness mode resonators. Journal of the Acoustical Society of America, January 1963, pp 36-42.

34 PAPADAKIS, E. P., Ultrasonic transducer evaluation in five 'domains': time, space, frequency, surface motion and theory. Ultrasonics Symposium Proceedings, 1977, pp 104-112.

35 PREIS, D., Block diagrams: a tutorial alternative to dynamical analogies. IEEE Trans. on education, November 1976, pp 143-148.

36 REDWOOD, M., Transient performance of a piezoelectric transducer. Journal of the Acoustical Society of America, Vol 33, No 4, April 1961, pp 527-536.

37 REDWOOD, M., A study of waveforms in the generation and detection of short ultrasonic pulses. Applied materials research, April 1963, pp 76-84.

38 REDWOOD, M., Experiments with the electrical analogue of a piezoelectric transducer. Journal of the Acoustical Society of America, Vol 36, No 10 (1964), pp 1872-1880.

39 REDWOOD, M. and LAMB, J., On the measurement of attenuation in ultrasonic delay lines. Proc. IEEE Vol 103, Part B, (1956), p 773.

40 RHYNE, T. L., An improved interpretation of Mason's model for piezoelectric plate transducers. IEEE Trans. on sonics and ultrasonics, March 1978, pp 98-103.

41 ROBINSON, D. E., LEES, S. and BESS, L., Near field transient radiation patterns for circular pistons. IEEE Trans. ASSP Vol 22 (1974) pp 395-403.

42 SEITCHIK, J. A., The determination of transducer coupling coefficients by time domain analyses. IEEE Trans. on sonics and ultrasonics, January, 1972, pp 23-27.

43 SHOTTON, K. C., BACON, D. R. and QUILLIAM, R. M., A pvdf membrane hydrophone for operation in the range 0.5 to 15 MHz. Ultrasonics, May 1980, pp 123-126.

44 SILK, M. G., Calculations on the effect of some constructional variables on ultrasonic transducer performance. Materials Physics Division, AERE Harwell Report, June 1980, (UK).

45 SILICONIX LTD, VMOS Power FET Design Catalogue, January, 1979.

46 SINHA, D. K., Note on response in a piezoelectric plate transducer with a periodic step input. Indian Journal of Theoretical Physics, Vol 10 (1962), pp 21-28.

47 SINHA, D. K., Note on electrical and mechanical responses with ramp-type input signals in a piezoelectric plate transducer. Indian Journal of Theoretical Physics, Vol 11 (1963) pp 93-99.

48 SINHA, D. K., A note on the responses in a piezoelectric transducer. Indian Journal of Pure and Applied Physics (1967) pp 375-376.

49 SINHA, D. K., A note on mechanical response in a piezoelectric transducer owing to an impulsive voltage input. Proc. Nat. Inst. Sci. India, Vol 31A (1965) pp 395-402.

50 SITTIG, E. K., Transmission parameters of thickness-driven piezoelectric transducers arranged in multi-layer configurations. IEEE Trans. on sonics and ultrasonics, October 1967, pp 167-174.

51 SITTIG, E. K., Effects of bonding and electrode layers on the transmission parameters of piezoelectric transducers used in ultrasonic digital delay lines. IEEE Trans. on sonics and ultrasonics, January 1969, pp 2-10.

52 SMITH, W. R. and AWOJOBI, A. O., Factors in the design of ultrasonic probes. Ultrasonics, January 1979, pp 20-26.

53 STEPHANISHEN, P. R., Transient radiation from pistons in an infinite planar baffle. Journal of the Acoustical Society of America, Vol 49 (1971), 1629-1638.

54 STEUTZER, O. M., Multiple reflections in a free piezoelectric plate. Journal of the Acoustical Society of America, April 1967, pp 502-508.

55 STEUTZER, O. M., Impulse response measurement technique for piezoelectric transducer arrangements. IEEE Trans. on sonics and ultrasonics. January 1968, pp 13-17.

56 TIERSTEN, H. F., Linear piezoelectric plate vibrations. Plenum Press, New York, 1969.

57 THURSTON, R. N., Effect of electrical and mechanical terminating resistances on loss and bandwidth according to the conventional equivalent circuit of a piezoelectric transducer. IRE Trans. on ultrasonics engineering, February 1960, pp 16-25.

58 Unilator Technical Ceramics Ltd, Piezoelectric Ceramics.

59 Vernitron Applications Bulletins (Southampton Ltd), 66047/A, 66011/F and 66017/B.

60 WEIGHT, J. P. and HAYMAN, A. J., Letter, Ultrasonics, November 1978, p 282.

61 WEYNS, A., Radiation field calculations of pulsed ultrasonic transducers. Ultrasonics, July 1980, p 183.

62 YADAV, B., A note on the study of mechanical response in a piezoelectric composite transducer. Indian Journal of Physics, Vol 42 (1969), pp 649-655.

63 YAMAMOTO, Y., Equivalent electrical circuits of the quartz crystal transducer for analysis of ultrasonic systems. IRE Trans. on ultrasonics engineering, July 1962, pp 1-5.

64 YING, C. F., LI, M. X. and ZHANY, H. L., Ultrasonics, July 1981, pp 155-158.

65 ZITELLI, L. T., Experimental broad-band ultrasonic transducers using pvF_2 piezoelectric film. Electronics Letters, 12(1976) p 393.